2018

AFFECT-PRESERVING VISUAL PRIVACY PROTECTION

Wanxin Xu
University of Kentucky, wxbit0930@gmail.com
Author ORCID Identifier:
https://orcid.org/0000-0001-7399-5027
Digital Object Identifier: https://doi.org/10.13023/etd.2018.303

STUDENT AGREEMENT:

I represent that my thesis or dissertation and abstract are my original work. Proper attribution has been given to all outside sources. I understand that I am solely responsible for obtaining any needed copyright permissions. I have obtained needed written permission statement(s) from the owner(s) of each third-party copyrighted matter to be included in my work, allowing electronic distribution (if such use is not permitted by the fair use doctrine) which will be submitted to UKnowledge as Additional File.

I hereby grant to The University of Kentucky and its agents the irrevocable, non-exclusive, and royalty-free license to archive and make accessible my work in whole or in part in all forms of media, now or hereafter known. I agree that the document mentioned above may be made available immediately for worldwide access unless an embargo applies.

I retain all other ownership rights to the copyright of my work. I also retain the right to use in future works (such as articles or books) all or part of my work. I understand that I am free to register the copyright to my work.

REVIEW, APPROVAL AND ACCEPTANCE

The document mentioned above has been reviewed and accepted by the student's advisor, on behalf of the advisory committee, and by the Director of Graduate Studies (DGS), on behalf of the program; we verify that this is the final, approved version of the student's thesis including all changes required by the advisory committee. The undersigned agree to abide by the statements above.

Wanxin Xu, Student

Dr. Sen-Ching Samson Cheung, Major Professor

Dr. Aaron Cramer, Director of Graduate Studies

AFFECT-PRESERVING VISUAL PRIVACY PROTECTION

DISSERTATION

A dissertation submitted in partial fulfillment of the
requirements for the degree of Doctor of Philosophy in the
College of Engineering
at the University of Kentucky

By
Wanxin Xu
Lexington, Kentucky

Director: Dr. Sen-Ching Samson Cheung, Professor of
Electrical and Computer Engineering
Lexington, Kentucky

2018

ABSTRACT OF DISSERTATION

AFFECT-PRESERVING VISUAL PRIVACY PROTECTION

The prevalence of wireless networks and the convenience of mobile cameras enable many new video applications other than security and entertainment. From behavioral diagnosis to wellness monitoring, cameras are increasing used for observations in various educational and medical settings. Videos collected for such applications are considered protected health information under privacy laws in many countries. Visual privacy protection techniques, such as blurring or object removal, can be used to mitigate privacy concern, but they also obliterate important visual cues of affect and social behaviors that are crucial for the target applications. In this dissertation, we propose to balance the privacy protection and the utility of the data by preserving the privacy-insensitive information, such as pose and expression, which is useful in many applications involving visual understanding.

The **Intellectual Merits** of the dissertation include a novel framework for visual privacy protection by manipulating facial image and body shape of individuals, which: (1) is able to conceal the identity of individuals; (2) provide a way to preserve the utility of the data, such as expression and pose information; (3) balance the utility of the data and capacity of the privacy protection.

The **Broader Impacts** of the dissertation focus on the significance of privacy protection on visual data, and the inadequacy of current privacy enhancing technologies in preserving affect and behavioral attributes of the visual content, which are highly useful for behavior observation in educational and medical settings. This work in this dissertation represents one of the first attempts in achieving both goals simultaneously.

KEYWORDS: Pose Estimation, Human Body Reshaping, 3D Face Reconstruction, Facial Expression Transfer, Visual Privacy Protection

Wanxin Xu

July 16, 2018

AFFECT-PRESERVING VISUAL PRIVACY PROTECTION

By

Wanxin Xu

Director of Dissertation: Dr. Sen-Ching Samson Cheung

Director of Graduate Studies: Dr. Aaron Cramer

Date: July 16, 2018

To my family

ACKNOWLEDGEMENT

Looking back to the challenging but rewarding journey towards to pursue my PhD degree, I have received generous help and support from many people.

First of all, I would like to extend my sincerest gratitude to my academic advisor, Dr. Sen-ching Samson Cheung. It is my great pleasure to be supported and instructed by a mentor like him, who has masterful grasp of his field and is constantly considerable from his students' point of view to inspire them towards success. I sincerely appreciate the numerous recourses and facilities I have been provided from Dr. Cheung, without which I would not be able to accomplish the work of my dissertation. He is quite energetic and cheerful, has long-lasting enthusiasm in his career. I have learned a lot from his unique characteristics and they will continue to inspire me through all the challenges that I will face in my future endeavors

I also would like to thank Dr. Alberto Corso, Dr. Daniel Lau, Dr. Ruigang Yang and Dr. Yuming Zhang for their time serving as my committee member. I really appreciate their constructive feedback and comments on my dissertation, which give me the opportunity to revisit it and make it a better one.

I truly appreciate the help and support from all my colleagues and friends at UK. Because of them the years of challenging scientific exploration has turned to quite enjoyable memories, which I will remember for the rest of my life.

Finally but most importantly, I would like to thank all members in my family from the bottom of my heart, in particular my parents, my grandparents, my sister and my

husband. My deepest appreciation goes to them. Without their unconditional love and constant support, I cannot accomplish this today and would not be able to stick to the completion of my PhD study.

TABLE OF CONTENTS

ACKNOWLEDGEMENT iii

TABLE OF CONTENTS v

LIST OF TABLES viii

LIST OF FIGURES ix

Chapter 1 Introduction 1
1.1 Background 1
1.2 Motivation 2
1.3 Contributions 3
1.4 Outline of the dissertation 5

Chapter 2 Related Work 7
2.1 De-identification of Visual Identifiable Information 7
2.2 Facial Expression Capture and Reconstruction 10
2.3 Human Pose Estimation 16
2.4 Human Shape Reconstruction 21
2.5 Body Reshaping 27

Chapter 3 Preliminary Works: General Pipeline for The Application of Face and Human Shape Manipulation 31
3.1 Geometric Data Collection and Processing 31
3.2 Surface Reconstruction from Point Cloud 35
3.3 Motion Capture for Face and Body Shapes 38

Chapter 4 Facial Image Manipulation with RGB Images 41
4.1 Facial Image Manipulation with Recolor and Component Blending 41
4.1.1 Overview of our system 41
4.1.2 Skin recoloring and facial component blending 42
4.1.3 Experimental results 44
4.2 Fully Automatic Photorealistic Facial Expression and Eye Gaze Correction with a Single Image 46

4.2.1 Overview of the system 48
4.2.2 Coarse and fine face reconstruction 48
4.2.2.1 Coarse model fitting 49
4.2.2.2 Geometry refinement 50
4.2.3 Facial expression transfer and eye gaze correction 52
4.2.4 Experimental results 53

Chapter 5 Human Body Reshaping with Single and Two Depth sensors 57
5.1 Skeleton-driven Approach for Human Body Reshaping with Single Depth Sensor 57
5.1.1 Data preparation and mesh generation 59
5.1.2 2D shape manipulation 60
5.1.3 Experimental results 61
5.2 Human Pose Estimation with Two RGB-D Sensors 62
5.2.1 System overview 63
5.2.2 Data acquisition and preprocessing 64
5.2.3 Non-rigid point set registration 65
5.2.4 Skeleton estimation using bone-based approach 68
5.2.5 Experimental results 69

Chapter 6 Model-based Approach for Human Body Reshaping with Sensor Network 73
6.1 Overview of the System 73
6.2 Data Collection and Pre-processing 75
6.3 Pose and Shape Estimation with Multiple Depth Sensors 77
6.3.1 SCAPE model 77
6.3.2 GMM-based pose and shape fitting 78
6.3.2.1 GMM-based point set registration 79
6.3.2.2 Human pose and shape optimization 81
6.3.3 Detailed motion reconstruction 84
6.3.4 Bone-based approach for skeleton estimation 85
6.4 Human Body Reshaping 86
6.5 Experimental Results 87
6.5.1 Evaluation of poses 87
6.5.2 Evaluation of shapes 90
6.5.3 Evaluation of human body reshaping 93
6.6 Application on Visual Privacy Protection 93

6.6.1 Evaluation of human body reshaping with depth sensor network for visual privacy protection 94

Chapter 7 Conclusions and Future Work 100

Bibliography 102

Vita……..... 119

LIST OF TABLES

Table 6.1 Average step length with different reshaping parameters (mm)..... 98

LIST OF FIGURES

Figure 2.1 Early method for face de-identification: (a) Original image; (b) Blurring; (c) Pixelization. 8
Figure 2.2 Examples of Animoji with iPhone X..... 10
Figure 2.3 Double counting error [137]. (a) Estimated pose; (b) Max marginal..... 16
Figure 2.4 Illustration of SCAPE model, θ - parameter for pose, β - parameter for shape. 22

Figure 3.1 Examples of Kinect Sensor v1 (a) and Kinect Sensor v2 (b)..... 32
Figure 3.2 Example of imperfect depth data captured by Kinect sensor with noises and black holes [155]..... 33
Figure 3.3 Calibration result using the method from [155], (a) uncalibrated scene; (b) calibrated scene..... 34
Figure 3.4 Comparison of three methods for point clouds simplification using CGAL [36]: (a) Original input; (b) Random simplification result; (c) Grid simplification result; (d) WLOP simplification result. 36
Figure 3.5 Duality of Delaunay triangulation [37] (a) Delaunay triangulation with all the circumcircles and their centers (red); (b) Voronoi diagram (red) overlaid to Delaunay triangulation..... 38
Figure 3.6 Template and embedded skeleton for human body and the hand [116]. (a) Human body with skeleton; (b) Hand with skeleton. 39

Figure 4.1 Face image editing procedure..... 42
Figure 4.2 Skin Color Transfer with input source image in (a), target image in (b) and the skin-recolored source image in (c)..... 42
Figure 4.3 Generation of the ROIs. (a) Landmark detection. (b) Landmark refinement by linear interpolation. (c) Initial ROIs. (Mouth (blue), eyebrows (yellow), eyes and nose (green)). (d) Final generated ROIs by erosion and dilation..... 43
Figure 4.4 Poisson blending result. (a) Source image. (b) Mask obtained from the ROIs generation. (c) Blended image. 44
Figure 4.5 Fame image editing result. (a) Source image. (b) Skin recolored result. (c) Facial component blending result. 45
Figure 4.6 The Overview of our proposed face expression transfer pipeline..... 47
Figure 4.7 Coarse face reconstruction: (a) labeled 3D face landmarks; (b) 2D landmarks detected on the input image; (c) reconstructed model projected to the input image 49
Figure 4.8 Geometry refinement: (a) coarse shape; (b) shape after refinement; (c) reconstructed fine shape with texture; (d) Facial expression transfer with coarse (left) and refined (right) 51
Figure 4.9 Eye gaze transfer: (a) original pairs of image with detected eye mask; (b) direct transfer without refinement; (c) final synthesized image 52
Figure 4.10 3D reconstruction evaluation: (a) Input RGB image; (b) Ground truth; (c) reconstructed model by our method; (d) error map between our model and ground truth; (e) error map between model obtained by method of [210] and ground truth. 53

Figure 4.11 Face reconstruction on unconstrained image: Input RGB image; reconstruction with our method; reconstruction with method from [210]; reconstruction using our method with texture. 55
Figure 4.12 Result of our proposed system: (First row) source input and target input images; (Second row) manipulated image after expression transfer from source to target without eye gaze correction; (Third row) final output image with gaze correction. 56

Figure 5.1 Human body reshaping with single depth sensor 58
Figure 5.2 (a) Original mask. (b) Refined mask and contour. (c) Generated mesh. 59
Figure 5.3 (a) Selected original image frame from two environments. (b) Reshaped image frame (taller and thinner). 62
Figure 5.4 The Overview of our proposed pose estimation pipeline 63
Figure 5.5 Point cloud alignment from two depth sensors: (a) before alignment; (b) after alignment. 64
Figure 5.6 Visual comparison of our proposed method using the dataset in [70] with its ground truth data. Blue line (Our method estimation) and Black dot (Ground truth). 69
Figure 5.7 Comparison of average joint position error for six sequences from the evaluation dataset: Kinect [156] (Dark blue), Baak.et al [13] (Light blue), Helten et al [70] (Yellow) and Ours (Red). 70
Figure 5.8 Pose estimation visualization results: (a) Color image from depth sensor (front); (b) pose estimation from KinectSDK (front); (c) pose estimation from KinectSDK (back); (d) pose estimation from our proposed system. 71
Figure 5.9 Poisson reconstruction with and without holes filling: (a) without holes filling before Poisson reconstruction; (b) with holes filling using our proposed way before Poisson reconstruction. 72

Figure 6.1 Overview of our proposed system. 74
Figure 6.2 Point cloud alignment from four depth sensors: (a) before alignment, (b) after alignment. (c) alignment with texture and camera position (1,2,3,4) 75
Figure 6.3 Point cloud outlier removal and simplification: (a) Original aligned point cloud; (b) after outlier removal using Gaussian filter; (c) after denoising using WLOP 76
Figure 6.4 SCAPE Model with 16 parts of different poses and shapes 78
Figure 6.5 View direction transformation (a) Morphable model with view direction (b) Original observed data with view direction (c) After transformation (Red: Y-axis; Blue: Z-axis; Green: X-axis) 81
Figure 6.6 Detail reconstruction (a) Initial registration result. (b) Reconstruction with details. (c) Detailed model with texture. 86
Figure 6.7 Human body reshaping (a) Original; Reshaping to different shape parameters (b) shorter; (c) thinner; and (d) fatter. 86
Figure 6.8 Visual comparison of our proposed method using the dataset in [70] with its ground truth data. Black line (Our method) and Red dot (Ground truth). 87
Figure 6.9 Comparison of average joint position error for six sequences from the evaluation dataset: Blue - [156], Orange - [70], Yellow - [192] and Purple - Ours method. 88

Figure 6.10 Pose estimation visualization result: (a) Color image from depth sensor (Kinect2); (b) (c) (d) (e)pose estimation from KinectSDK; (f) pose estimation from proposed system; (g) Reconstructed model with texture. 89
Figure 6.11 Error map for body shape fitting. (a) Original scan. (b) The estimated model overlaid with the ground truth, and (c) the difference between the estimated model and the ground truth, the unit is in millimeter. 90
Figure 6.12 Visual results of our shape fitting. Input model (gray) are overlaid on our result (red). 91
Figure 6.13 Detail visualization of shape fitting. 91
Figure 6.14 Body reshaping visualization result (a) Original reconstructed model (b), (c) and (d) Reshaped result with our method with different parameters of morphable model. 92
Figure 6.15 Our system reshapes the human body using multiple RGB-D sensors. (Left) Original reconstructed human model; (Right) 4 different views of the reshaped human body with shorter legs and longer body. 93
Figure 6.16 Average score of questionnaire results on the naturalness of our reshaping method. 95
Figure 6.17 Axis of rotation and relative angle of knees. 96
Figure 6.18 Joint Angle in one gait cycle. (a) Sequence1. (b) Sequence2. 97
Figure 6.19 Foot Joint position in one gait cycle. (a) Sequence1. (b) Sequence2. 99

Chapter 1 Introduction

Recent advances in digital image technologies have made it easier to capture and share data online. The captured images or videos enable a variety of applications such as video surveillance, intelligent monitoring system, etc. On the other hand, such forms of data gathering raise concerns on protecting sensitive information, such as identify of a child, that participant may want to keep hidden. As a result, an increasing amount of attention has been gathered to prevent the violation of privacy of individuals from both academia and industry.

1.1 Background

Privacy enhancing technologies for video data is a relatively new topic of research with the explicit goal of visually protecting the identity of selected individuals. From the early work at IBM on simple obfuscation [153] to the latest work on privacy in visual sensor networks [191], visual information management [115], and location/activity protection in surveillance [149], many aspects of enterprise surveillance have been investigated. Despite the significant research effort, there are few systems that are actually deployed in practice. Besides the questionable robustness of these research prototypes, the market needs from large corporations and public facilities do not seem to be significant enough to warrant large-scale deployment.

On the other hand, the prevalence of wireless network and the ease of capturing and viewing videos enable many new applications other than security and surveillance. Many of these applications have strong privacy need as required by law. The most notable examples are the use of video for behavior observations for educational and

medical purposes. Behavioral observation is an important tool for early diagnosis of many neurodevelopmental disorders in children. Behaviors like repetitive movements, staring spells, and tantrums can be early signs of serious conditions including autism spectrum disorder, epilepsy and Attention Deficit Hyperactivity Disorder (AD/HD). Such intermittent behaviors either are not exhibited or are difficult to capture during brief clinical visits. The gold standard in behavioral science is accurate recording of problematic behaviors based on observation over a period of time in naturalistic environments such as home or school. Such an approach is difficult to achieve in practical terms because setting up recording devices in naturalistic environments faces stringent privacy protection requirements as covered by HIPAA [174], FERPA [175], COPPA [176], and other related regulations. It is in this context that visual privacy protection is the most relevant and pressing to address.

1.2 Motivation

Visual privacy protection techniques, such as blurring, object removal or pixelation, have been applied to some of these studies to obfuscate everything in the video besides the subject of observation [64][66][65]. Besides these simple blurring or removal techniques, more advanced techniques have been proposed. Since people often identify a person by observing his/her face, large majority of the existing work focus on face de-identification. Newton et al. [125] proposed a privacy enhancing algorithm called k-Same, taking advantage of the concept of k-anonymity to face image databases. The algorithm determines similarity between faces based on a distance metric and creates new faces by averaging image components. More recently, Mosaddegh et al. [119] relied on a set of face donors from which it can borrow various face components (eyes, chin, etc.).

However, it is not enough to protect visual privacy only by modifying the face area. Even when the person's face is obscured, other elements could exist in the image, which can be used to perform person identification, for instance, using inference channels and previous knowledge [149]. Visual cues such as clothes, height and gait can be also used to identify the person. Others deal with the de-identification of the whole human body instead of just face. Tansuriyavong et al. [164] proposed to use a silhouette for privacy protection of a person. They remove information about textures while maintaining the shape of the person to complicate the identification. In [3], Agrawal et al. proposed person de-identification method in videos by using different blurring function. Flores and Belongie proposed to protect the privacy of a person in the image by removal [53]. Unfortunately, all these privacy-enhancing techniques obfuscates affect behaviors and detailed social interaction such as eye gaze between the subject and other individuals in the scene. Often, these behaviors are the key behavioral episodes that are of high diagnostic values. Finding a proper trade-off between the privacy and the utility of data remains a challenging problem. The research presented in this dissertation aims to preserve the utility like expression and pose of a person while protecting his/her privacy by making use of advanced computer vision technologies.

1.3 Contributions

The research work presented in this dissertation address the problem of protecting visual privacy while preserving most of the observable affect cues of an individual that are of high value either for security or medical purposes. I hypothesize that affect-preserving privacy protection can be achieved by digitally manipulating the identifiable attributes of an individual (body shape and facial features) while preserving the behaviors

(pose and expression). Capitalizing on the advances in visual data capturing and computer graphics, I argue that such an approach would be able to produce more naturalistic results compared to transferring behaviors to an animated avatar. Major contributions in this dissertation are listed as follows:

1. I propose a novel body reshaping scheme that, unlike typical 3D morphable approaches, does not require any user interaction in fitting the model to the original image. The proposed scheme uses a Kinect sensor to automatically capture and back-project 3D skeleton to the image in driving the mesh deformation process for reshaping.
2. I propose a novel human pose and shape estimation system that is more robust than existing systems in capturing complex body movements and require no manual initialization. The robust performance of the proposed system is due to the use of data captured from multiple depth sensors that are fused via a non-rigid fitting scheme. The subsequent estimation of pose and shape from the fused data is based on the celebrated SCAPE parametric model [10].
3. I propose a novel facial privacy protection scheme that, unlike existing approaches, protects privacy while preserving facial affect. The proposed scheme protects privacy by recoloring skin tones and replacing key facial features with those from other people, while preserving affect by blending these components to match the original expression.
4. To address the inadequacy of existing facial privacy protection in handling head pose variations and privacy leakage through the shape of the skull, I propose a new privacy protection scheme that transfers facial expression and

eye gaze from one person to another. The proposed scheme solves these problems by first using a coarse-to-fine scheme in reconstructing a detailed 3D face surface model from a single image in the wild, and then applying mesh deformation in transferring facial expression and eye gaze between the source and target models.

5. I propose a novel evaluation scheme to measure the effectiveness of body reshaping schemes in protecting privacy while preserving the utility of the videos. To the best of our knowledge, no evaluation schemes have been previously developed for this purpose. The utility is measured based on the subjective opinions on the naturalness of the reshaped videos. The privacy is measured based on whether the identity of the individual can be recognized after reshaping based on soft biometric techniques such as gait information.

1.4 Outline of the dissertation

The rest of this dissertation is organized as follows. Chapter 2 reviews the necessary background and previous works on de-identification for privacy protection, pose and shape estimation using depth information, and face reconstruction from RGB image. A brief introduction about the general pipeline for human body and face manipulation is presented in Chapter 3. In Chapter 4, the proposed method to hide the identity while preserving the utility information of individual by face recolor and facial component blending is first discussed. We then move to model-based approach for facial expression synthesis and eye gaze correction. In Chapter 5, I introduce the skeleton-driven an approach for human body reshaping in RGB images with single depth sensor. In addition, a scheme for pose estimation to improve the performance of human body

reshaping with single depth sensor is discussed. In Chapter 6, a model-based approach to reshape the body shape with multiple depth sensors and an application using human body reshaping for visual privacy protection is presented. The conclusion and future work are finally presented in Chapter 7.

Chapter 2 Related Work

2.1 De-identification of Visual Identifiable Information

Images, videos or other forms of data always contain rich information about the individuals in them – from facial features, body shapes, clothing styles to unique ways of walking and interactions with others. Such kind of information makes it easier to infer the identity of that person. However, most applications including those used in health and education research and general safety surveillance like people counting and crowd control, the knowledge of the identities of individuals are not necessary or required. Therefore, a need to use de-identification to remove all personal information of individual from an image or video draws much attention in recent years. Different from recognition, which makes use of all possible features to recognize the identity of a person or the label of an object, de-identification defined as an opposite process to conceal the identity of the person from been recognized. Instead of removing all information of the target person in image or video, the ideal goal for de-identification is to hide the identity of the person without obscuring his/her action and expression. In this section, we give a brief review on the most important work related to the pipeline for our visual privacy protection. More comprehensive reviews on previous literature can be found in [53][127].

Most of previous works proposed for de-identification of person in image or video focus on face de-identification, the primary biometric feature. Early approaches for face de-identification use simple transformation like blurring (see Figure 2.1(b)) or pixelization (see Figure 2.1(c)). While these methods are capable to protect the privacy of

(a) (b) (c)

Figure 2.1 Early method for face de-identification: (a) Original image; (b) Blurring; (c) Pixelization.

person in the image, some forms of data utility, such as facial expression, fails to be preserved due to heavy obfuscations of facial features. Most recent approaches attempt to preserve such features in a more systematic manner. Newton et al. proposed the k-same algorithm for face de-identification [125]. In their algorithm, they computed the average of k most similar faces from a dataset and replace each face image with the obtained average face. Some extensions to the k-same algorithm named k-same select [60] and model-based k-same [61] were proposed by Gross et al. aiming to improve data utility of the output. A large image gallery is required by the k-same select algorithm since there must be an image for each individual in every utility subset. In addition, the utility classifier need to be retrained if a new subset is added making this algorithm less flexible. Bitouk et al. in [20] introduced a system for privacy protection by replacing the face with another similar unrelated face selected from the database. Their algorithm blends the two faces by replacing the eyes, nose and mouth area and further adjust the color and illumination of the face in order to generate visually realistic result. Inspired by k-same algorithm, Jourabloo et al. in [90] proposed an approach to hide the identity of person while preserving a large set of facial attributes, such as gender, age, race, etc. by fusing faces with similar attributes. It can achieve impressive result on grayscale image with

attribute annotations, but the expression of the person fails to be preserved, which is not suitable for the applications like action recognition or behavior observation. In [104], the author presented a face de-identification method that enables the preservation of important face clues which is useful for behavior or emotions analysis. Their approach preserves the most important non-verbal facial features such as eyes, gaze, lips and lips corners by applying variational adaptive filtering. However, the approach on the basis of filtering fails to generate photo-realistic result.

Even though face plays the dominant role, other body features such as silhouette and gait are also important clues contained in image or video that have been shown useful for biometric identification. There are several works proposed to replace the object of interest in image or video by their abstracted version to achieve the goal for privacy protection. Williams et al. made use of silhouette representation for privacy protection in a fall detection and object finder system [190]. In addition to silhouette representation, Fan et al. proposed to use a generic 3D avatar to replace the person in video to protect the privacy of content in the video [45]. Their system provides a number of ways to obscure the person at different level, in addition to replace people within the video with 3D avatar or virtual objects, blurring the video also available. An interesting approach for body de-identification was presented in [126] - they proposed to replace a person with another one selected from a dataset gallery. However, the movement of the new person is different from the original one, which not proper for the applications like behavior observation or video monitoring. Ruchaud and Dugelay [148] proposed an approach to make the identity of people not be recognizable while preserving enough information such as body shape and motion that are required for the surveillance. They replace the body shape by

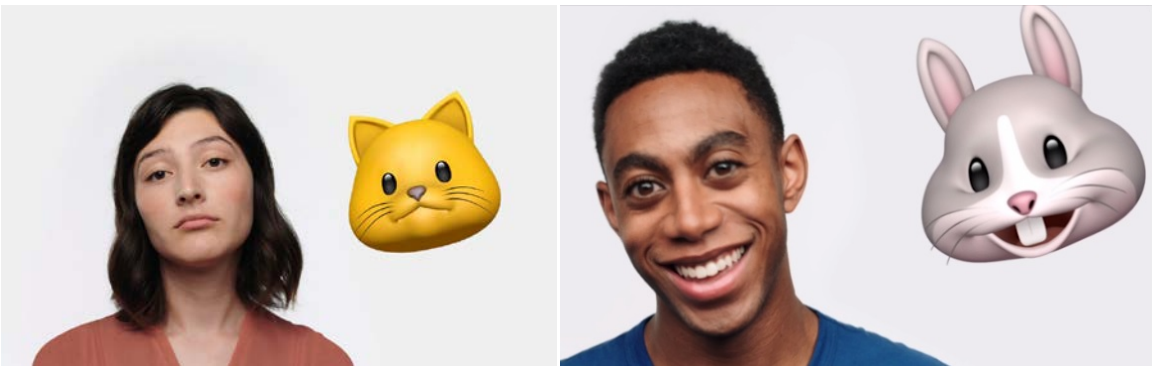

Figure 2.2 Examples of Animoji with iPhone X.

applying polygonal approximation on it with the help of a predefined model. It should be noted that the privacy of an individual can be protected or concealed by these schemes. Unfortunately, most of these methods suffer from artifacts, fail to emphasize the data utility and to preserve the naturalness of output image and video, which are key to subsequent vision processing. In this dissertation, we aim to preserve the *facial expressio*n and *body pose* of a person through reshaping while protecting his/her privacy.

2.2 Facial Expression Capture and Reconstruction

Human face plays a key role in human visual perception because it conveys a wide variety of information about an individual such as identity, emotion and intention. Reconstruction of a 3D model of a person's face from RGB images is important with various applications in face recognition, animation, video editing and more. For example, the latest iPhone X released by Apple using Face ID technology to unlock the phone, mimic and turn the expression of a person into an animated emoji, as is shown in Figure 2.2. Due to the variability in pose and environmental condition, this problem is fundamental but challenging in computer vision and computer graphics. Because it is

easy for human to recognize the inaccuracies in face appearance, tremendous efforts have been made to model the face with high quality.

The last few years have seen great progress on 3D face reconstruction from RGB images. Various methods have been proposed to solve the problem of facial model reconstruction and can be roughly categorized into three groups: shape from shading based approach (SFS), structure from motion based approach (SFM) and statistical model-based approach.

Shape from shading It is an approach to recover the shape information from a single image with use of information on shading variations. Many approaches are proposed to estimate the shape of a person's face which is optimized to match the input image and can be considered as an extension of shape from shading method. SFS-based methods can recover the fine geometric details that may not be available from low-dimensional models with the knowledge of lighting conditions and surface reflectance properties. The original shape from shading algorithm was proposed by Horn [73] and has been further investigated by others. Atick et al. in [12] used a statistical shape shading algorithm to reconstruct the 3D shape of a human face from a single image. Their work assumes the facial albedo to be constant and a linear constraint on the shape is imposed. The drawback of this algorithm is its time for computation and complexity. Dovgard and Basri [44] presented a SFS-based approach by combining the statistical constraints from [207] and the geometric constraint of facial symmetry into a single framework. Their framework is simple and has low cost in computation, however, the main drawback of this approach is that it is more compatible to frontal faces and the performance of the algorithm will be limited if the given human face is not symmetric.

Kemelmacher and Basri [94] introduced an approach to reconstruct the face model from a single image using just a reference model. They assume Lambertain reflectance and use spherical harmonics to represent the reflectance, which allows for and can handle unknown lighting coming from multiple unknown light sources.

Structure from motion One major constraint of SFS-based methods is that the lighting should be known as a prior or require a relatively simple model to approximate the illumination. Therefore, it is hard to apply it directly to the image in the wild if the configuration of the light sources is unknown or complicated. To overcome the limitation of SFS-based methods, the structure from motion based approach making use of multiple images is proposed to reconstruct the model of a human face. Fidaleo and Medioni [49] estimated the 3d shape of a person's face from the corresponding 2d facial feature points of multiple facial images. With use of this method, a dense and accurate person-specific 3d face model can be obtained. However, it often requires many consistent face images from different views, and self-occlusion or non-rigid variations which may lead to the correspondence error in 2d images can easily cause the SFM-based methods to fail. Lee et al. [103] proposed a SFM-based method for 3d face reconstruction which is robust to self-occlusion. They first build a coarse 3d face model using facial landmarks detected on multiple images. After that a dense 3d mean face model is warped to fit the coarse 3d face by thin-plate spline fitting. Ichim et al. [80] introduced an approach to build dynamic 3d avatar from a collection of facial images captured by mobile devices, which can be used to create avatar with low cost and hardware requirement. Their approach deforms the template model with a constraint of noisy point cloud built from SFM. Compared to SFS-based approaches, SFM-based methods are more robust to illumination. However, it

is challenging for SFM-based approaches to reconstruct a dense 3d face model because reliable feature point correspondences among facial images captured in the wild is hard to establish. Another limitation is that the SFM-based approaches cannot handle the non-rigid transformation of a person's face caused by variations in facial expression, which serves as an important component in 3d face modeling.

Statistical Face Model Different from SFS-based and SFM-based methods, statistical face model based approaches achieve face reconstruction on an image using a training dataset to learn a deformable model and then infer the 3d model of face in the given image by fitting a set of feature points between the 2d image and the obtained 3d deformable model. The popular approach for this type of facial reconstruction methodology is based on 3D morphable model (3DMM), an example-based approach proposed by Blanz and Vetter [21]. It uses the principal component analysis to learn the principal variations of face shape and appearance from the example faces, and then fitting these properties to a specific face in an image as a linear combination of principal components. This was extended by Vlasic et al. [180] who study and synthesize the variations on the facial shape along several axes, such as identity and expression by using a multilinear model. A variety of methods have been proposed in the last few years to reconstruct the face model from images or video. Most of them make use of 3D morphable model or a multilinear face model for face reconstruction [177][86][210]. Zhu et al. in [211] proposed a discriminative approach for 3d face model fitting by using local facial features and learn a cascade of regressor to estimate and update the parameters of 3d morphable model iteratively, achieving promising results. Some efforts in the field for face reconstruction have also focused on trying to build face model from other type of

source data. For example, building face model from large unstructured photo collections has been proven to be very successful [95][146][147]. Roth et al. [146] took a collection of unconstrained facial images with various poses and expressions as input and finally generated a person-specific face model of the individual. Their method first detects 2d landmarks on all input images and a 3d template mesh is warped and projected to 2d to match the 2d landmarks to get an initial model. A photometric stereo approach is further applied to improve the reconstruction. They extended their work in [146] by using a 3d morphable model instead of a simple template mesh to improve the fitting performance on image with arbitrary face shape and pose in [147]. These techniques, however, are not suitable for face reconstruction of individuals with only limited samples.

Other recent works have shown promising results for by integrating the 3d morphable model with deep neural networks for reconstructing the model of faces in images [24][43][166][172][173]. Richardson et al. [143] proposed a method to regress the parameters of 3d morphable model for face images with use of convolutional neural network. While their network can recover the facial shape from real image successfully, external algorithms are required for pose alignment and detail refinement. To recover the detailed information on face image, Richardson et al. [144] introduced an end-to-end network-based approach to improve the coarse face model generated by 3d morphable model with the help of a fine-scale network. A limitation of their method is that it may not performs well for face image with large geometric variations beyond the given subspace. To overcome this problem, Sela et al. [152] proposed a fully convolutional network to predict correspondence and depth by learning the unconstrained geometry directly in the image domain. They merge the model-based and data-driven geometries to

improve the quality for face reconstruction with details. In this dissertation, we extend the work in [210] to develop a coarse-to-fine scheme to reconstruct a 3D face model from 2D images. Different from [210], we capture the person-specific features like winkles using shading information from the image. This is essential to making the result photorealistic.

With the success of face reconstruction from images, several algorithms have been proposed for facial expression synthesis. In [107], Li and others proposed a method for facial expression retargeting in video, but the scheme relies on a pre-captured dataset. Song and others presented an analogy-based approach that uses the vertex tent coordinate transfer to perform geometric warping [159]. A Face2Face framework proposed by Thies et al. [177] allows for expression transfer between a captured RGB video of one actor and another arbitrary target face video in real time. They use a blendshape model to estimate the person's identity, expression, appearance and lighting. Further work on expression mapping and image-based mouth re-rendering enables the generation of photo-realistic target video sequence. Suwajanakorn et al. [162] introduced a framework to synthesize the lip movement by learning the mapping between audio and lip motion. Their work requires a large amount of person specific training data and does not take gaze direction into consideration. Thies et al. [167] presented an approach for real-time gaze-aware facial reenactment in virtual reality using a RGB-D camera to capture a person wearing a head-mounted display (HMD), and track the eye gaze with use of two internal infra-red (IR) cameras. A recent work proposed by Wen et al. in [187] achieve the tracking for 3D shape and motion of eyelids in real time from a single view RGB-D input. The reconstructed face is integrated with the tracked eye region making the result more

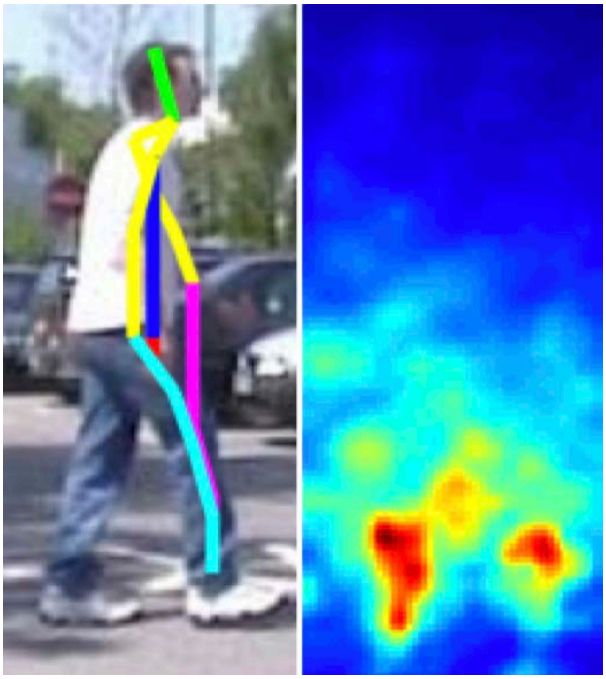

(a) (b)

Figure 2.3 Double counting error [137]. (a) Estimated pose; (b) Max marginal.

realistic. They represent eyelid variation with two linear models and detect semantic edges using a DNN, and further reconstruct the eyelid in real-time by a projective edge fitting method. Our work, however, differs from the previous approaches as it does not require any pre-captured dataset or neural images of the source and the target. We extend the work proposed in [160] to manipulate the expression of target input image using mesh deformation. Besides expression, we also transfer the eye gaze of the source actor to the target actor by using geometry warping approach.

2.3 Human Pose Estimation

Existing approaches for pose estimation mainly fall into two classes: marker-based and markerless. Most of the commercial motion capture (Mocap) systems use marker-based techniques because of their robust and accurate performance. However, the

significant hardware cost, as well as the need of a highly controlled environment and a special suit with markers significantly limit the use of Mocap in many of the aforementioned applications. Fueled by advances in commodity video cameras, marker-less Mocap systems are becoming more prevalent in recent years. Early markerless systems are based on carefully-calibrated color camera networks [15][55]. Recent advances using marker-less Mocap systems for human motion capture can be found in a number of excellent survey articles [118][136][157]. However, these approaches often require complex setup, careful control of illumination and background for foreground extraction. The quality of the scan is often poor, making these types of markerless systems impractical for casual usages like home entertainment. The related work I am going to discuss here will focus on 2d pose and 3d pose estimation in color and depth image. Based on this division, I first introduce the method of 2d pose estimation, and then 3d pose estimation will be presented in detail.

2D Pose Estimation. Many existing works estimate the pose of a person from a single, monocular image or video depending on image features that are chosen to represent the salient parts of the image with respect to the pose of a person. In the last few decades, many features are proposed for pose estimation. The early approach for pose estimation proposed by Hogg [71] makes use of edge information. Agarwal and Triggs [2] proposed to separate the person from background in image using image silhouettes. The author in [138][47] used color features to model the un-occluded skin or clothing for pose estimation. Color and texture provide more information compared with geometric features such as edge and silhouette, but the appearance model need to be updated during tracking to account for the change of illumination. To achieve good

performance for pose estimation, the features like edge, silhouette, color and etc. are combined together. Yang and Ramanan used oriented gradient descriptor for pose estimation with low computation cost, which can be combined with other descriptors [198].

In addition to image features, some researchers estimate the pose of person by modeling the articulated relationships between rigid human body parts with use of part-based models. In particular, tree-structured pictorial structure models are popular and widely used for human pose estimation. For instance, Johnson and Everingham [87] used a cascade of body parts detectors to obtain discriminative template. Other approach extended part-based model to a more flexible spatial body model implemented based on poselet features [134]. Despite impressive result, one of the limitation for tree structure is double counting, it occurs because of the symmetric appearance of body parts (left and right arm), more than one part is assigned to the same region of the image with high confidence, an example is shown in Figure 2.3 [137]. To overcome this, a lot of efforts have been focused on constructing more representative models and adding additional constraints [182][48][85][169][38]. Ferrari et al. [48] included repulsive edges to kinematic model to overcome double counting problem in upper-body pose estimation in video.

Recently, the development and surge of interest of deep convolutional neural networks (CNN) for vision task enables the state-of-art performance on pose estimation by employing convolutional architectures [8][27][171][133][185]. Among these approaches, DeepPose [171] is the first attempt using CNN to estimate the pose of a person. It regressed the joint coordinates of body parts with a cascade of ConvNet. Chen and Yuille [34] combined a part-based model with ConvNets to improve CNN performance. They used a mixture model to represent the spatial relationships between pairs of joint and learning the probabilities for the presence of joints and their spatial relationships within image patches by DCNNs, to improve the overall performance. Most recent approach for single person pose estimation is proposed by Newell et al. in [124]. They proposed a novel CNN architecture that replies on skip connections for feature learning and

a “stacked hourglass” network on the basis of repeated pooling and upsampling for the task of human pose estimation. Thereafter many methods are proposed based on stacked hourglass architecture. For example, Chu et al. [35] extended the work in [124] with a multi-context attention mechanism and the author in [197] adopted hourglass as their basic structure and replace the residual units with a Pyramid Residual Module.

Single person pose estimation in image or video has been studied extensively, parsing the pose of multiple person in the scene is much more challenging due to occlusions and interactions between people. The approaches for multi-person pose estimation can be categorized into two groups: top-down and bottom-up. Top-down approaches [82][130][46][59] employ a person detection and then perform single-person pose estimation for each detection. The performance of these kind of method highly depend on the reliability of person detector and the runtime of these approaches rely on the number of people. Bottom-up approaches [31][81][99][123][129] predict the body joints of all person in the scene and further partition them to corresponding person instances. These methods rely on context information and more robust to occlusion and complex poses. Cao et al. [28] proposed part affinity fields to encode location and orientation of limbs, and then used a greedy algorithm to parse the joints for all people in the image.

3D Pose Estimation. Estimate the 3D pose of a person from an image or video has been of significant interest, it can be used in many applications such as gaming, human motion capture and analysis, and human-computer interaction. Different methods have been proposed depending on the input type and the number of capture devices [9][25]. Belagiannis et al. [16] estimated the 3d human pose of all person from images captured by synchronized cameras. Similar to the work in [16] that integrates 2D pose detections in each view, Joo et al. proposed the first system to infer the pose of more than five people engaged in social interactions with use of hundreds of VGA cameras, HD cameras and Kinects sensors [88]. The application of these methods might be limited due to the requirement of multi-camera system in a controlled environment. Instead of estimating the 3d human pose with multiple images as input, some recent works are proposed rely

on deep-net frameworks for 3d human pose estimation from single image. The work of [108] extended the structured-SVM model to deep neural networks for 3d human pose estimation from monocular image by learning a similarity score between feature embedding of the image and the pose. Zhou et al. [209] estimated the pose from monocular video using temporal and spatial information with Expectation-Maximization algorithm.

With the recent advances in low cost and compact depth sensors such as Microsoft Kinect cameras, several approaches have been proposed using depth sensors to estimate human pose without any markers. The approach for human pose estimation with one or more depth camera system can be classified into three categories: generative approaches based on local or global optimization, discriminative approaches based on learning from exemplars or exemplar pose retrieval and hybrid approaches [69].

Generative approaches: The earlier approach for real time depth-based motion tracking from single view was presented in [22]. Ganapathi et al. [57] proposed a method to track the pose of human by extending the traditional ICP with free space constraints. Ye and Yang [201] performed a GMM-based optimization over a rigged mesh model for human body tracking. A drawback of generative approaches is that its accuracy is limited by the fidelity of the model used. Some of these generative models, however, fail to preserve important surface details like the folds and winkles of the clothes and thereby cannot produce high quality rendering. Different from the existing work, our proposed pipeline can generate a human model with details of hairstyle and cloth wrinkles rather than a rough shape.

Discriminative approaches: To address the limitation of generative models, Shoton et al. in [156] trained a regression forest classifier to cluster the input single depth image into parts using a large training dataset of realistic human body shapes, and

estimated the joint locations using mean shift. Similarly, based on regression forests, Taylor et al. in [165] proposed an approach to predict dense correspondences between image pixels and the vertices of an articulated mesh model directly. Since the effort used to train classifiers can be quite significant for many learning-based methods, our proposed methods have the advantage that it does not require significant effort in acquiring training data to build customized classifiers.

Hybrid approaches: Combining the advantages from both generative and discriminative approaches, the first hybrid approach for human motion capture was presented in [56]. Baak et al. [13] and Ye et al. [200] both proposed a data-driven approach for pose estimation, which used a discriminative approach to initialize the pose estimation based on a set of pre-captured motion exemplars and refine the estimation via a generative process. Contrary to these approaches, our goal is to estimate the pose and shape of the actor with multiple stationary depth sensors and allow the actor to move freely in the capturing space.

2.4 Human Shape Reconstruction

There is a vast amount of applications with human shape reconstruction, such as computer games, animation, virtual reality and etc. It has been extensive studied both theoretically and algorithmically by researchers in computer vision and computer graphics. Over the last few decades, a number of approaches for modeling of human shape has been developed with depth images [205][121], 3D scanners [10][188] and multi-view images [55][75][110]. According to the number of camera used, existing approaches can be classified as single and multi-view.

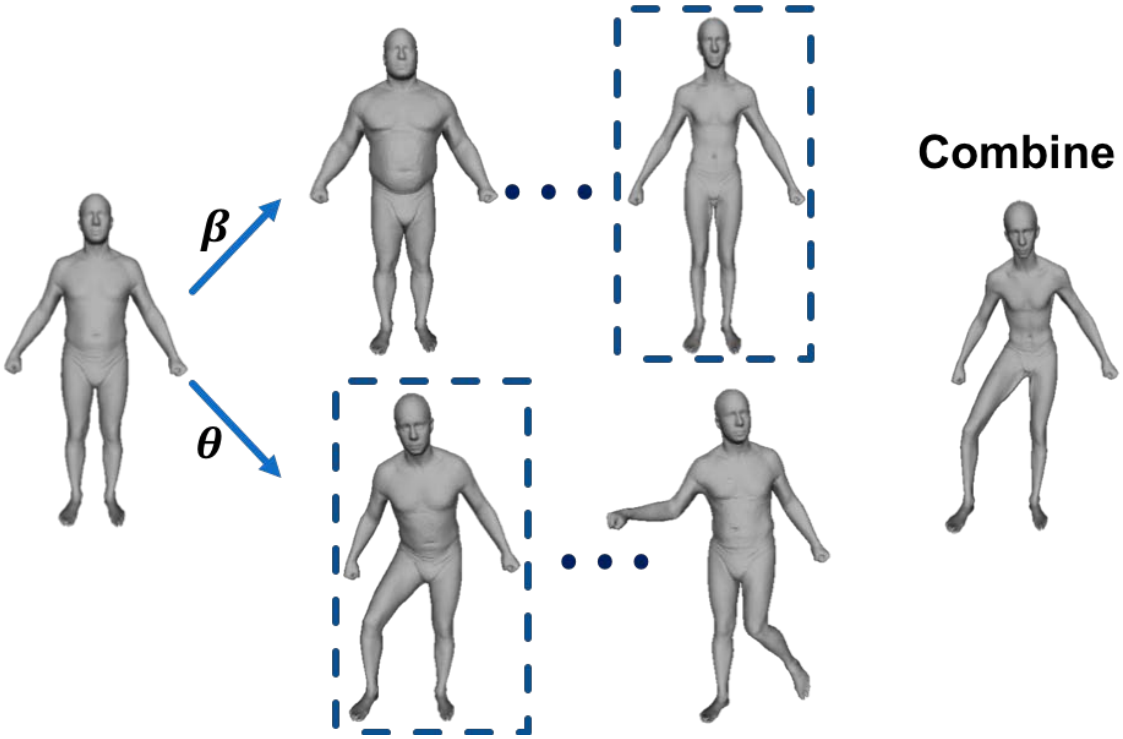

Figure 2.4 Illustration of SCAPE model, θ - parameter for pose, β - parameter for shape.

Single-view reconstruction: Some works rely on a good detection of silhouettes in image. Sigal et al. [158] used silhouette to compute the shape features and then estimate the shape of the person by a mixture of experts model. In addition to silhouette, Guan et al. [62] proposed to use edge and shading information to improve the performance of shape estimation with self-occlusion. Zhou et al. [208] introduced a body-aware image warping approach to recover the 3D body shape. In their approach, it is required for user to manually label the body parts and joints before the fitting, in order to estimate the body shape dependent parameters. Bogo et al. [23] presented the first method to simultaneously extract the 3D pose and body shape from a single image fully automatically, without any user interaction, and without requiring a background image for background extraction. The author in [194] proposed an approach to reconstruct the

human body shape from monocular video using a pre-captured shape template. Recently, several methods are proposed to capture both shape and pose of a parametric human body model with depth cameras, such as Microsoft Kinect sensor. Weiss et al. [186] proposed to estimate the shape of human body by fitting the parameters of a SCAPE model (see Figure 2.4) to the depth data with a single depth sensor. Zhang et al. in [205] used a single depth sensor to capture and register several scans of a user at multiple poses from different views and used these data to build a personalized parametric model. Newcombe et al. in [121] extended their previous work on Kinect-Fusion to capturing dynamic 3D shapes including partial views of moving people. BodyFusion [202] reconstructed the dynamic motion of a person from a single depth camera in real-time with use of skeleton prior. The author in [203] further extended the work in [202] to be able to handle the challenging scenario like fast motion and infer the inner body shape apart from clothing. A recent system for real-time generation of 3D human model using ICP-based alignment was proposed in [5]. However, this kind of approach may fail to track human pose from noisy depth data due to its sensitive to initial poses and prone to local minima.

Multi-view reconstruction: Marker-less performance capture from multi-view have been well studied. Aguiar et al. [4] achieved human performance capture by volumetric deformation from multi-view video. Their approach requires the user to specify the key vertices used to refine the surface for each pair of subsequent time instants. Liu et al. [112] introduced a combined image segmentation and tracking framework for capturing the motion of two characters from multi-view videos. They extended the work to handle motion capture for more than two persons and gave a comprehensive overview and thorough evaluation of the system in [110]. Rhodin et al.

[141] proposed a volumetric shape model and estimated the shape parameters by fitting a parametric shape model to image edges and silhouette. However, their approach only reconstructs a coarse shape model without cloth-level details, for instance, wrinkle or folds. Robertini et al. [145] proposed a model-based performance capture algorithm to capture the shape of human body with detailed in less controlled and outdoor environments from multi-cameras. In [89], Joo et al. proposed an interesting approach to capture the body movement with use of a unified deformation model in a multi-view camera system. Their approach can capture the total body motion including facial expressions, body motion, and hand gestures. Using multiple depth cameras for the reconstruction of human body have received significant interests in recent literatures. Helten et al. in [68] proposed a method for estimating a personalized human body model with two depth sensors, and then they used the estimated model to track the user's pose in real time from a stream of depth images. Tong et al. presented a full body scanning system by letting the user standing still on a turntable with multiple Kinect sensors [178]. Ye et al. [199] presented an algorithm to capture the performance of multi-person with three handheld Kinects. Their proposed method removes the constrains that the cameras have to be static and in controlled settings. Similar to the camera setting in [199], Wang et al. [183] proposed a method to reconstruct the complete textured models of moving subjects using a new pairwise registration algorithm to register partial scans with little overlap without the knowledge of initial correspondences from three or four handheld sensors. Fusion4D [42] used multiple depth cameras to capture human subject with challenging motions in real-time and demonstrated pretty impressive results on dynamic scenes modeling. A system named FlyCap was proposed in [195], this system aimed to

capture the human motion using multiple autonomous flying cameras equipped with RGB-D sensors which was solved by a non-rigid surface registration approach for tracking of moving object.

Understanding and manipulating the range of human body shape variation has applications ranging from body beautification to computer animation. Recently, many statistical methods have been proposed to model human body shape variations due to different identities, postures, and motions.

Statistical shape models are commonly used as a prior when the goal is to predict the body shape in motion. Early works in [6][154] used principle component analysis (PCA) to characterize a space of human body shapes without considering the shape changes with the pose. More recently, other approaches were introduced to model non-rigid deformations caused by posture changes based on triangle transformations [10][7][63]. These works resulted in a morphable human model that can be used to produce body models of different people with different poses. A simplified SCAPE model called S-SCAPE was proposed by Pishchulin et al. in [135] to model the variations caused by different identity and postures as linear factors. This kind of model can be used to represent the shape of human body and to generate the corresponding mesh models for posture and shape fitting purposes. The limitation of global model is that a large available dataset is required to train the parameters for shape and posture variations. To solve this problem, Zuffi and Black [212] proposed a part-based statistical model, in which the body is represented by a graphical model and can be deformed to represent the variation of different postures and shapes, while ensuring the joint connected parts to be close. Compared to SCAPE model, this part-based model is more efficient and flexible.

Recent advances in deep neural networks provide an alternative approach to capture the human body shape from the data. Dibra et al. [40] presented an accurate and fully automatic method to estimate the body shape of a person from silhouettes or shaded images by using convolutional neural networks. A limitation of this method is that it assumes a frontal view input and cannot handle poses with a significant difference from the neutral pose or contain self-occlusions. In [163], the author proposed a novel encoder-decoder architecture to estimate the pose and shape of a person. The proposed framework makes it possible to indirectly learn the body shape and pose parameters from real images and corresponding silhouette without knowing the ground truth on corresponding 3D pose and shape parameters. Kanazawa et al. [91] proposed an end-to-end framework to reconstruct the human body. The proposed architecture can infer the 3d pose and shape of a person from image in-the-wild with complex background. Different from previous approaches to estimate the human shape with arbitrary posture using a parametric model, Varol et al. [179] proposed the BodyNet, a fully automatic end-to-end framework on the basis of neural network to predict the human body shape from a single image in natural scene, which contains four subnetworks and use a volumetric representation for body shape estimation. The network is fully differentiable and provide segmentation on body part.

Many applications, like reshaping human bodies in still images [208], reshaping in video [84], and estimating body shape under clothes [196], all make use of such types of morphable human models. In this dissertation, we use the SCAPE model from [11] and a GMM based fitting approach for human body reshaping. Different from our previous work in [193] that can only change the shape of the body along the direction of the

skeleton in 2D space, the current work uses a parametric model for mesh deformation transfer in 3D space. Unlike our previous work in [192] that focused only on pose, the proposed approach can simultaneously estimate both the human pose and shape for body reshaping.

2.5 Body Reshaping

Realistic human performance capture is an active research area in computer vision and computer graphics. It enables many applications from character animation in films and computer games, to behavior analysis and monitoring in medical rehabilitation. In recent years, great progress has been made in the field of human performance capture. Many existing works specifically designed for pose tracking without the estimation of human body shape or pre-obtain the shape of an actor and track it over time. Our goal, in this dissertation, is to reshape the body shape of an actor by simultaneously estimating his/her pose and shape.

Many existing commercial image-editing tools can only provide basic functionality, and it may takes the user hours of manual work to change the appearance of the body in an image. To provide an easy way to do such manipulation, [208] proposed a semi-automatically approach to modify the shape of the person in image. They fit the 3d model to image and allow the synthesis of image by deforming the model following a body-aware image warping approach to transfer the effect of reshaping from the model to image. However, a good 3d skeleton and segmentation of body is required from the user. A system for quickly and easily manipulating the body shape of a human actor in video footage is demonstrated in [84]. They change and modify the shape of the actor by transforming the deformation of a body model fitted to the shape and pose of the actor.

The manipulated result on human body reshaping in video footage is obtained by performing an imaged-based warping. Different from manipulating the shape of human body in image or video, more recent work [51] develop a system to generate and reshape avatar with a 3D body scan as input. However, user annotation or a good initialization between the input and the morphable model is required by the aforementioned works, which may limit the wide usage of the approach. Chen et al. [32] presented a system that is able to produce realistic and plausible result for editing the clothed 3D body by using a 3D body-aware warping scheme. It is achieved by fitting a revised SCAPE model to the actor and control the shape of the actor by a few semantically meaningful parameters. Different from theirs with a good initial value for pose and shape parameter during fitting, we combine the GMM with SCAPE to get correspondence between the model and the actor and thus can handle more complex pose that are different from the neural pose.

Despite the great success of previous work, there still remains lots of difficulties to produce global consistent and natural looking manipulation result. In this dissertation, we explore a novel system to reshape the human body using noisy depth data from multiple stationary depth sensors. Accurate and reliable estimation of pose and shape plays a key role in our system, which is a challenging task because of the complexity of human motion and complicated occlusions from self and environment. Using a well-calibrated network of RGB-D sensors, our approach can accurately estimate the non-frontal poses and poses with significant self-occlusions. Different from previous approaches that require manual annotations or segmentations, we devise a fully automated approach for surface representation of an actor move freely in the capturing space with the help of a Gaussian mixture model (GMM) based framework. By taking all

data points into consideration, it enables the fitting without a prior knowledge of correspondence between the model and the observed data practical and more robust to noisy and outliers. Once the model is fitted to the observed data, a bone-based approach is applied to find the location of skeletal bones.

Another advantage of our system is that it provides an easy and quick way to make the observed actor getting taller, shorter, fatter or thinner by applying deformation transfer across consistent captured frames. The physical attributes like height, weight or leg length of the observed actor can be manipulated by changing the parameters of the morphable model. Such reshaping enables new form of visual privacy protection that can obfuscate soft biometrics of a person, like gait, height or weight, while maintaining the cognitive behavioral patterns useful for many health-related observation tasks. A model-based cloth try-on system with privacy protection using mobile Augmented Reality is presented in [151]. They use secret sharing and secure computation technique to help the selection of a 3d model of user to ensure the privacy protection. Different from theirs, our approach provides a new way to build the 3d model of user and hide the identity by the idea of avatar animation. Liu et al. [111] proposed to use linear blend skinning to achieve the mesh deformation for image-based rendering. They can only change the pose of person but the shape of person is still preserved, which cannot be used to preserve the data utility and protect the privacy for the application of behavior observation. Contrary to previous work for privacy protection by blurring the body or replace it with an avatar [128], reshaping on real image can generate a more realistic image that preserve useful information like the posture while hide the identity of the person which is crucial for psychological and behavior analysis. Experimental results demonstrate the effectiveness

of our system to automatically estimate the pose and shape of human as well as the reshaping of the estimated human body.

Chapter 3 Preliminary Works: General Pipeline for The Application of Face and Human Shape Manipulation

In this chapter, a high-level overview of the main components and steps for the application of face and human shape manipulation is introduced and discussed. Even though the pipeline of these methods highly depend on their applications and goals, therefore, may varying significantly, a number of components tend to be common: the input geometric data capture and preprocessing, surface reconstruction, and rendering. The followings provide a detailed description for each of the most common components used to achieve the goal of face and human shape manipulation.

3.1 Geometric Data Collection and Processing

Many applications benefit from or even require geometric information acquired from the scenes in real world, such as virtual reality, human computer interaction, and health care. Digital cameras are commonly used to obtain the 3D information of an object captured from the physical environment through image-based 3D reconstruction techniques, structure from motions, for example. In recent years, the availability of low-cost and contact-free RGB-D cameras offer new possibilities for the capturing of more complexed structures. This kind of sensors acquire range images in real-time, i.e. with 30 frames per second or more. Among them, the Time-of-Flight (ToF) and Structure-Light sensor have experienced a remarkable success in developer and research communities. Such range imaging-based devices make use of optical properties and use their own light source for the active illumination of a scene. As is shown in Figure 3.1 (a), the technology of Kinect v1 released in 2010 was based on the structured light approach. It

(a) (b)

Figure 3.1 Examples of Kinect Sensor v1 (a) and Kinect Sensor v2 (b).

consists of two cameras, one RGB and one IR, and one laser-based IR projector [116]. The depth information for each pixel is calculated by triangulating the known pattern through the projection of structured light emitted by the projector. Different from Kinect v1 sensor, Kinect v2 sensor (see Figure 3.1 (b)) employs a time-of-flight (ToF) camera for depth sensing. These technologies offer a cheap and easy access to measure the distance to the nearest objects through every single pixel of the acquired depth maps. Because of their geometric imaging capabilities, a lot of works have been explored using RGB-D cameras in the last decade. Simultaneous Localization and Mapping (SLAM), human pose recognition, face tracking, hand articulations and others have been explored using RGB-D cameras by researchers from industry and academia [167][187][201][156][202].

Depending on the type of RGB-D sensors, several pre-processing operations may be required, such as noise removal, camera calibration and alignment. Take Kinect sensor as an example and two sample depth images are shown in Figure 3.2. Darker grayscale represents smaller depth measurements. Both images suffers excessive noises like inaccurate depth pixel, values or holes, which could influence the performance and may result in inaccurate estimation for pose detection, image localization or 3D reconstruction.

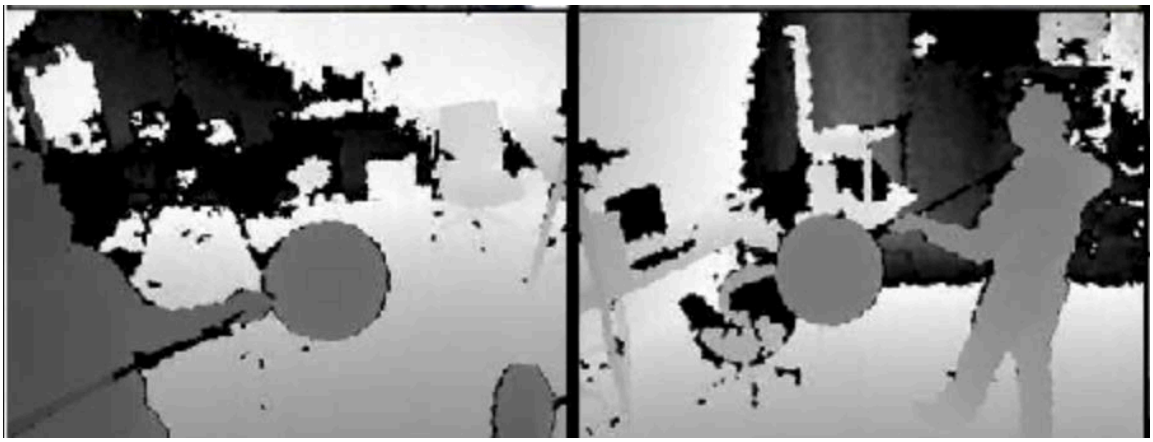

Figure 3.2 Example of imperfect depth data captured by Kinect sensor with noises and black holes [155].

The removal of noise is a challenging task because it is not easy to distinguish noise from the true surface. An optimal noise removal algorithm is often expected to remove the undesired outliers, while preserving the detailed geometrical information. Traditional denoising approaches are effective in removing sporadic noise and filling in small missing values. For example, Fleishman et al. [52] extended the concept of bilateral filtering, first proposed for image smoothing [170], to remove the noises while preserve the edge information. A modification of bilateral filtering named divisive normalized bilateral filtering was proposed by Fu et al. [54] to achieve temporal and spatial filtering. Holes on depth data can be caused by self-occlusion or specular reflection of the underlying surface and in turn affect the performance of applications such as surface reconstruction, action recognition, object segmentation etc. Some of the holes on depth data are small and isolated, and others are large and connected. Small to medium size holes can be filled by applying an interpolation technique such as linear interpolation, bi-linear interpolation or polynomial interpolation.

(a)

(b)

Figure 3.3 Calibration result using the method from [155], (a) uncalibrated scene; (b) calibrated scene.

Large holes can be filled using depth image inpainting approaches. Doria et al. [41] introduced a method to fill holes in the LiDAR datasets by combining the concept from patch-based image inpainting and the gradient field image editing. The author in [114] clustered RGB-D image patches into groups and filled in missing depth data by employing the low-rank matrix with the help of the corresponded color images.

After obtaining cleaned depth data, reliable and accurate calibration or registration may be required to align the subsequent captured depth data from different cameras to produce high quality-spatial data and 3D models. The well-known Kinect Fusion technique used a single moving Kinect sensor and aligned all frames to build static 3D model of the environment [122]. The alignment in Kinect Fusion is achieved with the help of Iterative Closest Point (ICP) algorithm, which provides an estimation of

the extrinsic parameters of the sensor. In the case of using multiple Kinect sensors for dynamic 3D scene reconstruction, estimating camera extrinsic parameters often require a calibration object of known geometry. Traditional calibration methods with checkerboard or laser pointers do not work well for depth camera as the specific color or texture pattern are not observable for depth sensors. In addition, because of the wide baseline, the overlapping views between adjacent sensors are small and using ICP algorithm to estimate the extrinsic parameters of sensor cannot product a robust estimate. A possible way is to use a separate calibration object to establish correspondences for registration parameters estimation. One such example is to use a spherical calibration object [155]. Such a calibration technique can be used for scene reconstruction with multiple wide-baseline RGB-D cameras without much user interaction, an example of multiple sensor registration is shown in Figure 3.3. ICP algorithm can be further used to refine the result of registration by optimizing the extrinsic parameters.

3.2 Surface Reconstruction from Point Cloud

Point Clouds are the measured scene points in 3D space, and they can be calculated from the depth data obtained in the previous stage. A typical way to convert the depth map produced by the RGB-D sensor to point cloud is to apply the perspective projection with the information of calibration about the sensor. It can be achieved by using the mapping function between the depth data and the camera space provided by the Kinect SDK, a software development kit, to convert the depth data to point cloud [98].

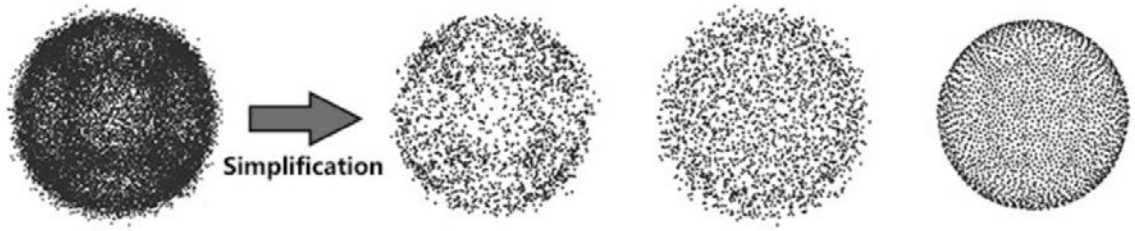

(a) (b) (c) (d)

Figure 3.4 Comparison of three methods for point clouds simplification using CGAL [36]: (a) Original input; (b) Random simplification result; (c) Grid simplification result; (d) WLOP simplification result.

The direct use of these point clouds is not suitable for most applications because of the massive amount of redundant data they contain. Many works have been conducted to simplify the dense point clouds by removing the redundant points while keeping the feature points to represent the 3D geometry of the scene or object [77][67][78][113]. These works can be roughly divided into two categories: mesh-based and point cloud-based. Mesh-based approaches construct triangular mesh from the point cloud in the first step and then removing the redundant triangles. Because of the large amount of the data to be processed, the time for computation is high. In contrast, the point-based methods for simplification rely on the point information to simplify the point cloud without reconstruction of mesh model and have lower computational complexity than mesh-based methods. As such, they are more widely used and supported by open-source computational geometry library such as Computational Geometry Algorithms Library (CGAL) [36]. There are a number of different point-based simplification methods. Figure 3.4 shows the comparison result of three methods for point cloud simplification. The first one is to let the user specify the desired size of the point cloud and remove the points from the input point set randomly, see Figure 3.4 (a). The grid-based approach

shown in Figure 3.4 (b) clusters all points into grid cells and replace all points inside a cell with an arbitrarily chosen representative point. The speed for this algorithm is slower compared to the first approach. The Weighted Locally Optimal Projection (WLOP) algorithm proposed by Huang et al. in [77] simplifies the point cloud and also regularizes the resampled points to be evenly distributed adhere to the original shape, as is shown in Figure 3.4 (c), upon which is more useful and proper for further mesh reconstruction.

With the point clouds in hand, the process of converting such a discrete point set into a continuous surface representation is defined as surface reconstruction. The reconstructed surface mesh is good representation for the topology and geometric shapes. During the last few decades, many algorithms for surface reconstruction have been proposed depending on the output requirements, the properties of input point cloud data, the preference of user, etc. Depending on how the mesh is constructed, these algorithms can be roughly divided into three groups: implicit surface-based approaches, region growing approaches, and Delaunay-based approaches [97]. Implicit surface-based methods use weighted sum of basis functions such as the radial basis function to fit the point cloud data. Region growing approach starts with a seed triangle and then continually grows or expands from this seed triangle until all the points have been considered. Different from the implicit surface-based approach, the region growing approach takes all the points from the point cloud as the vertices of the reconstructed triangle mesh. The details of the original object, therefore, will be preserved and tend to produce more accurate reconstructed surface mesh. The Delaunay-based approach aims to turn a set of points to a set of triangles for the desired triangle mesh surface reconstruction. As is shown in Figure 3.5, in Delaunay triangulation, it is defined that no

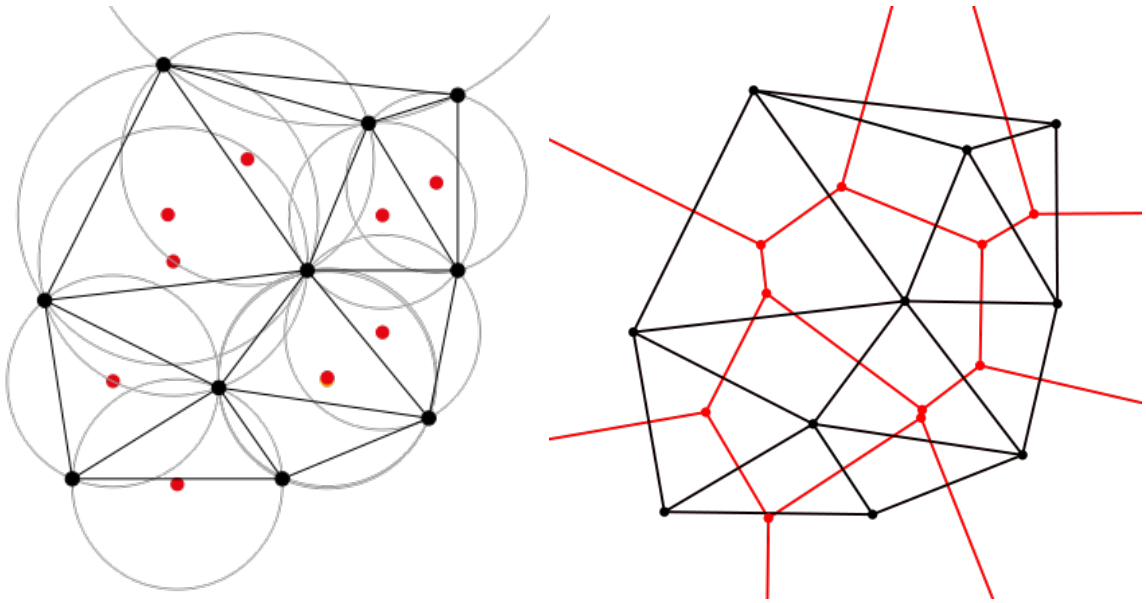

(a) (b)

Figure 3.5 Duality of Delaunay triangulation [37] (a) Delaunay triangulation with all the circumcircles and their centers (red); (b) Voronoi diagram (red) overlaid to Delaunay triangulation.

points other than the three points that define the aforementioned triangle can be contained by each circumcircle. The dual of Delaunay triangulation is called Voronoi diagram and is generated by connecting the centers of the circumcircles as displayed in Figure 3.5 (a). Both are important geometric data structures in computational geometry, which provide a possible way to approximate the neighbor points in the point cloud data.

3.3 Motion Capture for Face and Body Shapes

Motion capture is the process to record the motion information of objects or people. Due to the emergence of new types of sensors such as Kinect and the improvement of computational performance, motion capture has found increasing usage in many fields, like character animation for games and entertainment, motion analysis for medical, sports and virtual reality.

In general, motion capture techniques can be classified into two categories: marker-based systems require the attachment of different kinds of sensors or markers on the subject being captured; markerless systems, on the other hand, capture motion based on statistical inferences on captured images [22][110][112][195]. For consumer markets and other domains like health care where it is desirable to have the least amount of restriction, markerless systems provide a much more promising solution for motion capture. In this work, we concentrate on markerless motion capture using single or multiple depth sensors.

A surface mesh template with embedded skeleton is a widely used data structure to model the tracked subject in markerless motion capture system [135][196][212]. This kind of mesh template can be a generic model, SCAPE, for example, or a laser-scanned mesh model with detailed surface geometry. The skeleton model can be represented by a tree structure, as is shown in Figure 3.6. The red dots in this figure represent the joints.

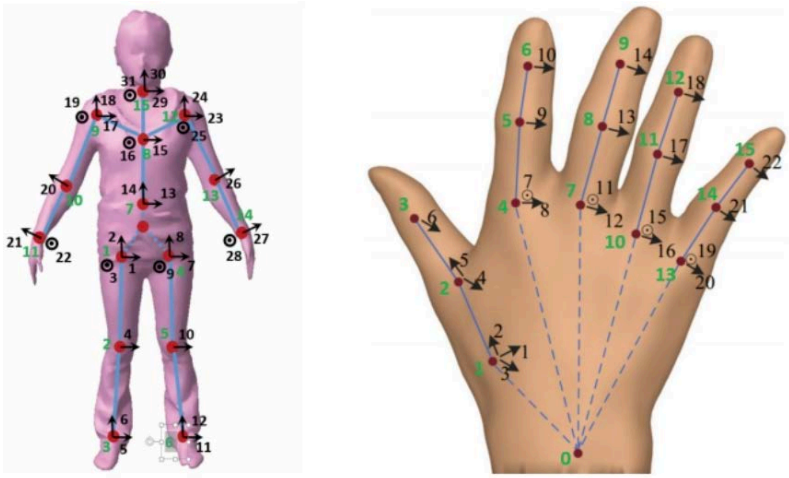

(a) (b)

Figure 3.6 Template and embedded skeleton for human body and the hand [116]. (a) Human body with skeleton; (b) Hand with skeleton.

The movement of each joint is controlled by different rigid body motion as indicated by

the black arrows. A rigid motion of a joint can be represented in several ways, like Euler angles, quaternions, twist, etc. The motion of a subject can be obtained by optimizing the energy function which contains the data term and the regularization term.

Compared to body motion capture, facial motion capture is more challenging because of the requirement for higher resolution in detection and tracking of subtle expressions movement. The captured and processed facial movements can then be used for facial animation in games or avatars. In recent years, blendshape has been used successfully to create 3D dynamic models for the application of facial animation and retargeting [106]. Such model contains a neutral face and a set of face with different expressions, ranging from stereotypical (like happy and sad) to extremely subtle (like narrow eyes). A new facial model can be created by combining different blendshapes with different weights.

Chapter 4 Facial Image Manipulation with RGB Images

In this chapter, two different ways to manipulate the expression of human face in RGB images are presented. I first discuss image a retouching technique to manipulate the face image while preserving the expression [193]. Then, a system to transfer expression from one person to another is introduced.

4.1 Facial Image Manipulation with Recolor and Component Blending

Face image editing typically involves a set of image editing tools, such as recoloring, image composition, tone adjustment and etc. Many of them have already been widely studied and applied in face image editing. Bitouk et al. in [20] proposed a face swapping system based on a large collection of face images. Another face swapping method under large pose variation was proposed by Lin et al. [109]. Our work combines recoloring and composition of facial component to produce a new face image while preserving the general configuration of different facial features so as to preserve the expression.

4.1.1 Overview of our system

The procedure of face image editing in our system is illustrated in Figure 4.1. Given an input source image and a selected target image that best fits the facial expression of the source image from the dataset, we first segment the skin part from the rest of the image. Then, we use the color transfer method proposed by Reinhard et al [139] to recolor the source image. To change the face component of the source image, like eyes, nose or mouth, we first detect the facial component to be changed and then blend it with

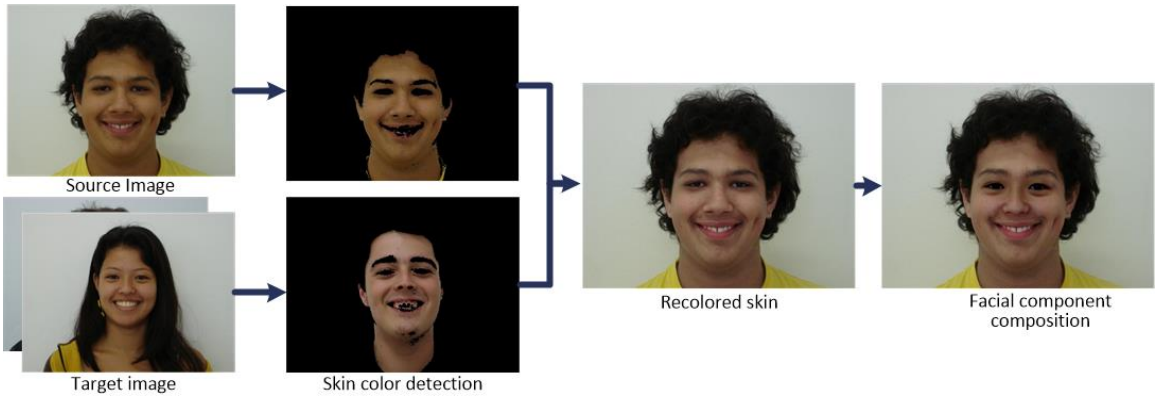

Figure 4.1 Face image editing procedure

the corresponded parts from the target image using Poisson blending method [132]. Details of our implementation and the results are presented in the following section.

4.1.2 Skin recoloring and facial component blending

Given an input source image, we first search for the best fitted image from the dataset that has a similar expression and head pose with the source image. Then we segment the skin region from the rest of the image for source and target image. In this step, we first manually select a patch to identify the proper skin color and then apply the skin color detection algorithm. Our system uses a combination of HSV and YCrCb color-

(a) (b) (c)

Figure 4.2 Skin Color Transfer with input source image in (a), target image in (b) and the skin-recolored source image in (c).

spaces to model the skin color. Then, we use a simple thresholding scheme to classify the skin pixels. To transfer the skin color of the target image to that of the source image, we take advantage of the color transfer algorithm described in [139]. At the first step, segmented source and target images are converted from RGB space to $l\alpha\beta$ space. Then, we compute the mean $\bar{l}_s, \bar{\alpha}_s, \bar{\beta}_s$ and variance $\hat{l}_s, \hat{\alpha}_s, \hat{\beta}_s$ of the source and target images for each color channel. The final mapped distributions of the data points in $l\alpha\beta$ space are obtained by Equation (4.1), (4.2) and (4.3):

$$l_{mapped} = (l_s - \bar{l}_s)\frac{\hat{l}_t}{\hat{l}_s} + \bar{l}_t \tag{4.1}$$

$$\alpha_{mapped} = (\alpha_s - \bar{\alpha}_s)\frac{\hat{\alpha}_t}{\hat{\alpha}_s} + \bar{\alpha}_t \tag{4.2}$$

$$\beta_{mapped} = (\beta_s - \bar{\beta}_s)\frac{\hat{\beta}_t}{\hat{\beta}_s} + \bar{\beta}_t \tag{4.3}$$

The last step for the color transfer procedure is to convert the result back to RGB space. Figure 4.2 shows the result for color transfer.

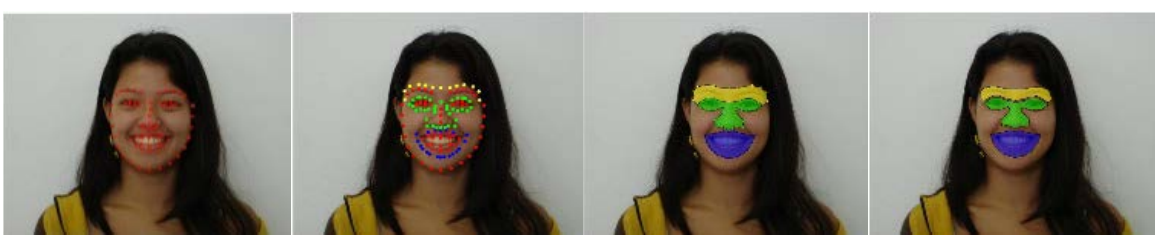

(a) (b) (c) (d)

Figure 4.3 Generation of the ROIs. (a) Landmark detection. (b) Landmark refinement by linear interpolation. (c) Initial ROIs. (Mouth (blue), eyebrows (yellow), eyes and nose (green)). (d) Final generated ROIs by erosion and dilation.

(a) (b) (c)

Figure 4.4 Poisson blending result. (a) Source image. (b) Mask obtained from the ROIs generation. (c) Blended image.

The next part of face image editing in our system is to replace the specified facial component of the source image with the target image. We first use the facial feature detection algorithm proposed in [11] to detect the eyes, nose or mouth in source and target image. Inspired by the work in [119], we then segment the face image into different regions of interest (ROI) by linear interpolation, image erosion and dilation on the basis of the detected feature point. The process to generate the ROIs is completely automated, as illustrated in Figure 4.3. After cropping the corresponded ROIs from source and target images, we apply the Poisson blending method [132] to blend the cropped part from the target image with the source image seamlessly. The result of image blending is shown in Figure 4.4.

4.1.3 Experimental results

The objective of the experiment in this part is to show that the resulting image have the same general expression as the original one. In addition, the identity of the person should not be revealed from the resulting image. To demonstrate the performance of our method, we use FEI Face Database [79], which contains 2800 images of 200 different subjects, and Caltech Faces dataset [184] which contains 450 images of 27

(a) (b) (c)

Figure 4.5 Fame image editing result. (a) Source image. (b) Skin recolored result. (c) Facial component blending result.

different subjects. The choice of these datasets is led by the ease to find similar expressions from different individuals. Figure 4.5 shows results obtained from our face image editing method. We can see the result looks natural and the expression of the person is preserved while some of the key facial biometric features including eyes, nose, and mouths are replaced. One limitation of our method is that the source and target image should have similar head pose and the change of head pose need to be small in order to

produce realistic rendering. One possible way to fix this problem is to align the face image using 3D face model as discussed in the next section.

4.2 Fully Automatic Photorealistic Facial Expression and Eye Gaze Correction with a Single Image

Nonverbal information like facial expression and eye gaze plays a crucial role in social interaction. Generating a photorealistic facial expression from a single image while preserving the identity of the actor has many applications in film making, gaming and telepresence. In recent years, several approaches have been proposed to animate the expression of a real actor on a virtual avatar in real time [150][29]. Instead of transferring the expression to a virtual avatar, Thies et al. presented an algorithm to transfer the captured expressions from the source video to another real actor [177]. While these approaches have demonstrated impressive results on facial animation to real actor or avatar, synthesizing a wide range of facial expressions accurately and realistically on arbitrary real actors remains a challenging problem due to significant difference between source and target actors, self-occlusion, uncontrolled illuminations, etc.

Recent advancements in low cost and compact depth sensors make it easier to acquire depth information for facial performance editing. In [168], Thies et al. proposed a method for face reenactment based on RGB-D data. Hsieh et al. in [74] developed a system to capture and retargeting facial expressions using a commercialized depth sensor. However, compared to 2D RGB cameras, depth devices are still not widely available and the resolution of the captured images is low. Cao and others proposed a regression-based algorithm on webcam, with robustness and accuracy comparable to RGB-D based methods [29]. Similarly, the expression transfer method proposed in [177] can achieve

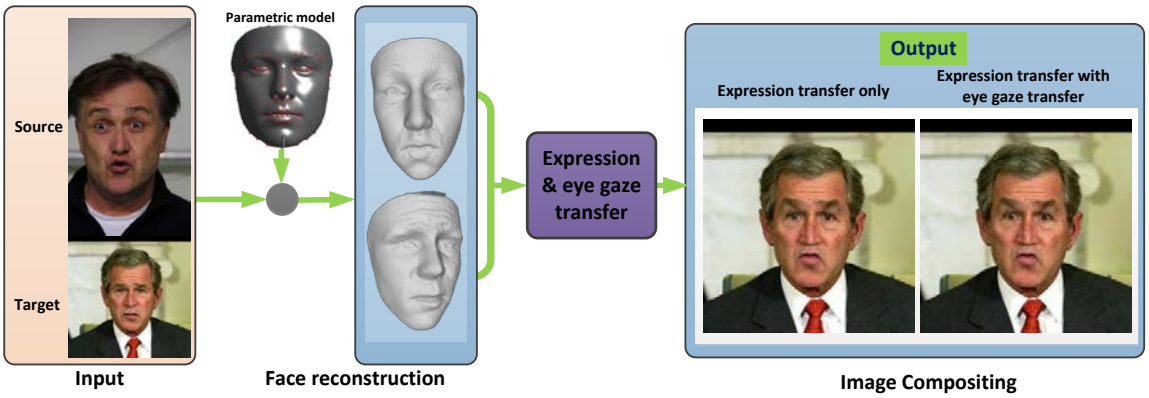

Figure 4.6 The Overview of our proposed face expression transfer pipeline

real-time transfer of facial expressions captured from a source actor to a target actor with different identity. The main drawback of the previous systems for facial performance capture is that they lack the capability to get information of eye gaze. Often ignored in most facial expression transfer systems, eye gaze has been shown to significantly contribute to our perception of social attention [100], and is of significant value in medical evaluations of conditions like autism spectrum disorder. In [181], Wang et al. presented the first approach to capture the eye gaze, head pose and expression simultaneously using a single RGB camera.

In this section, we propose a facial reenactment system that takes a source and a target image with arbitrary facial expressions, and generates a new image of the target actor with both facial expression and eye gaze similar to those of the source actor while preserving all the background information. To achieve photorealistic transfer, we propose a novel coarse-to-fine scheme for reconstructing the 3D geometry of the face based on details from a single image. The facial expression information is then transferred in a fully automatic manner from source image to target image using mesh deformation.

4.2.1 Overview of the system

To manipulate the facial expression and eye gaze according to the source image with minimal artifacts, I propose a system consisting of three main parts: 3D face reconstruction, expression and eye gaze transfer, as well as image compositing (see Figure 4.6).

3D face reconstruction: We start the whole pipeline by building the 3D models for a single source and target images respectively. At the same time, we capture the person-specific features like winkles using shading information from the image. This is essential to making the result photorealistic.

Expression and eye gaze transfer: The second part in our system is to transfer the expression and eye gaze from the source to the target. We manipulate the expression of target input image using mesh deformation with a reference to the source input image. In addition to expression, the eye gaze of the source actor is also transferred to the target actor by using geometry warping approach.

Image compositing: The last component in our system blends the re-rendered target image with its original background by using modified Poisson image editing [1], where they take the pixels on source and target boundary into consideration, in addition, alpha blending is added to the editing process.

4.2.2 Coarse and fine face reconstruction

In this section, we first discuss the use of a parametric face model for face representation. Then, we introduce an approach to capture wrinkles and high frequency details on image to generate a mesh with fine details.

4.2.2.1 Coarse model fitting

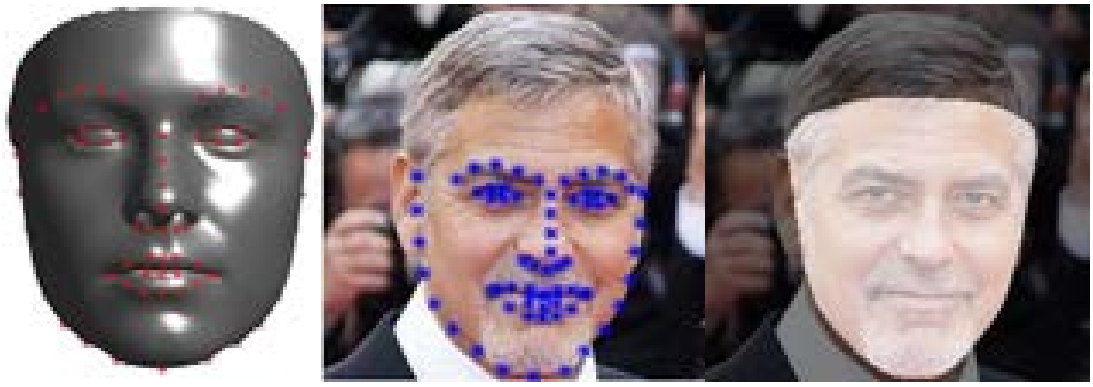

(a) (b) (c)

Figure 4.7 Coarse face reconstruction: (a) labeled 3D face landmarks; (b) 2D landmarks detected on the input image; (c) reconstructed model projected to the input image

We encode the face shapes by making use of a parametric face model created based on publicly available 3D facial expression datasets. We control the expression and shape of the 3D face on a lower-dimensional subspace with principle component analysis (PCA):

$$S = \bar{S} + E_{id}\alpha_{id} + E_{\exp}\alpha_{\exp} \tag{4.4}$$

where S is the desired 3D shape, $\bar{S}$ denote the shape of the average face among the scans, E_{id} is the principle axis extracted from a collection of 3D face meshes with a neutral expression. $E_{\exp}$ is the principle axis trained on the offset between expression mesh and neutral mesh of each individual contained in the scans. α_{id} and $\alpha_{\exp}$ are the representations of shape and expression weight for modeling. Basel Face Model [131] and FaceWarehouse [30] are used for constructing E_{id} and $E_{\exp}$ respectively.

Following the scheme of [210], we fit the parametric model to the source input image and target input image. With the assumption of weak perspective projection:

$$S_{2d} = f \begin{bmatrix} 1 & 0 & 0 \\ 0 & 1 & 0 \end{bmatrix} RS + T \tag{4.5}$$

where S_{2d} represents the 2D positions of vertices in S projecting from the world coordinate to image plane, f is scalar factor, R and T are rotation and translation matrices respectively. After we find the 2D landmark alignment result S_{land_2d} [140], all unknowns in Equation (4.4) and Equation (4.5) can be solved by minimizing the projection error of labeled 3D landmarks on the parametric model S_{2d} and S_{land_2d}:

$$E = \min_{f,R,T,\alpha_{id},\alpha_{\exp}} \left\| S_{land\_2d} - S_{2d} \right\|^2 \tag{4.6}$$

An example of our coarse face reconstruction is shown in Figure 4.7. It shows the labeled 3D landmarks on parametric model, the 2D alignment on image, and the rendered coarse model overlay to the image respectively.

4.2.2.2 Geometry refinement

A good estimate of the overall shape of an individual in the image can be obtained by fitting the parametric model from the previous stage but person-specific facial features like wrinkles are not adequately captured. To refine the geometric details in this stage, we deform the obtained mesh to fit its shading with the input image. Inspired by the work in [161], we assume Lambertian reflectance and approximate the image intensities with the

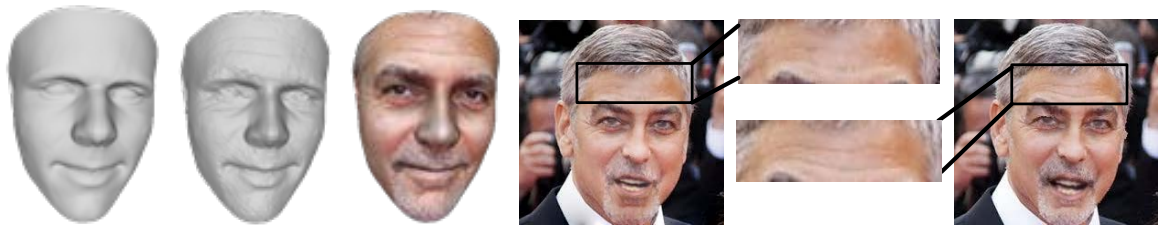

(a) (b) (c) (d)

Figure 4.8 Geometry refinement: (a) coarse shape; (b) shape after refinement; (c) reconstructed fine shape with texture; (d) Facial expression transfer with coarse (left) and refined (right)

surface normal using the first-order spherical harmonics. The objective function for shading based geometry refinement is as follows:

$$E = \sum_{v} \left\| I(P(v)) - l^T h_v(z(v)) \right\|^2 + \beta_1 E_{reg} + \beta_2 E_{LP} \tag{4.7}$$

where $I(P(v))$ is the image intensity of vertex v projected to the image plane with the projection matrix P, l is a vector of 4×1 representing the spherical harmonics coefficients, and $z(v)$ is the z-coordinate of vertex v. β_1 and β_2 are weights for the regularization term E_{reg} that constrains the final mesh to be close to the original shape, and the Laplacian smoothing term E_{LP}. h_v is 4D spherical harmonics approximation to surface reflectance defined as $h_v = (1, \frac{(w_r - w)\times(w_c - w)}{\|(w_r - w)\times(w_c - w)\|})$, where $w = (v_x, v_y, v_z)$ and w_r, w_c are neighboring vertices of w along horizontal and vertical direction on the surface. Equation (4.7) can be solved by updating and fixing l and v iteratively with linear least squares optimization. Figure 4.8 shows the result of geometry refinement. Figure 4.8 (a) shows the coarse shape obtained from the previous stage, Figure 4.8 (b) shows the shape with geometric refinement, Figure 4.8 (c) shows the refined shape with texture

information and Figure 4.8 (d) shows the effectiveness of geometry refinement for facial expression transfer.

4.2.3 Facial expression transfer and eye gaze correction

After obtaining the 3D models for both the source and the target images, we apply the mesh deformation to transfer the expression from the source to target. Our approach is similar to that of [160]. However, instead of finding correspondences based on the user selected markers, we register the models with coarse shape parameters to the refined shape obtained by geometry refinement. In this way, the correspondences can be easily treated as all of the triangles in the mesh. Thus, the efficiency for facial expression transfer can be improved significantly without finding correspondence points. The difference around the mouth of the source and target actors are reduced by piecewise affine warping in the image domain.

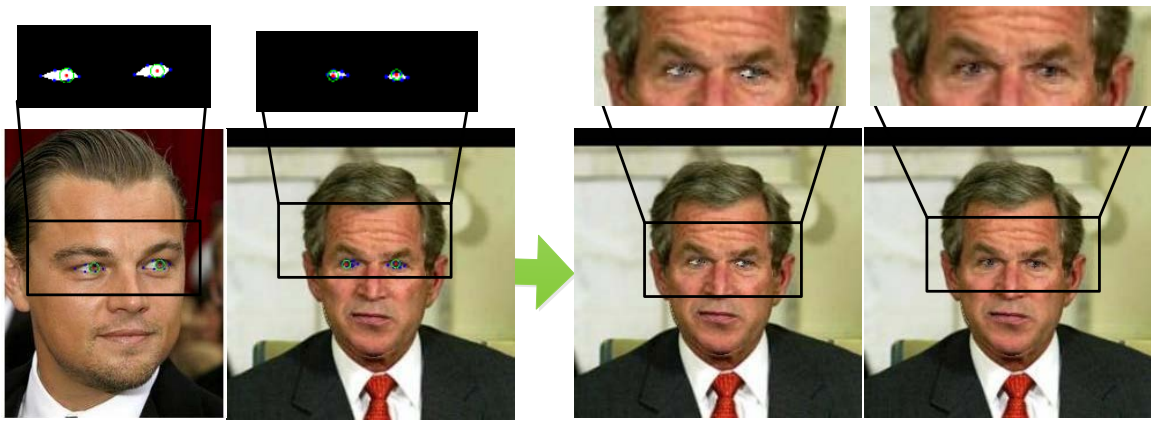

(a) (b) (c)

Figure 4.9 Eye gaze transfer: (a) original pairs of image with detected eye mask; (b) direct transfer without refinement; (c) final synthesized image

In addition to expression transfer, we take the eye gaze difference into consideration to make the final re-rendered image more realistic. As is shown in Figure 4.9, we first extract the eye mask from source and target image by morphological operations. The gaze is estimated by sphere fitting, colored with the green circle and red point in Figure 4.9 (a). Then, we use the correspondence points extracted from source and target images around the eye area to compute the transformation matrix to warp the eye mask. The relative location for eye gaze is calculated using the center of eye gaze and the eye corner. The synthesized eye gaze is finally estimated by the aspect ratio from the relative location. The final manipulated image is generated by blending the eye and the mouth area with the re-rendered image together. More results are shown in the experimental section.

4.2.4 Experimental results

We evaluate the performance of our system on face reconstruction from single image using both qualitative analysis and quantitative evaluation.

(a) (b) (c) (d) (e)

Figure 4.10 3D reconstruction evaluation: (a) Input RGB image; (b) Ground truth; (c) reconstructed model by our method; (d) error map between our model and ground truth; (e) error map between model obtained by method of [210] and ground truth.

We first present the experimental result for face reconstruction. We evaluate the accuracy of our system for face reconstruction on a public available dataset provided by MPI Informatik [18]. The dataset contains three sequences captured indoor with 200k vertices and one sequence captured outdoor with 50k vertices. The scanned models from this dataset serve as the ground truth. To measure the difference between the ground truth and our reconstructed model, we first align them by ICP algorithm [76] and search the nearest point from the ground truth model along the normal direction of each vertex in our reconstructed model. The Euclidean distance is then calculated for each pair of the points. One example from the dataset is shown in Figure 4.10. The mean error distance between our reconstructed model and the ground truth is 2.48mm, comparing with the method from [210] which is 2.71mm. We also compare our method for face reconstruction with the method from [210] on more unconstrained images of different illumination and poses. Figure 4.11 presents the result of comparison, from left to right, showing the reconstructed model and the model with texture.

To evaluate the performance of our method for facial expression and eye gaze transfer, we choose images with different expression or head pose from the LFW dataset [100]. The result of our method for transferring the expression and eye gaze between two different identities with single image is shown in Figure 4.12. The leftmost row in each of the three pairs is the input of source and target image, the transfer result of expression is shown in middle column, the final result with eye gaze transfer is displayed in the rightmost column. It can be seen that our system is able to generate realistic result for various facial expression transfer with eye gaze correction.

Figure 4.11 Face reconstruction on unconstrained image: Input RGB image; reconstruction with our method; reconstruction with method from [210]; reconstruction using our method with texture.

Figure 4.12 Result of our proposed system: (First row) source input and target input images; (Second row) manipulated image after expression transfer from source to target without eye gaze correction; (Third row) final output image with gaze correction.

Chapter 5 Human Body Reshaping with Single and Two Depth sensors

Automatic reshaping of human bodies is a computer vision and graphics technique with many applications. It manipulates various shape attributes of the visual appearance of a person without any manual editing. Keeping coherent reshaping results across many video frames is more challenging and the recent advance in RGB-depth sensors have significantly advanced key processing steps including pose and skeleton estimation. In order to develop a system that can be used in the consumer market, it is important to minimize the number of sensors required and the initialization setup. In the first part of this chapter, I introduce a single RGB-D sensor based for human body pose and shape reshaping system. This system features a novel pipeline for pose estimation that can be used to improve the performance of human body reshaping with single depth sensor. The limitation of a single sensor is that the estimation of pose from the 3D data our reshaping system based on is not robust due to significant occlusions. In the second part of this chapter, we extend our system to utilize two RGB-D sensors and introduce a new pipeline for pose estimation.

5.1 Skeleton-driven Approach for Human Body Reshaping with Single Depth Sensor

Reshaping of human body in image or video is an active area of research in computer graphics [208][84]. Most existing works rely on the use of 3D Morphable Model to edit the human shape. In our first system, we achieve this by manipulating the 3D skeleton data provided by a single Kinect V2 Sensor. We then apply the linear blend skinning procedure with bounded biharmonic weights as described in [83] to perform a

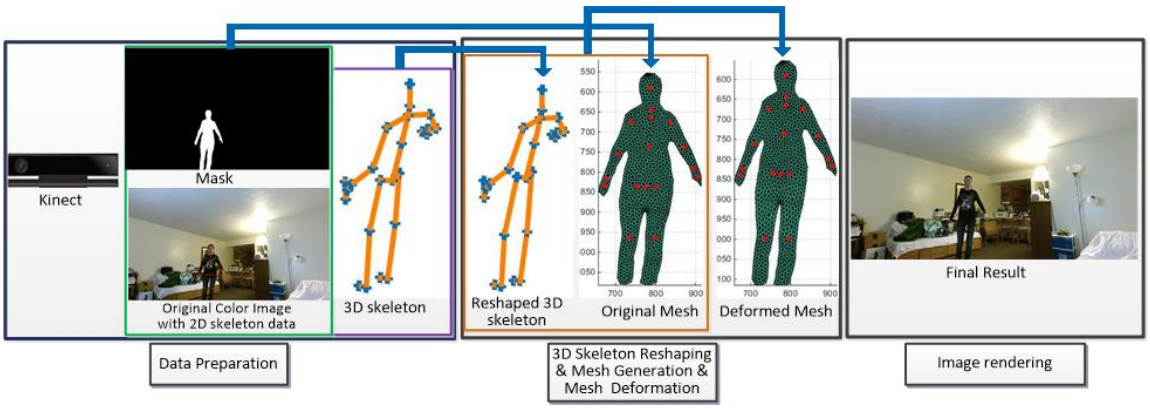

Figure 5.1 Human body reshaping with single depth sensor

smooth 2D mesh deformations. Figure 5.1 gives an overview of our human body reshaping procedure, which consists of three stages. The first stage of body reshaping is data preparation. We use Microsoft Kinect Sensor to acquire 3D skeleton data, back projected 2D skeleton data and human shape mask simultaneously. These data are computed using the Kinect V2 SDK by Microsoft. Next, we manipulate the 3D skeleton data by scaling each body part along its direction to get new 3D skeleton data and back project it to 2D image using coordinator mapper provided by Kinect V2 Sensor. The shape deformation is achieved using linear blend skinning [83] by moving the 2D skeleton data obtained in first stage to the corresponded projected 2D joints position obtained in the second stage. Finally, we render the new image using 2D image rendering tool. Details of our implementations and the results are presented in the following section.

5.1.1 Data preparation and mesh generation

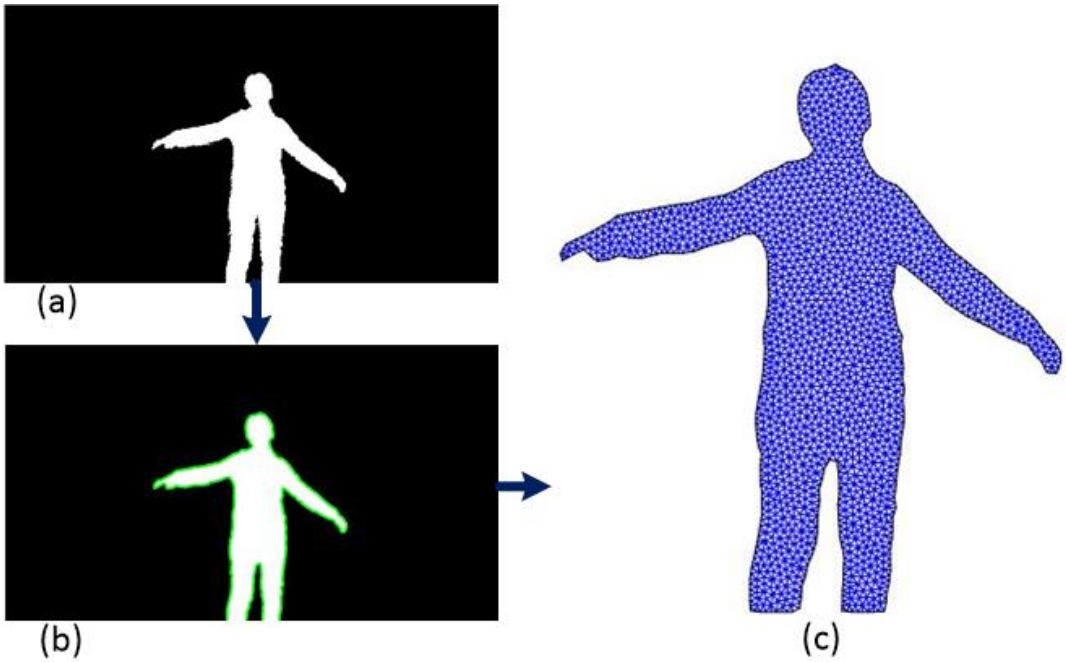

Figure 5.2 (a) Original mask. (b) Refined mask and contour. (c) Generated mesh.

The process starts by capturing the color image frame of the whole environment which will be used for further rendering. The Kinect SDK also provides the associated body mask data, 3D skeleton data and back projected 2D skeleton data. The segmentation of the human body from the color image frame can be achieved by overlaying the body mask data on the color image. Due to the poor contrast and bad lighting of the image, we use morphological operations to refine the segmentation. The contour of the human shape is then obtained from the mask data. Note, the obtained contour must be a closed polygon. We use the triangulation algorithm in [22] to generate the triangulated mesh inside the contour. The entire procedure is demonstrated in Figure 5.2.

5.1.2 2D shape manipulation

The 3D Skeleton data contains the 3D positions for 25 human joints. We use 19 of them for body shape editing, excluding the unrelated hand thumb, hand tip, and foot for our applications. Suppose each joint position in the skeleton space is represented as (X, Y, Z). The skeleton space coordinates are expressed in meters. The back projected 2D skeleton data on the color image is represented as (x, y) in pixel. To change the shape of the human body in each frame sequence and preserving their consistence, we propose a method that are able to scale the correlated bone length without changing the human pose. Using $P_i = (X_{i1}, \ldots, X_{in}; Y_{i1}, \ldots, Y_{in}; Z_{i1}, \ldots, Z_{in})^T$ to represents the 3D joint position set in i^{th} frame and $n = 1, 2, \ldots, 19$. We first calculate the length of the bone for each joint pair in 3D space. Then, we divide the reshaping process of the 3D skeleton into five parts: left arm, right arm, left leg, right leg and body. The target length of each part is based on the skeleton of an average man/woman in the U.S. The scaling is computed in the 3D space, mapping the original P_i to the target P_i' in each frame in the video sequence. After 3D skeleton reshaping, we use the built-in function of Kinect SDK to map the new 3D skeleton data P_i' to the color image to obtain the new 2D skeleton data. The 2D mesh deformation is finally achieved using linear blend skinning [83] by moving the 2D skeleton data on the mesh to the corresponded new projected joint position. To obtain the final result, we render the new mesh by patching the color of the original appearance of the human to the deformed mesh. In the last step, we embed the reshaped colored human body image to the background image obtained in the first stage.

5.1.3 Experimental results

To evaluate the performance of our proposed human body reshaping method, we conduct the experiment in two different environments. The spatial resolution of the image captured by the Kinect is 1920×1080. The practical ranging limit of Kinect is 0.4 to 4m. The first column and second column in Figure 5.3 demonstrate a sample of the original video frames and the corresponding reshaped video frame. The result shows that our method can reshape the human shape under different and complex environment. The limitations in segmentation and 3D skeleton tracking from the Kinect might influence our reshaping results. In the future, we plan to combine advanced segmentation and tracking under occlusion approach with those from the Kinect to improve the performance of our approach and make it more robust.

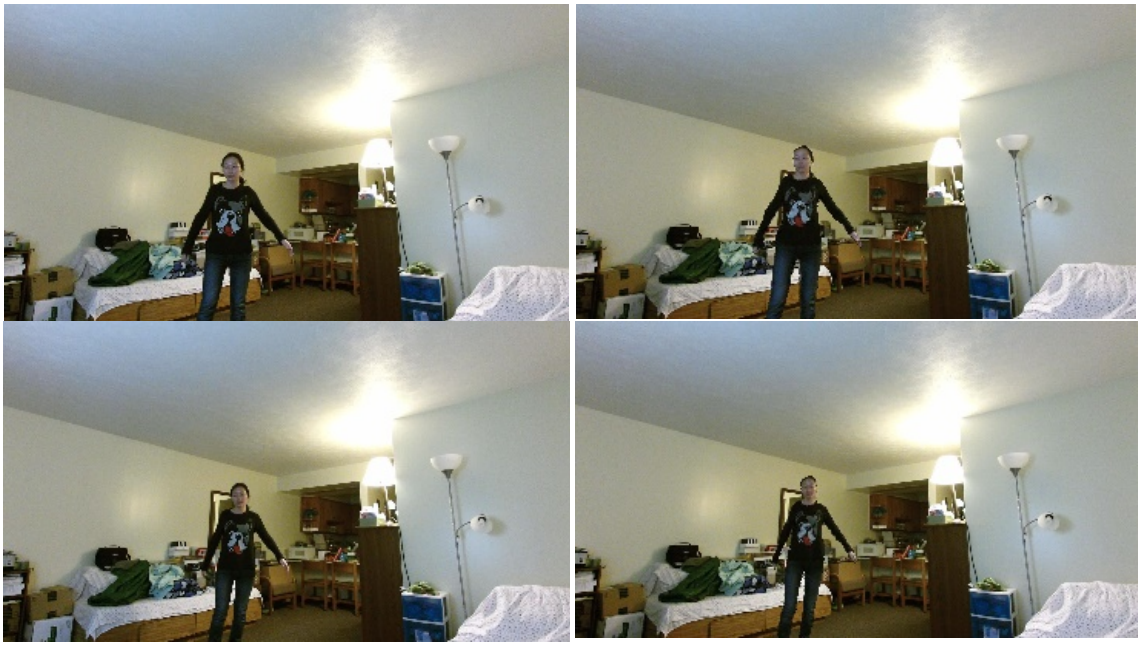

(a) (b)

Figure 5.3 (a) Selected original image frame from two environments. (b) Reshaped image frame (taller and thinner).

5.2 Human Pose Estimation with Two RGB-D Sensors

Even though recent approaches have shown that 3D positions of body joints can be estimated from a single depth sensor, the depth data often suffer from sensing noise

and self-occlusion. Before going to our model-based approach for human body reshaping, I first introduce a system to estimate the pose of human subject using two RGB-D sensors to improve the performance of the skeleton-based approach for human body reshaping as described in Section 5.1.

5.2.1 System overview

The two sensors simultaneously capture the front and back of the body's movement. Using a wide-baseline RGB-D camera calibration algorithm, the two 3D scans are first geometrically aligned, and then registered to a generic human template using a Gaussian-mixture-model based point set registration procedure with local structure constraints. The new pose of person is finally estimated by a rigid bone-based pose transformation. Experimental results demonstrate the effectiveness of our system in estimating the body pose over other state-of-the-arts techniques.

The overall pipeline of our proposed framework is illustrated in Figure 5.4. It consists of three main components: data acquisition & preprocessing, non-rigid

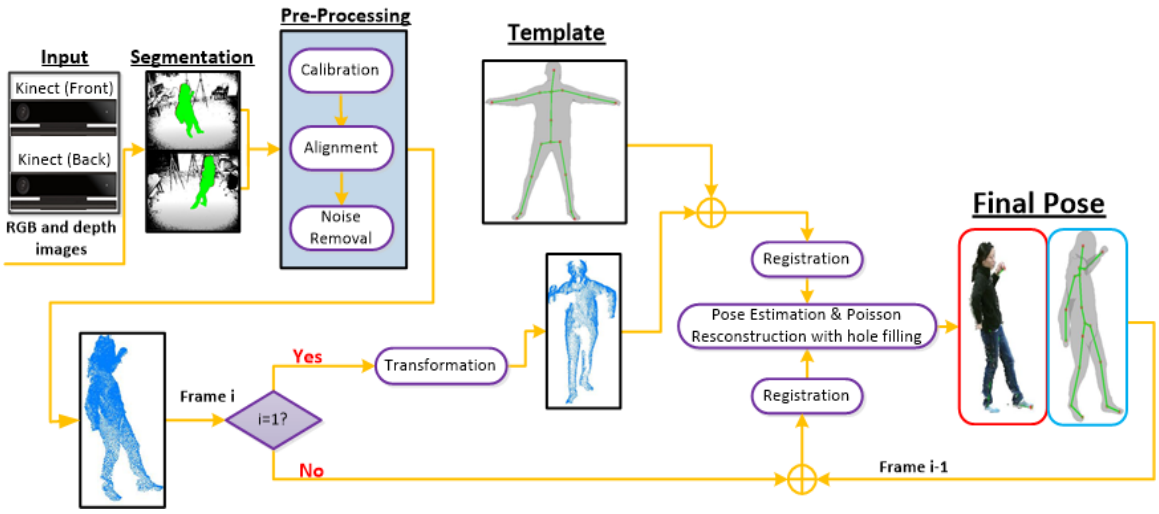

Figure 5.4 The Overview of our proposed pose estimation pipeline

registration, and skeleton estimation. We first discuss the acquisition and preprocessing of the data used in our framework in Section 5.2.2, followed by the method to register the template to the target model in Section 5.2.3. In Section 5.2.4, we introduce how we estimate the pose from the template and registered input scans. The experimental result is finally discussed in Section 5.2.5.

5.2.2 Data acquisition and preprocessing

In our framework, two Kinects are mounted in opposite direction facing toward the front and back of the subject being captured. The subject can move freely within the intersecting view frusta of the two Kinects during the capture. The input data is a set of color and depth images. Each pair of input images are aligned and transformed into a point cloud representation. As shown in Figure 5.4, we first detect and segment the person from the scene using background subtraction and morphological operations. Since

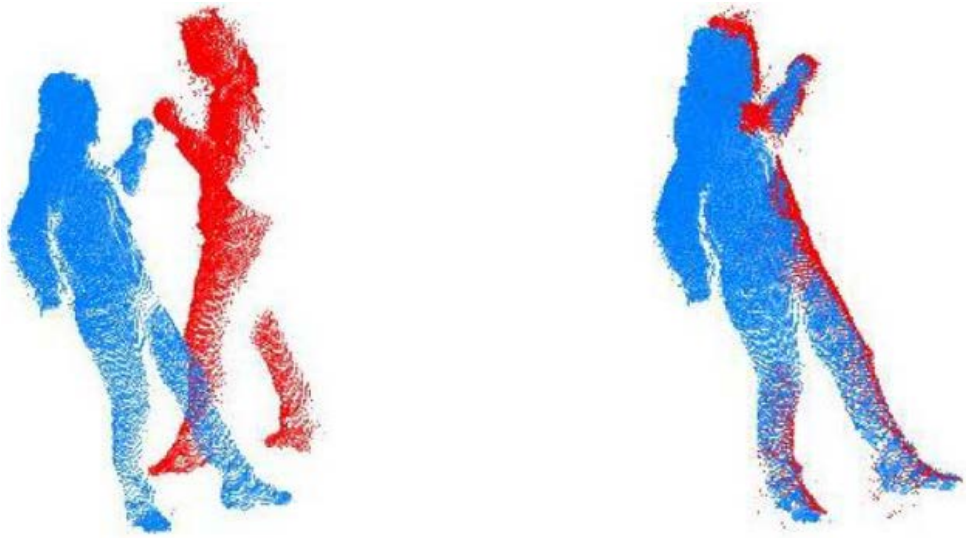

(a) (b)

Figure 5.5 Point cloud alignment from two depth sensors: (a) before alignment; (b) after alignment.

the 3D positions of point cloud is obtained with respect to the local coordinate system of each depth sensor, we first provide a coarse alignment of the point clouds from those two depth sensors using the extrinsic camera parameters. Different from traditional calibration methods using a checkerboard [206], we use a wide-baseline RGB-D camera network calibration method proposed in [155]. This approach makes use of a spherical object with distinct color as a calibration object and identifies the correspondences across different views based on the estimated locations of the center of the sphere. The calibration procedure produces the relative camera pose between the two cameras, which we use to provide a rough alignment of the two point clouds. Figure 5.5 shows the alignment of the two point-clouds.

After the initial alignment process, the combined point clouds are roughly aligned but there are still noise and outliers that could affect the pose estimation. To remove these noises, we follow a two-stage process. By assuming the distribution of the distances of each point to its closest K neighbors follows a Gaussian distribution, we first remove those points whose mean distance between all its neighbors significantly deviate from the global mean distance. Even though this stage can remove most outliers, the surface of the point cloud is still noisy and unevenly distributed. Surface reconstruction directly on these low-quality data would be highly unreliable. As such, we apply Weighted Locally Optimal Projector (WLOP) to further denoise these data points and resample them evenly across the surface [77].

5.2.3 Non-rigid point set registration

In the next stage of our proposed pipeline, similar to [201], we create a 3D template model that consists of the surface vertices, the surface mesh connectivity, the

skeleton and the skinning weight, by having the person posed a T-shaped posture in the overlapped region of the two frusta. We use the approach from Baran et al. [17] to automatically get the kinematic skeleton with $n = 18$ joints and the skinning weight, which describes the association of each vertex to each bone. The generation of this template model is done offline and only once over the entire pipeline.

For registration, the first frame of the sequence is registered with the template while the rest of the frames are registered with the neighboring frames. Since the view direction of the input scan might be different from that of the template, we first transform the input scan according to the estimated view direction of the template. Applying principle component analysis to the point cloud, the 3D orientations for the template and the input scan are obtained. We then transform the input scan into the same view direction with the template. Afterwards, we use the Coherent Point Drift (CPD) algorithm proposed in [120] to register the input scan with the template. However, as the input scan can be quite incomplete, direct application of CPD for registration can be problematic as it fails to take spatial relationship between the neighboring points into consideration.

In our framework, inspired by the work in [58], we preserve the local structure of the template through Laplacian coordinate. Similar to [120], we assume the template data, $Y = \left\{ y_n \in R^D \mid n = 1, 2, \ldots, N \right\}$ represents the centroids of GMM. The goal is to derive an optimal GMM parameters to fit the input scan $X = \left\{ x_m \in R^D \mid m = 1, 2, \ldots, M \right\}$ to the GMM centroids by minimizing the objective function defined below:

$$E(W, \sigma^2) \equiv Q(W, \sigma^2) + \lambda_{lc} E_{lc} + \lambda_g E_g \tag{5.1}$$

Following the same approach as [201][120][58], we use the Expectation Maximization (EM) algorithm [19] to solve the objective function in Equation (5.1) iteratively. Using a weighted uniform distribution account for outliers, with the assumption that the variance σ^2 for all Gaussians is same, the first term in Equation (5.1) is defined as:

$$Q(W,\sigma^2) \equiv \sum_{m,n} \frac{P_{mn}}{2\sigma^2} \left\| x_m - \Psi(y_n, W) \right\| + \frac{N_P D}{2} \log \sigma^2 \tag{5.2}$$

$$P_{mn} \equiv p^{old}(n \mid x_m) = \frac{\exp(-\frac{\left\| x_m - \Psi(y_n, W) \right\|^2}{2\sigma_{old}^2})}{\sum_{n=1}^{N} \exp(-\frac{\left\| x_m - \Psi(y_n, W) \right\|^2}{2\sigma_{old}^2} + \frac{(2\pi\sigma^2)^{\frac{D}{2}} uN}{(1-u)M})} \tag{5.3}$$

where Ψ can be considered as a function of Y with parameters W; u is the weight of uniform distribution; $\sum_{m,n} \equiv \sum_{m=1}^{M} \sum_{n=1}^{N}$; $N_P = \sum_{m,n} p^{old}(n \mid x_m)$ and p^{old} denotes the posterior probabilities of GMM. Two more terms, E_{lc} and E_g, in Equation (5.1) are used for regularization:

$$E_{lc} \equiv \sum_{n=1}^{N} \left\| L(y_n) - L(\Psi(y_n, W)) \right\|^2 \tag{5.4}$$

$$E_g \equiv \left\| W \right\|^2 \tag{5.5}$$

where L is Laplacian matrix with cotangent weights. The E_{lc} term is used to preserve the local shape structure of the template. The E_g term ensures the continuous motion. λ_{lc} and λ_g are trade-off parameters specified by user.

5.2.4 Skeleton estimation using bone-based approach

Once the input scan is registered to the template, the correspondence between them is obtained. Inspired by the work in [101][102], we treat the template as a rest pose, which is used to estimate the pose of the input scan. According to the skeleton and weights provided by the template, we can obtain $B = 17$ parts for the rest pose, the vertices in the same cluster have the same rigid motion. The clustering in our framework is achieved by assigning the vertices to the bone with the largest weights.

Since the vertices in the registered input scan $\chi = \{v_i \mid i = 1, \ldots, N\}$ has correspondences to the vertices in the rest pose $\varphi = \{u_i \mid i = 1, \ldots, N\}$, the estimation of the new pose becomes the problem of finding a set of rigid bone transformations $\{R_j, T_j \mid j = 1, 2, \ldots, B\}$ to associate the vertices in the input scan to the vertices in the rest pose through minimization the following objective function:

$$\min_{R_j, T_j} \sum_{i=1}^{N} \left\| S_j R_j u_i + T_j - v_i \right\|^2 + \lambda E_{diff} \tag{5.6}$$

$$E_{diff} \equiv \sum_{(j,k) \in Edge} \left\| S_j R_j C_{jk} + T_j - S_k R_k C_{jk} - T_k \right\|^2 \tag{5.7}$$

where $j = 1, 2, \ldots, B$; S_j is the scaling factor for each bone transformation, which helps to fit the bone length of the input scan; $(j,k) \in Edge$ means bone j and bone k share the same joint C_{jk}; λ has the value of 1 in our framework. E_{diff} ensures that the difference of new positions of joints connecting two bones will be small after transformation. Similar to [101][102], we find the solution to the Weighted Absolute Orientation problem

[72] to solve Equation (5.6). The new pose of the input scan can be obtained by applying transformation to the rest pose.

In our framework, the last step in this stage is to build the detailed human pose model. The original incomplete input scan contains the detailed information, like clothes winkles, hair style etc., and the registered input scan can be used to fill the gap of the missing data. As such, we fuse them together and then apply Poisson surface reconstruction [93] to obtain a detailed human pose model.

5.2.5 Experimental results

In this section, we experimentally demonstrate the effectiveness of our framework from two perspectives: qualitative analysis and quantitative evaluation. Our system was first tested on a publicly available dataset provided by MPI Informatik [70]. This dataset contains six sequences (D1-D6) of motion with varying difficulties performed by one actor including kicking, rotation, and circular walking. The ground truth of joint position of the actor is also provided in this dataset obtained by a marker-based Mocap system.

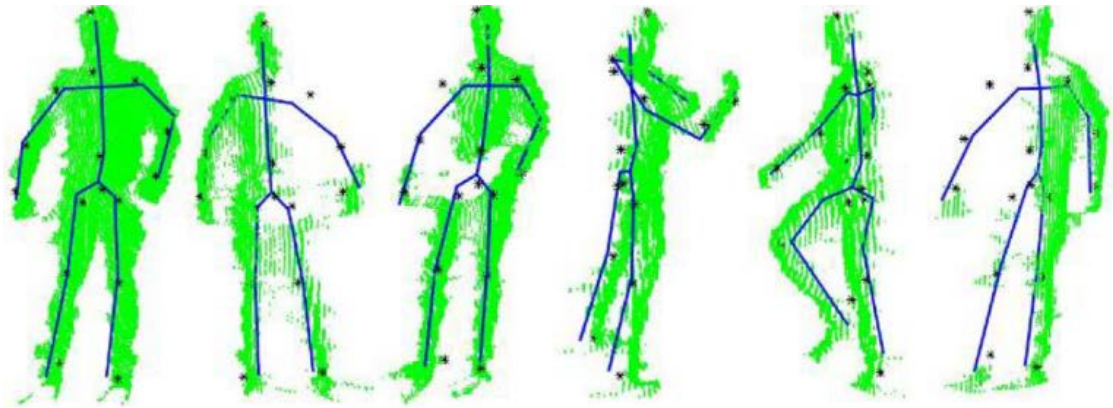

Figure 5.6 Visual comparison of our proposed method using the dataset in [70] with its ground truth data. Blue line (Our method estimation) and Black dot (Ground truth).

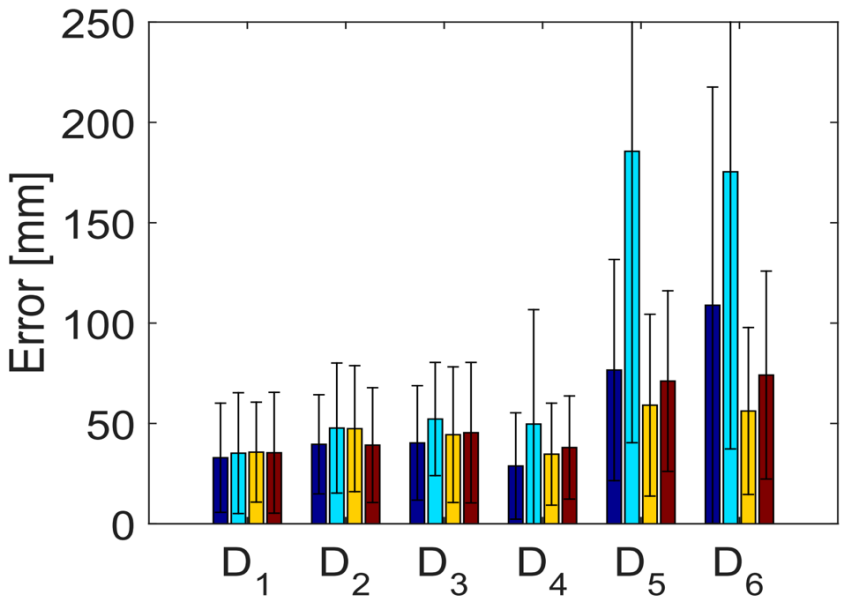

Figure 5.7 Comparison of average joint position error for six sequences from the evaluation dataset: Kinect [156] (Dark blue), Baak.et al [13] (Light blue), Helten et al [70] (Yellow) and Ours (Red).

We can qualitatively and quantitatively evaluate our system by comparing the joint position error against the ground truth data.

Even though this dataset is captured by one depth sensor, our proposed system can be used. We first applied Hidden Point Removal (HPR) method in [92] to detect the visible part of the template and then estimated the pose by our proposed pipeline. We followed the same strategy as described in [70] to estimate the average joint error. Figure 5.6 shows the pose estimation of our system on this dataset. As shown in Figure 5.6, our system can produce good estimation even with heavy occlusion and missing data. The average joint position error of our method versus other state-of-art approaches on this dataset are shown in Figure 5.7. The results clearly show that our system achieves higher or comparable performance [70][156][13].

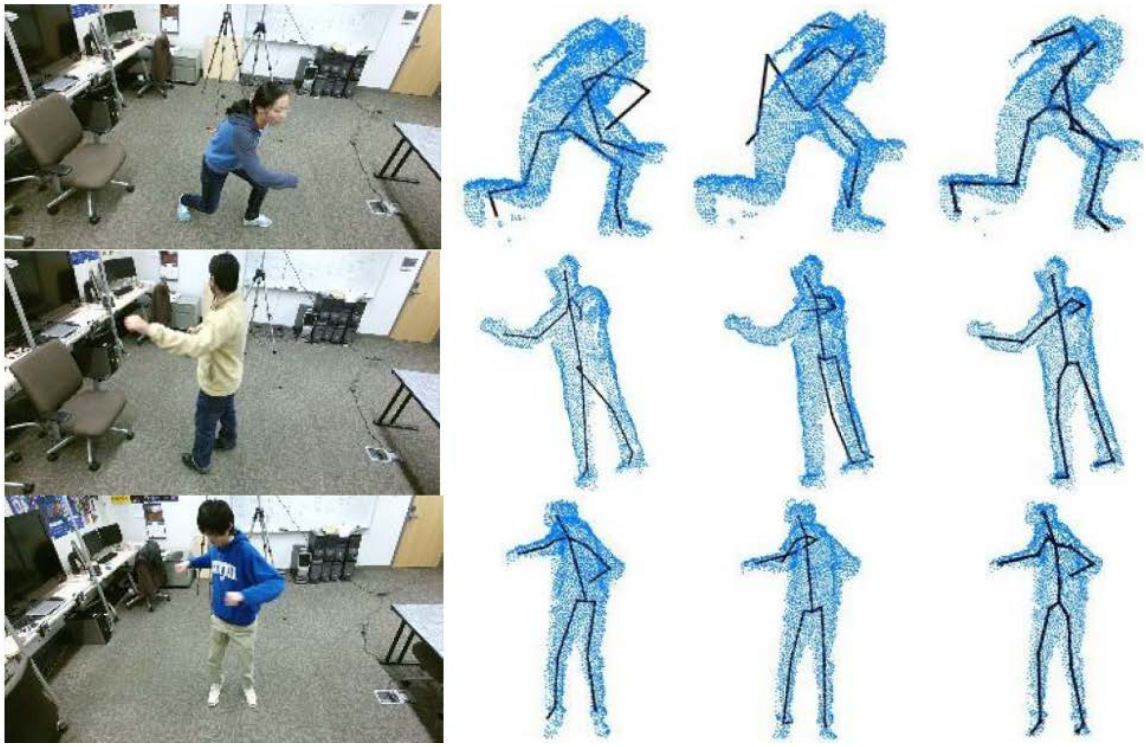

(a) (b) (c) (d)

Figure 5.8 Pose estimation visualization results: (a) Color image from depth sensor (front); (b) pose estimation from KinectSDK (front); (c) pose estimation from KinectSDK (back); (d) pose estimation from our proposed system.

In addition, we compare the accuracy of pose estimation on our pipeline by comparing it with Kinect SDK [96]. We captured three sequences of three actors with different weight and height, performing a variety of complexity movements like crossing arm, rotation, running, etc. The first column of Figure 5.8 shows the captured color images from the depth sensor in front; the second and third column show the pose estimation by Kinect SDK for the depth sensors in front and behind respectively; the last column shows the pose estimation by our proposed pipeline. It can be observed that the Kinect SDK based method produce poorer pose estimation than our proposed system under significant occlusion. Some joint positions deviate from the supposed position if the body parts are occluded.

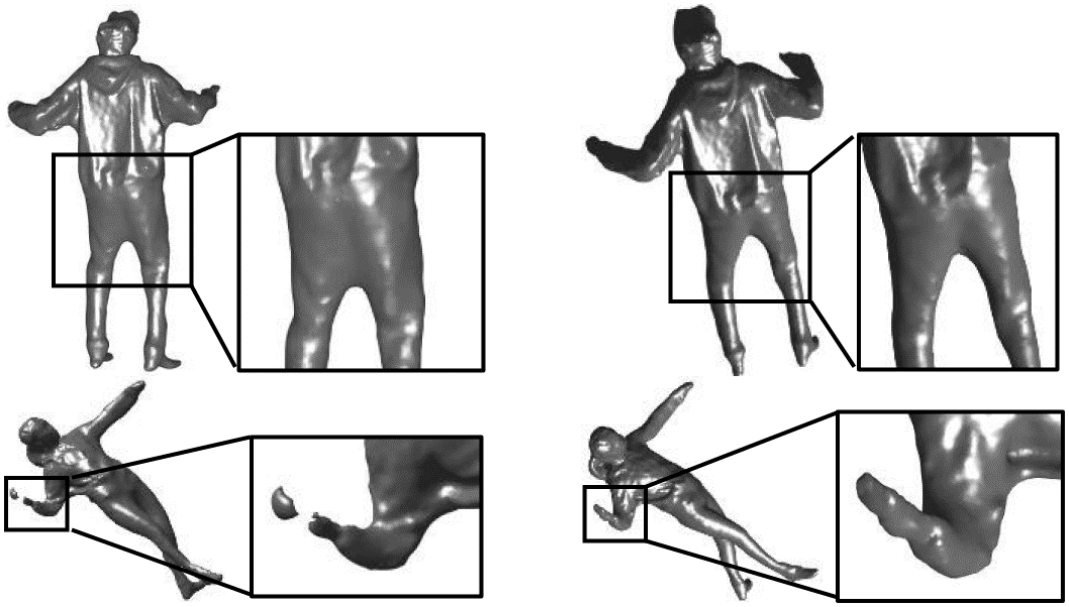

(a) (b)

Figure 5.9 Poisson reconstruction with and without holes filling: (a) without holes filling before Poisson reconstruction; (b) with holes filling using our proposed way before Poisson reconstruction.

In our last experiment, we visually show the comparison of the detailed model generated with and without holes filling before the Poisson reconstruction. The data here is the same as that from Figure 5.8. The comparison is shown in Figure 5.9. We can see the reconstructed model with holes filling before Poisson reconstruction looks more natural. The first column shows the reconstruction result without holes filling, some of the body part (e.g. leg) is miss-connected or disconnected (e.g. hand).

Chapter 6 Model-based Approach for Human Body Reshaping with Sensor Network

In this chapter, a novel pipeline to reshape the human body using noisy depth data from multiple RGB-D sensors (sensor network) is presented. Compared with a single view reshaping system introduced in Chapter 5, multiple RGB-D sensors provide more constraints and better coverage, leading to more consistent results. However, there exist several challenges in estimating the pose and shape of human simultaneously in RGB-D data due to self-occlusion and motion complexity. To cope with the time-varying articulated human shape, we propose a new approach that combines a Gaussian Mixture Model (GMM) based fitting approach as introduced in Section 5.2.3 with a morphable model learned from range scans. Without any user input, this approach can automatically account for the variations in pose and shape. It also enables different types of reshaping by manipulating body attributes such as height, weight or other physical features. Experimental results are provided to demonstrate the effectiveness of our system in manipulation of human body shapes. In the last part of this chapter, we demonstrate the feasibility in using our proposed system for visual privacy protection.

6.1 Overview of the System

The schematic of our proposed framework is shown in Figure 6.1. It consists of three main components: data acquisition & preprocessing, pose & shape estimation, and human body reshaping. Inputs are aligned color and depth data captured from multiple RGB-D cameras. Based on offline calibration parameters, we first perform denoising on

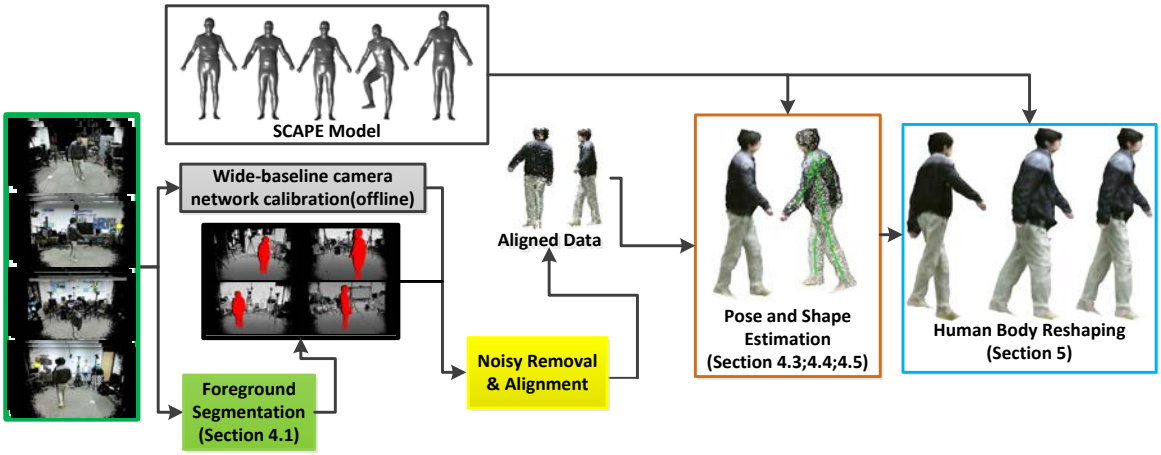

Figure 6.1 Overview of our proposed system.

the depth data and align them onto the same coordinate system based on the system described in [155].

To estimate the pose and shape of the actor, we use a morphable model along with the GMM based framework to fit the observed data. We optimize the model to the observed data in two stages. The first stage (Section 6.3.2) estimates the posture and coarse body shape of the observed actor, by combining a modified approach from [10] with the GMM based point set registration [120]. While this initial step produces accurate pose and coarse shape, it fails to reconstruct the non-rigid deformations caused by clothing of the actor. In the second stage (Section 6.3.3), the details of the surface shape are estimated by finding the difference along the normal directions between the reconstructed shape in the first stage and the original refined point cloud.

After finding the correspondence between the observed data and the morphable model, we can now reshape the observed actor by modifying the semantic body attributes of the morphable model and applying the deformation transfer to the fitted model fully automatically (Section 6.4).

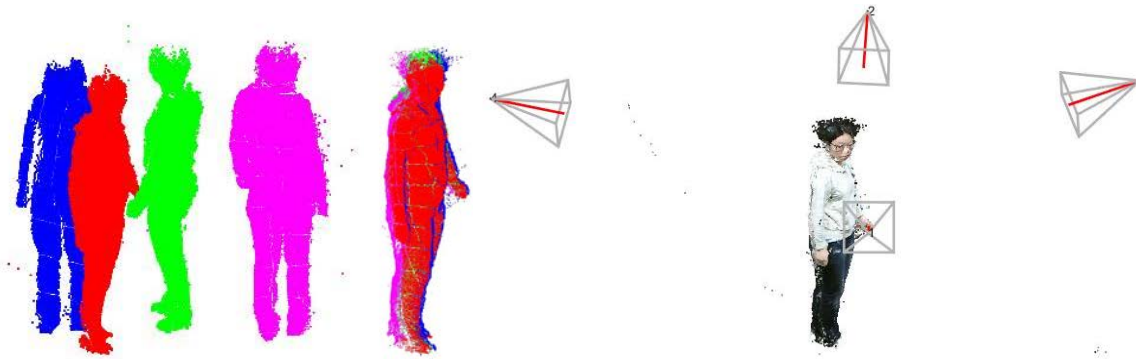

(a) (b) (c)

Figure 6.2 Point cloud alignment from four depth sensors: (a) before alignment, (b) after alignment. (c) alignment with texture and camera position (1,2,3,4)

6.2 Data Collection and Pre-processing

In our experimental setup, we used four Kinect cameras mounted in four directions perpendicular to each other for data capture. This configuration helps to minimize any interference between adjacent Kinect cameras. The actor can move freely within the four intersecting view frusta during the capture. The input data is a set of color and depth images. Each pair of input images are aligned and transformed into a point cloud representation [26].

As shown in Figure 6.1, we first detect and segment the person from the scene using background subtraction and morphological operations. Since each depth sensor produces point clouds in its own local coordinate system, we need to estimate the extrinsic camera parameters before aligning the local point cloud data into a global coordinate system. Different from traditional calibration methods using checkerboard [206], we estimate the extrinsic parameters using a wide-baseline RGB-D camera network calibration method from [155]. This approach uses of a spherical object with distinctive color as a calibration object, and identifies the correspondences across

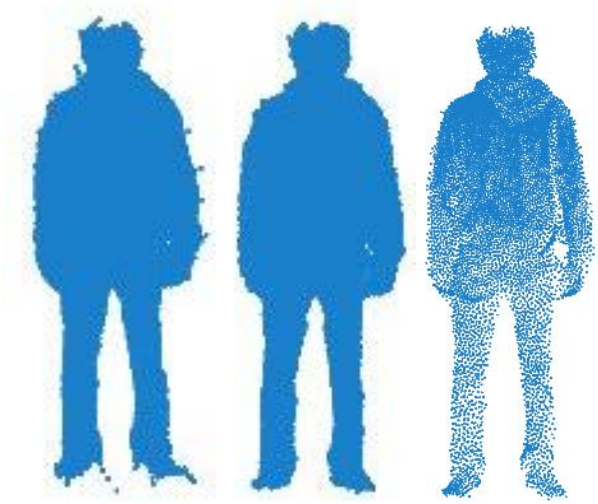

(a) (b) (c)

Figure 6.3 Point cloud outlier removal and simplification: (a) Original aligned point cloud; (b) after outlier removal using Gaussian filter; (c) after denoising using WLOP

different views based on the estimated trajectory of the sphere's center. The calibration procedure produces the relative rigid transformation between the two cameras, which we use to provide a rough alignment of the point clouds. Figure 6.2 shows a sample of point clouds from different views in their local coordinates in Figure 6.2(a), in the global coordinates in Figure 6.2(b), and with textures and cameras' position in Figure 6.2(c).

After the process of initial alignment process, we follow the same two-stage process to remove the noises and outliers as described in Section 5.2.2. By assuming the distribution of the distance of each point in the aligned input scan to its neighbors is Gaussian with a mean and a standard deviation, we first search for the nearest neighbors at each 3D point and remove the point whose mean distance between all its neighbors is greater than or smaller than the threshold defined by the global mean and standard deviation. Even though this stage can remove most outliers, the surface of the point cloud is still noisy and non-uniformly distributed. In this case, the assumption of a normal

distribution for further surface reconstruction would be unreliable. To solve this problem, we apply Weighted Locally Optimal Projector (WLOP) [77] to generate a set of denoised, simplified and evenly distributed point, as is shown in Figure 6.3.

6.3 Pose and Shape Estimation with Multiple Depth Sensors

6.3.1 SCAPE model

Unlike our previous work [192], we use the SCAPE model, instead of a non-parametric model, as prior for the goal of reshape human body caused by different identities and postures. This section briefly reviews the SCAPE model introduced in [10].

The SCAPE model uses separate parameters to control the deformation of the pose and the body shape, and then fuses them together under a single transformation. Denote the generic template model of shape and pose as X and the target model as Z. SCAPE computes a 3×3 transformation matrix A_f that deforms each triangle T_f^0 (defined by vertices $x_{f,k}, k=1,2,3$) in the template model to its corresponding target triangle T_f with vertices ($z_{f,k}, k=1,2,3$):

$$T_f \equiv A_f T_f^0 \equiv R_f(\theta) D_f(\beta) Q_f(\theta) T_f^0 \tag{6.1}$$

where the pose is governed by the rotation of triangle in part $R_f(\theta)$ and the pose-dependent non-rigid deformation $Q_f(\theta)$. The shape variations are controlled by a linear function $D_f(\beta)$. During the training phase, the pose of different individuals is fixed at

(a) (b) (c) (d)

Figure 6.4 SCAPE Model with 16 parts of different poses and shapes

θ_0. SCAPE models the shape variation using a PCA model $D_f(\beta) \equiv U\beta + \mu$, where U and μ are both pre-trained PCA parameters, μ is the mean body shape.

Given both θ and β, vertex positions $z_1, \ldots, z_N$ of the target mesh can be determined by solving the linear least square problem as follows:

$$E_m \equiv \underset{\{z_1,\ldots,z_N\}}{\operatorname{argmin}} \sum_{f=1}^{F} \sum_{k=2,3} \left\| R_f(\theta) D_f(\beta) Q_f(\theta) \Delta x_{f,k} - \Delta z_{f,k} \right\|^2 \tag{6.2}$$

where F is the total number of faces, N is the total number of vertices, and $\Delta x_{f,k} = x_{f,k} - x_{f,1}, \Delta z_{f,k} = z_{f,k} - z_{f,1}$ are edges for each triangle. As shown in Figure 6.4, we can synthesize realistic meshes for different people in a broad range of poses and shapes.

6.3.2 GMM-based pose and shape fitting

The next step is to fit the trained SCAPE model to the observed data obtained in Section 6.2. The goal of fitting is to optimize both θ and β such that the resulting

morphable model has good approximation for the observed data. Previous approaches based on morphable models such as [196][33] require initial guesses about the closest point correspondence or sparse tracking markers. Instead, we use a GMM based approach [204] that takes all the observed data points into consideration. Our approach is more robust against outliers and occlusions, and is also more effective in fitting between two complex non-rigid point data sets. In the followings, we first describe the GMM based non-rigid registration approach in Section 6.3.2.1, unlike the previous approach presented in Section 5.2.3 that focused only on pose, the proposed approach in this section can simultaneously estimate both the human pose and shape for body reshaping, and then provide the details in Section 6.3.2.2 on how we apply this approach in fitting the observable data with the morphable model.

6.3.2.1 GMM-based point set registration

Inspired by the work proposed in [120], we assume that the observed data $Y = \{y_m \in R^D \mid m = 1, 2, \ldots, M\}$ follows a N -component GMM distribution with component means initialized at the vertices $X = \{x_n \in R^D \mid n = 1, 2, \ldots, N\}$ of the deformed template with pose and shape parameter θ and β. Therefore, the probability of each observed data point can be expressed as:

$$P(y_m) = (1-u)\frac{1}{N}\sum_{n=1}^{N} P(y_m \mid x_n) + u\frac{1}{M} \tag{6.3}$$

$$P(y_m \mid x) = \frac{1}{(2\pi\sigma^2)^{D/2}} \exp\left(-\frac{\|y_m - x_n\|^2}{2\sigma^2}\right) \tag{6.4}$$

where D is the dimension of the observed data (e.g. $D=3$); u is the weight of the uniform distribution that accounts for outliers and the variance σ^2 for all Gaussians is assumed to be the same for simplicity.

The registration of these two point sets X and Y can be considered as a Maximum Likelihood problem, which is equivalent to minimize the following negative log-likelihood:

$$E \equiv -\sum_{m=1}^{M} \log P(y_m) \tag{6.5}$$

Using the same approach as in [120], we apply the Expectation Maximization (EM) [39] algorithm to minimize the objective function in Equation (6.5) iteratively until it converges. During the E-step, the posterior probabilities are calculated using the parameter obtained from the previous iteration based on the Bayes rule as:

$$P_{nm} \equiv p^{old}(x_n \mid y_m) = \frac{\exp(-\frac{\|y_m - x_n\|^2}{2\sigma_{old}^2})}{\sum_{n=1}^{N} \exp(-\frac{\|y_m - x_n\|^2}{2\sigma_{old}^2}) + \frac{(2\pi\sigma^2)^{\frac{D}{2}} uN}{(1-u)M}} \tag{6.6}$$

During the M-step, we can find the new parameters by minimizing the objective function in Equation

$$Q(X(\theta,\beta),\sigma^2) \equiv \sum_{m=1}^{M}\sum_{n=1}^{N} \frac{P_{nm}}{2\sigma^2}\|y_m - x_n\|^2 + \frac{N_p D}{2}\log\sigma^2 \tag{6.7}$$

where $N_p = \sum_{m=1}^{M}\sum_{n=1}^{N} P_{nm}$.

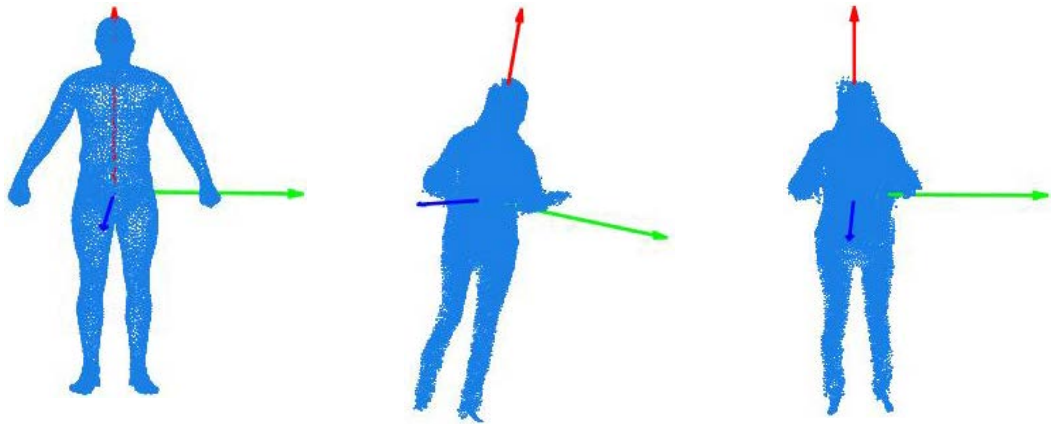

(a) (b) (c)

Figure 6.5 View direction transformation (a) Morphable model with view direction (b) Original observed data with view direction (c) After transformation (Red: Y-axis; Blue: Z-axis; Green: X-axis)

6.3.2.2 Human pose and shape optimization

Before applying the GMM registration, we need to first transform the observed data to the same view direction of the morphable model. Using principle component analysis on the point cloud, the 3D orientations of the morphable model and the observed data are obtained. We then construct a transformation to transform the observed data into the same view direction with the morphable model, as shown in Figure 6.5.

After the alignment process, we apply the GMM-based non-rigid registration approach to fit the morphable model X to the observed data Y. We solve this by jointly optimizing the two objective functions from Equation (6.2) and Equation (6.7) to obtain X, θ and β using the following objective function:

$$E_m + \omega_{data} * Q(X(\theta, \beta), \sigma^2) \tag{6.8}$$

where E_m from Equation (6.2) and $Q(X(\theta,\beta),\sigma^2)$ from Equation (6.7) are weighted by ω_{data} that controls the influence of observed data on the morphable model. To simplify the optimization problem, we use a coordinate descent strategy and solve for each variable iteratively. The followings describe the steps that are summarized in Algorithm 1.

Initialization. In the initial stage, the variance σ^2 is obtained by taking the derivative of the objective function defined in Equation (6.8) w.r.t. σ^2 and set it equal to zero, yielding:

$$\sigma^2 = \frac{1}{N_p D}\sum_{m=1}^{M}\sum_{n=1}^{N} P_{nm}\left\|y_m - x_n\right\|^2 \tag{6.9}$$

Iteration. There are three main steps in each iteration:

1) Fixing θ and β, update X.

We solve the vertices that gives the best correspondence between the morphable model X and the observed data Y. It can be obtained by minimizing the objective function defined in Equation (6.8).

2) Fixing β and X, update θ.

To estimate the pose change $\Delta\theta$, we use the twist change to rotation as an approximation, that is, i.e. $R_{new} \approx (I + \Delta\hat{\theta})R$, where $\Delta\theta = (\Delta\theta_1, \Delta\theta_2, \Delta\theta_3)$, and

$$\Delta\hat{\theta} = \begin{bmatrix} 0 & -\Delta\theta_3 & \Delta\theta_2 \\ \Delta\theta_3 & 0 & -\Delta\theta_1 \\ -\Delta\theta_2 & \Delta\theta_1 & 0 \end{bmatrix} \tag{6.10}$$

Then, the pose change can be solved by minimizing the following function to deform the morphable model into the pose that best approximates the observed data.

Algorithm 1. Human Pose and Shape Optimization

Input: Initial θ, β, σ^2 and observed data Y.

Output: The optimized θ^*, β^*.

$iter = 0$;

Repeat

$j = 0$;

E-step:

Compute posterior P_{nm} according to Equation (6.6);

M-step:

Repeat

Compute X by solving Equation (6.8);

Compute and update θ by Equation (6.11);

Compute and update β by Equation (6.12);

Adjust ω_{data} by simulated annealing;

$j++$;

Until (satisfy the stop criteria)

$iter++$;

Until (satisfy the stop criteria)

$\theta^* = \theta, \beta^* = \beta$

$$\min_{\Delta\theta} \sum_{f=1}^{F} \sum_{k=2,3} \left\| (I + \Delta\hat{\theta}_b) R_b D_f Q_f \Delta x_{f,k} - \Delta y_{f,k} \right\|^2 + \omega_R \sum_{b1,b2 \in adj} \left\| \theta_{b1} - \theta_{b2} \right\|^2 \qquad (6.11)$$

where D_f and Q_f are defined in Equation (6.2); ω_R is a trade-off parameter; and $b1, b2$ are indices of the adjacent bones. The second term in Equation (6.11) is used to prevent large joint rotation.

3) Fixing θ and X, update β.

For shape update, we find the best shape parameters to fit the observed data by minimizing the following function:

$$\min_{\beta} \sum_{f=1}^{F} \sum_{k=2,3} \left\| R_b \overline{(U\beta + \mu)} Q_f \Delta x_{f,k} - \Delta y_{f,k} \right\|^2 \tag{6.12}$$

Termination. The process fits the morphable model to the observed data iteratively. The process stops if it reaches to a maximum number of iterations (e.g. $\max\_iter = 10$) or the maximum movement of the vertices is small enough (experimentally set to 1mm).

6.3.3 Detailed motion reconstruction

After the registration in Section 6.3.2, we obtain a deformed mesh $X' \equiv \{x'_n \in R^D \mid n = 1, 2, \ldots, N\}$ that is a good approximation of the observed data. However, to preserve details like winkles and folds, they need to be transferred from the observed data to the deformed mesh.

To recover the details of observed data, we use a procedure similar to that proposed in [105]. For each vertex x'_i in the deformed mesh, we first find the nearest neighbor c_i from observed data along its normal direction n_i . Then, the detail coefficients d_i is obtained by optimizing the objective function as follows:

$$E_d = \sum_{i=1}^{N} (\left\| x'_i + d_i n_i - c_i \right\|^2 + \lambda_l \left\| d_i \right\|^2) + \lambda_s \sum_{i,j} \left\| d_i - d_j \right\|^2 \tag{6.13}$$

where i and j are neighboring vertices. The second term in the first summation in Equation (6.13) is used to prevent large movement. The weighting factor λ_l is

empirically set to 0.1. The last term accounts for smoothness with the weighting factor $\lambda_s = 0.5$. This is a least square problem and can thus be solved efficiently. Figure 6.6 shows how the details are preserved and the resulting reconstructions.

6.3.4 Bone-based approach for skeleton estimation

Once the observed data are registered to the morphable model, the correspondences between them can be obtained. Similar to the process of skeleton estimation introduced in Section 5.2.4, we treat the morhpable model as a rest pose and use it to estimate the skeleton of the observed data. According to the skeleton and weights

(a) (b) (c)

Fig econstru l regis) Re h
det model

(a) (b) (c) (d)

Figure 6.7 Human body reshaping (a) Original; Reshaping to different shape parameters (b) shorter; (c) thinner; and (d) fatter.

from the morhpable model, we can obtain $B = 16$ parts or clusters for the rest pose. Vertices in the same cluster are assumed to have the same rigid motion. The clustering in our framework is achieved by assigning the vertices to the bone with the largest weights. The new skeleton of the observed data can finally be obtained by applying the resulting transformation to the rest pose following the procedure as described in Section 5.2.4.

6.4 Human Body Reshaping

In Section 6.3.2, we describe the procedure to establish the correspondences between the morphable model and the observed data. Such correspondences can then be used to reshape the human body. In particular, we treat the morphable model as source mesh, and the deformed mesh with details as target mesh, the deformation transfer is applied to reshape the human body.

The goal of the deformation transfer is to transfer the change in shape from the source to that of the target. In our system, the attributes, like the weight, height or leg length of a human body can be modified by changing the shape parameter from β to β^*

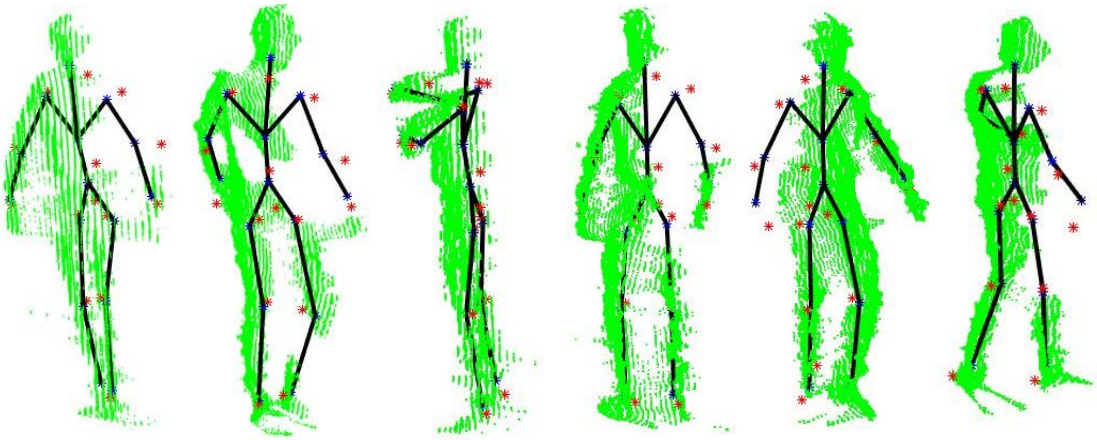

Figure 6.8 Visual comparison of our proposed method using the dataset in [70] with its ground truth data. Black line (Our method) and Red dot (Ground truth).

in the source mesh $X(\theta, \beta)$. Given a new β^*, we first obtain the deformed source mesh, and then transfer the deformation to the target by affine transformation similar to the procedure proposed in [160]. Figure 6.7 shows one example of reshaping the human body with different shape parameters.

6.5 Experimental Results

In this section, I experimentally evaluate our framework from two perspectives. First, we quantitatively measure the pose estimation and shape quality of our system using several publicly available datasets. The motion in these datasets ranges from simple movements to very challenging ones with heavy occlusion. Second, we demonstrate the effectiveness of our human body reshaping system.

6.5.1 Evaluation of poses

The IDT dataset [70] contains six sequences (D1-D6) of varying motion complexities, including kicking, rotation, and circular walking, performed by one actor.

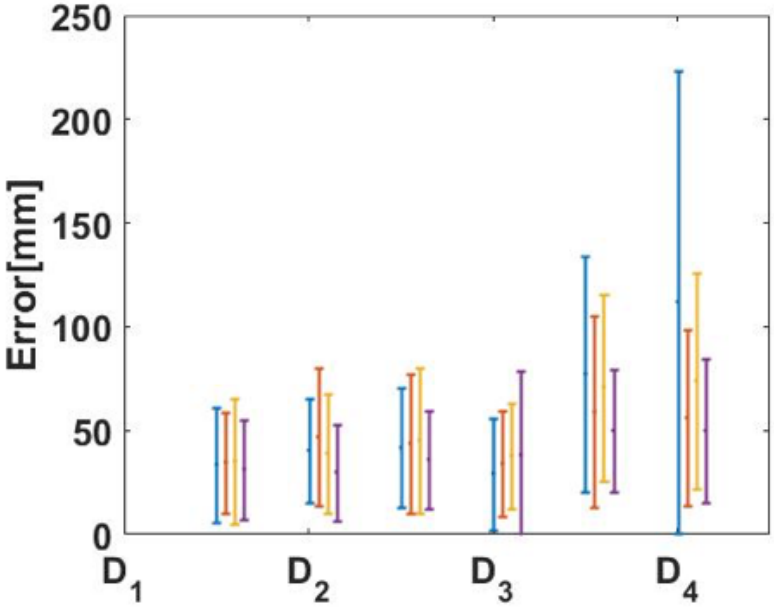

Figure 6.9 Comparison of average joint position error for six sequences from the evaluation dataset: Blue - [156], Orange - [70], Yellow - [192] and Purple - Ours method.

The ground truths of joint positions obtained by a marker-based MOCAP system are provided as part of this dataset. As such, we can qualitatively and quantitatively evaluate our system by comparing the joint position error against the ground truth data following the same strategy as in [70].

As shown in Figure 6.8, our system can produce good estimation even with heavy occlusion and missing data. The average joint position error of our method versus other state-of-art approaches on this dataset are shown in Figure 6.9. Among the three methods we compared ([156];[70];[192]) in which the dataset using in this paper is provided by their method, our proposed method gave the best results five out of the six sequences in the dataset.

In addition, we compare the accuracy of our pose estimation with that from the Kinect SDK V2 [96]. We captured three sequences of three different actors performing a

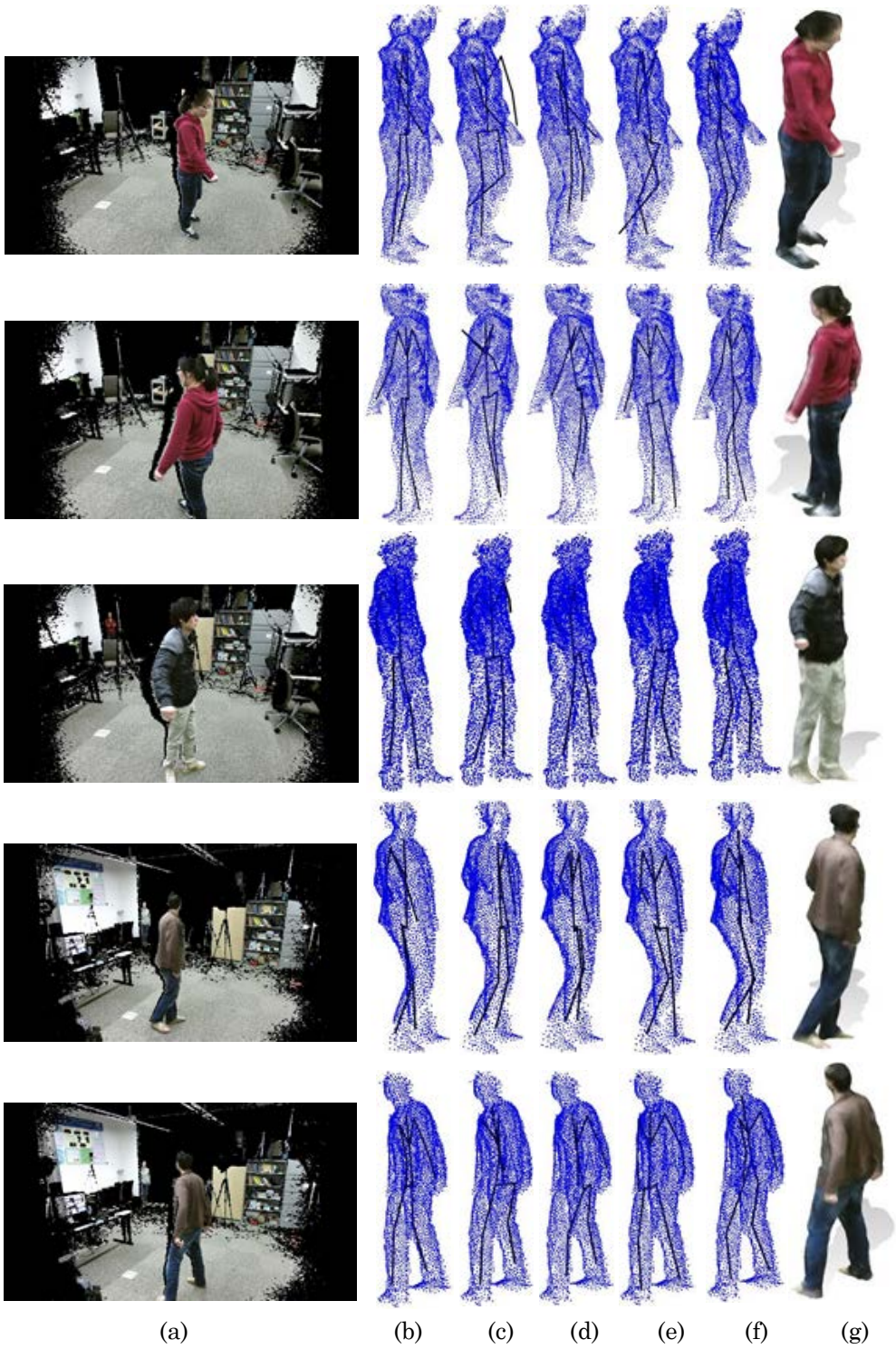

Figure 6.10 Pose estimation visualization result: (a) Color image from depth sensor (Kinect2); (b) (c) (d) (e)pose estimation from KinectSDK; (f) pose estimation from proposed system; (g) Reconstructed model with texture.

(a) (b) (c)

Figure 6.11 Error map for body shape fitting. (a) Original scan. (b) The estimated model overlaid with the ground truth, and (c) the difference between the estimated model and the ground truth, the unit is in millimeter.

variety of complex movements like crossing arm and running. The first column of Figure 6.10 shows the captured aligned color images from one depth sensor. The second to fifth columns show the pose estimations by Kinect SDK for each of the four depth sensors respectively. The sixth and seventh columns show the pose estimation and the reconstructed model with texture by our proposed pipeline. It can be observed that the Kinect SDK based method produces poorer pose estimation than our proposed system under significant occlusion. Some joint positions deviate from the supposed position if the body parts are occluded.

6.5.2 Evaluation of shapes

We evaluate the accuracy of body shape fitting using the SCAPE dataset [10], which contains 71 example poses with 12k vertices and 25k triangles, as well as the dataset in [196], which has 6 subjects (3 female and 3 male) performing 3 different motions (knees up, spin and walk) in 3 clothing styles (tight, layered and wide).

These two datasets are publicly available with high quality realistic 3D scans. We visually and quantitatively measure the accuracy of our shape estimation. For the SCAPE dataset, we calculate the Euclidean Distances between all pairs of correspondence points between the ground truth and estimated shape. Figure 6.11 shows the error map for the examples selected from the dataset. It is clearly visible that the optimized shape model closely resembles the targeted example pose even though the input scan with large missing area. The mean error and the maximum error distance between our estimated shape and the ground truth for this example are 7.6 mm and 34.3 mm respectively.

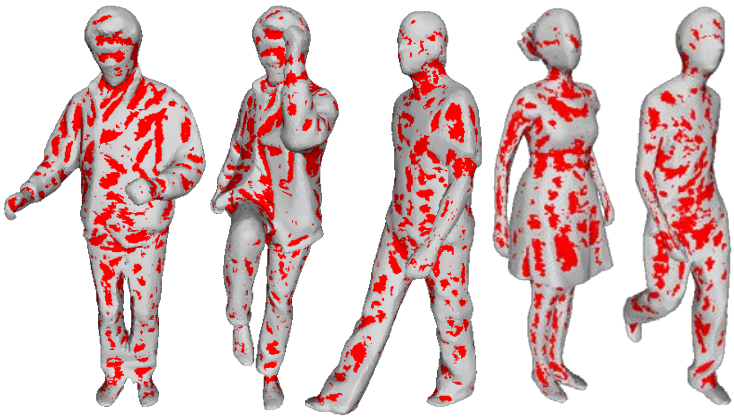

Figure 6.12 Visual results of our shape fitting. Input model (gray) are overlaid on our result (red).

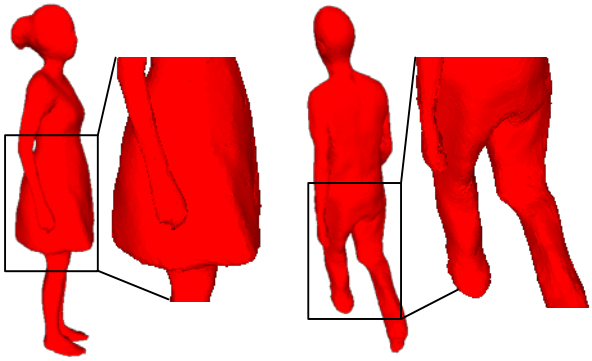

Figure 6.13 Detail visualization of shape fitting.

To visually validate our system, we compare our reconstruction result against the model from the dataset from [196]. The results are shown in Figure 6.12, which shows the overlay of our result with the model from the dataset. Figure 6.13 shows the shape reconstruction in detail. It can be noticed that our detail reconstruction algorithm can well preserve the winkles and folds of subject's clothing.

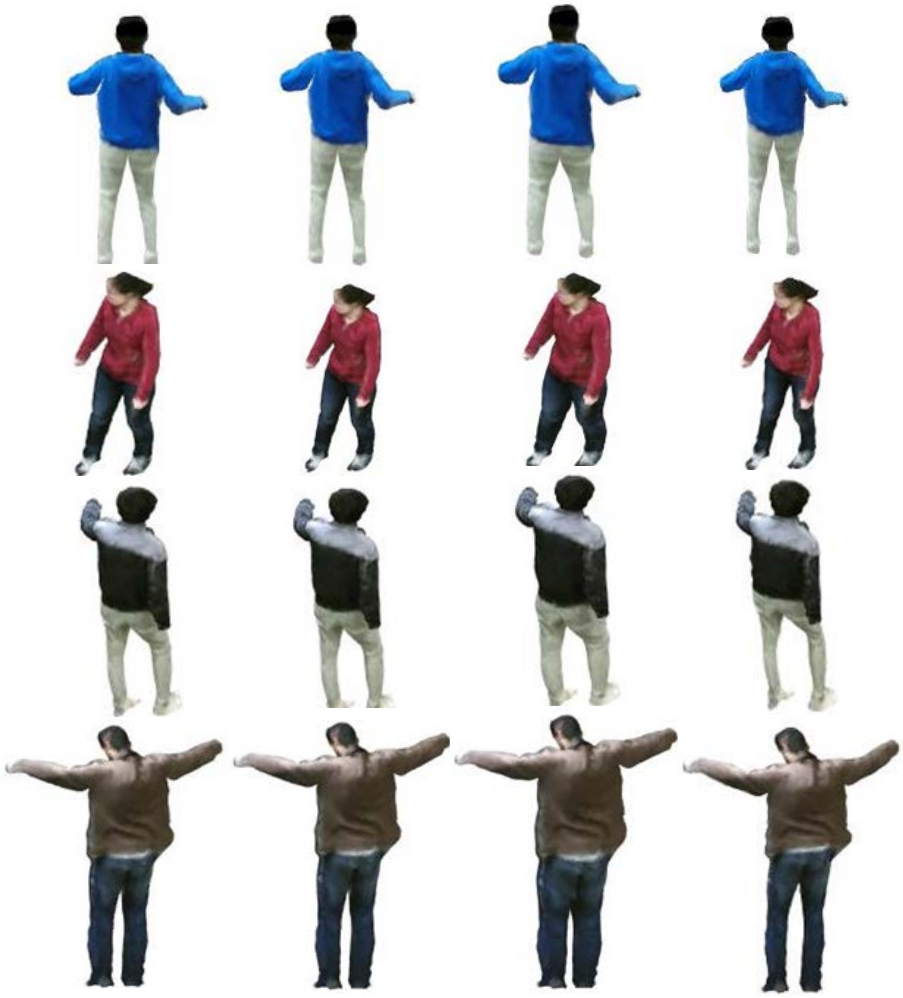

Figure 6.14 Body reshaping visualization result (a) Original reconstructed model (b), (c) and (d) Reshaped result with our method with different parameters of morphable model.

Figure 6.15 Our system reshapes the human body using multiple RGB-D sensors. (Left) Original reconstructed human model; (Right) 4 different views of the reshaped human body with shorter legs and longer body.

6.5.3 Evaluation of human body reshaping

In our last experiment, we evaluate the entire system from data capturing to human body reshaping. We capture four sequences of four individuals with different height and weight in the lab environment. By changing the parameters of the morphable models, we can produce various body types as shown in Figure 6.14.

6.6 Application on Visual Privacy Protection

The prevalence of wireless networks and the convenience of mobile cameras enable many new video applications other than security and entertainment. From behavioral diagnosis to wellness monitoring, cameras are increasing used for observations in various educational and medical settings. Videos collected for such applications are considered protected health information under privacy laws in many countries. At the same time, there is an increasing need to share such video data across a wide spectrum of stakeholders including professionals, therapists and families facing

similar challenges. Visual privacy protection techniques, such as blurring or object removal, can be used to mitigate privacy concern, but they also obliterate important visual cues of affect and social behaviors that are crucial for the target applications. In this section, an application using human body reshaping and facial image manipulation for concealing the identity of individuals while preserving the underlying affect states is discussed. The experiment results demonstrate the effectiveness of our method for visual privacy protection.

6.6.1 Evaluation of human body reshaping with depth sensor network for visual privacy protection

In this section, we evaluate the entire system from data capturing to human reshaping described in Section 6.1 for visual privacy protection. Our hypothesis is that the reshaped video will preserve the naturalness of human movements while obfuscating important soft biometrics such as height and weight for privacy protection. We use the same sequences captured in the lab environment as mentioned in Section 6.5.3. In order to objectively prove our hypothesis, we have devised two tests in measuring the naturalness and privacy preservation of the reshaping results.

In the first test, we have recruited 25 non-expert participants who were not familiar with the four actors in the videos. Each of them was shown 4 video sequences. Each sequence has 4 sub-sequences derived from the same data – the second one was always the original while the other three were different reshaped versions. However, the participants were not aware which was the original, and they were asked to rank the 4 sub-sequences ranging from 1 (least natural) to 4 (most natural). The participants were free to watch all sequences repeatedly.

As the ranks are not independent samples, we utilize the Wilcoxon signed-rank test [189] to analyze the result obtained from the questionnaire. In this two-sample statistical test, we set one sample to be the original video (sub-video 2), and the other one to be each of the reshaped videos. The null hypothesis is that the mean rank of the reshaped videos is the same as that of the original video. Our test results are shown in Figure 6.16, in which the y-axis in (a), (b), (c) and (d) represents the rank scores from the

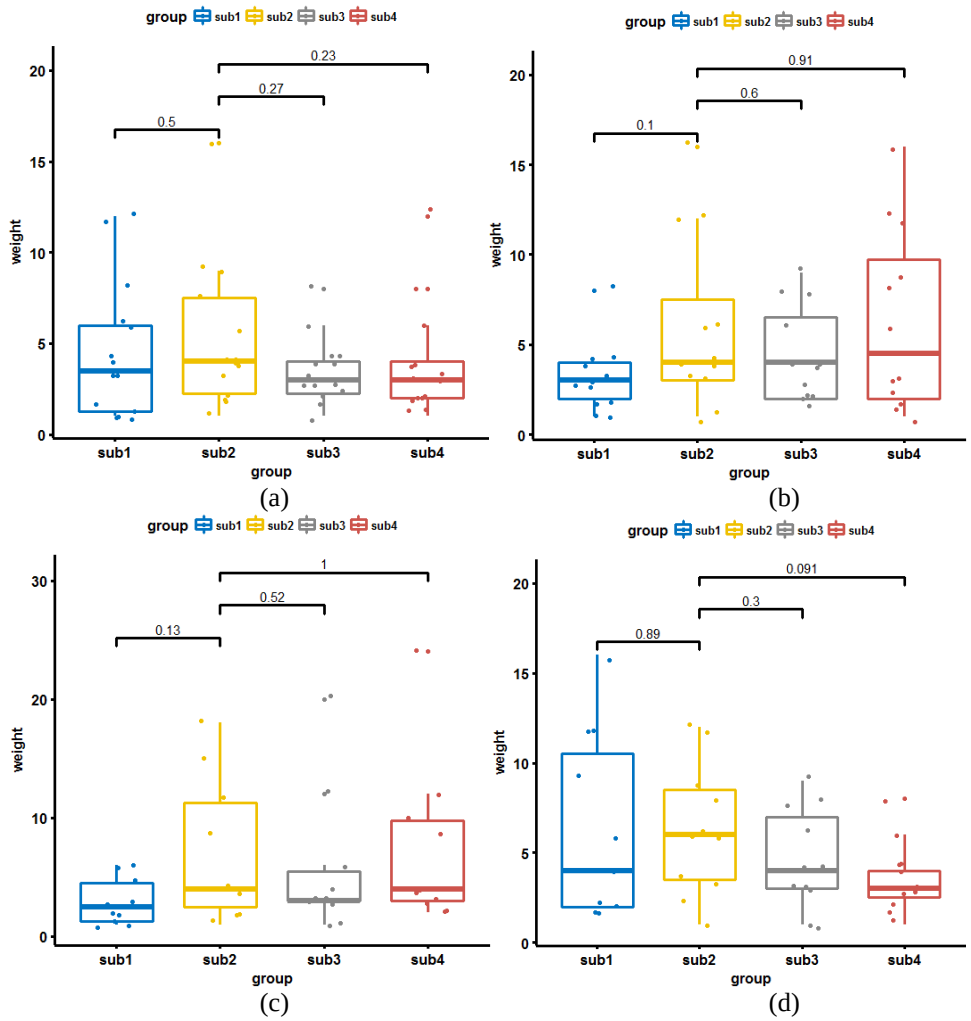

Figure 6.16 Average score of questionnaire results on the naturalness of our reshaping method.

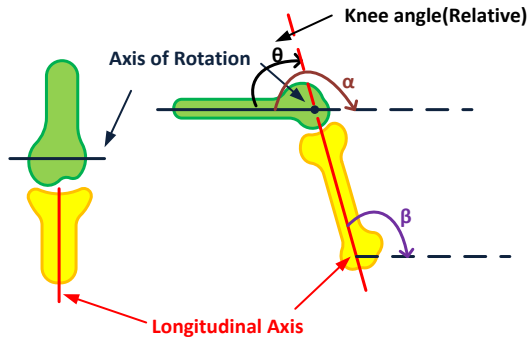

Figure 6.17 Axis of rotation and relative angle of knees.

questionnaire. The p-value of the test for each sub-video paired with the original video is marked on top of each box bar. None of the p-values are significant enough ($p < 0.05$ [50]) to reject the null hypothesis. As such, we conclude that the naturalness of our proposed method for human body reshaping is comparable with the real captured video.

In the second test, we evaluate the capacity of our reshaping method for privacy protection. We use gait analysis as an instance. In particular, the performer is required to first stand as an 'A'-pose and then walk normally towards the depth sensor for a few steps. The motion data are captured and extracted by using our skeleton estimation approach mentioned in Section 6.3.4. We use the foot step or stride length and rotation angle of knees as the gait features for analysis, which has been investigated and proved to be a key measurement for gait recognition in existing work [117].

Foot step: During a walking period, one foot serves as a pivot when the other foot moves, it's half of the stride length. In our experiment, we assume that the pivot foot not move in the short time interval. We compute the foot step by averaging the Euclidean Distance between the locations of left and right foot joint in several intervals.

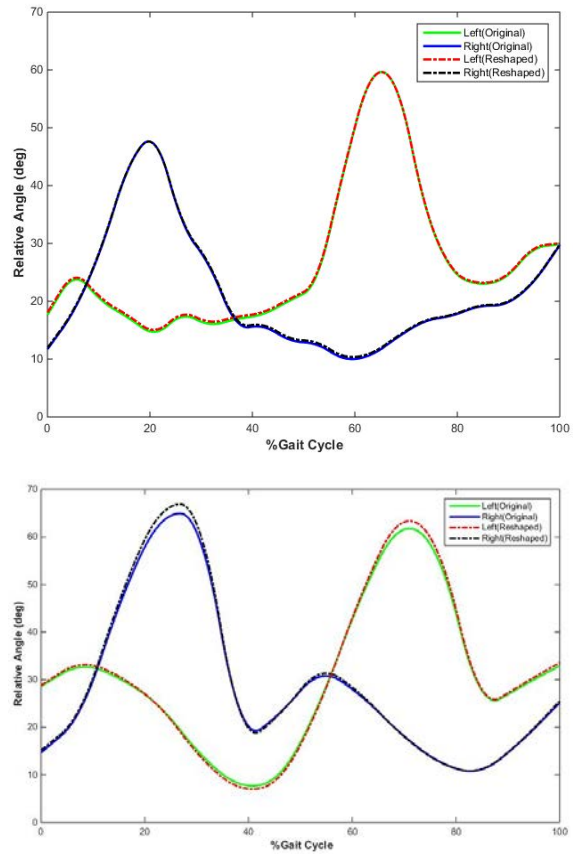

Figure 6.18 Joint Angle in one gait cycle. (a) Sequence1. (b) Sequence2.

Rotation Angle of knees: With the help of the obtained joint position from our system, we calculate the relative angle of left and right knee along the longitudinal axis, as shown in Figure 6.17. The knee angle can be computed as $\theta = \alpha - \beta$. After reshaping, if the foot step is changed to some extent while the relative rotation angle of knee is preserved, which indicates that the soft biometric feature, gait for example, is protected.

We test the effectiveness of our proposed method for privacy protection by capturing two sequences of people walking normally in the room. Figure 6.19 shows the result of foot joint position in one gait cycle before and after reshaping, respectively with different reshaping parameters. In Table 6.1, we show the average step length in several

intervals for different reshaping parameters. Reference to the work proposed by Middleton et al. in [117], we can conclude that the range for stride length used as gait feature to recognize the identity of a person from others is from 640mm~840mm, that is, 320mm~420m for each foot step. In other words, we can assume that the identities of two people are different if the difference of their step length is greater than 20mm. Figure 6.18 shows the result of joint angle of knee in one gait cycle before and after reshaping, respectively.

From Figure 6.19 and Table 6.1, we can see that the foot joint position after reshaping is quite different with that of the original one for two different actors, and the step length changes between 30-80mm according to different reshaping parameters. The significant difference in foot step length between the original and reshaped videos will be able to protect the identity of an individual from a gait biometric identification system. And from Figure 6.18 we can see that the joint angle after reshaping is almost similar with that of the original one for two different actors. The results, therefore, demonstrate the effectiveness of our proposed method for privacy protection.

Table 6.1 Average step length with different reshaping parameters (mm)

Category		Test1	Test2	Test3
Sequence1	Original	361.76	361.76	361.76
	After Reshaping	407.14	339.96	328.76
Sequence2	Original	354.49	354.49	354.49
	After Reshaping	434.40	329.95	299.80

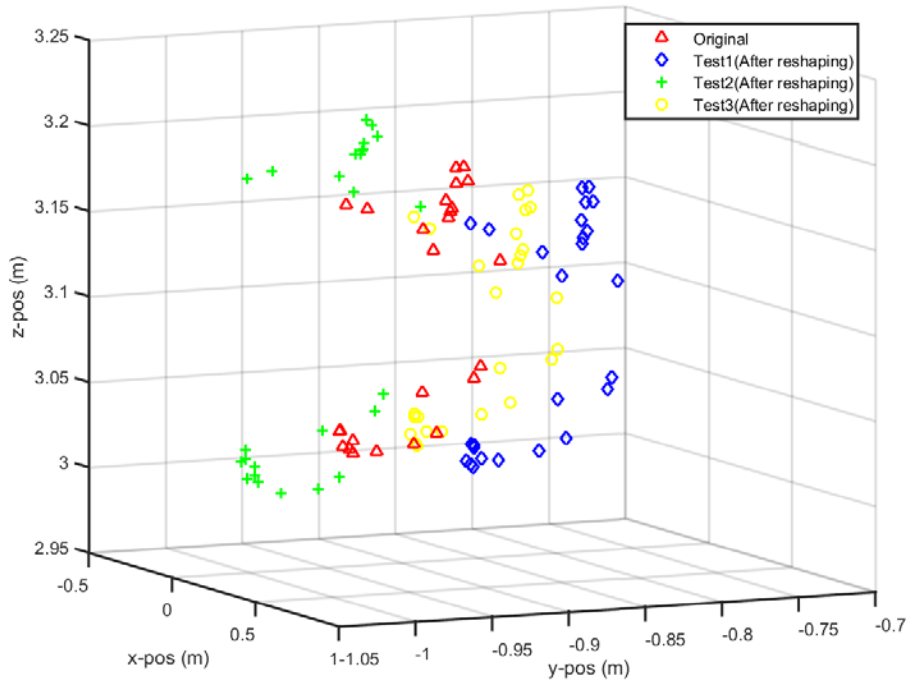

(a)

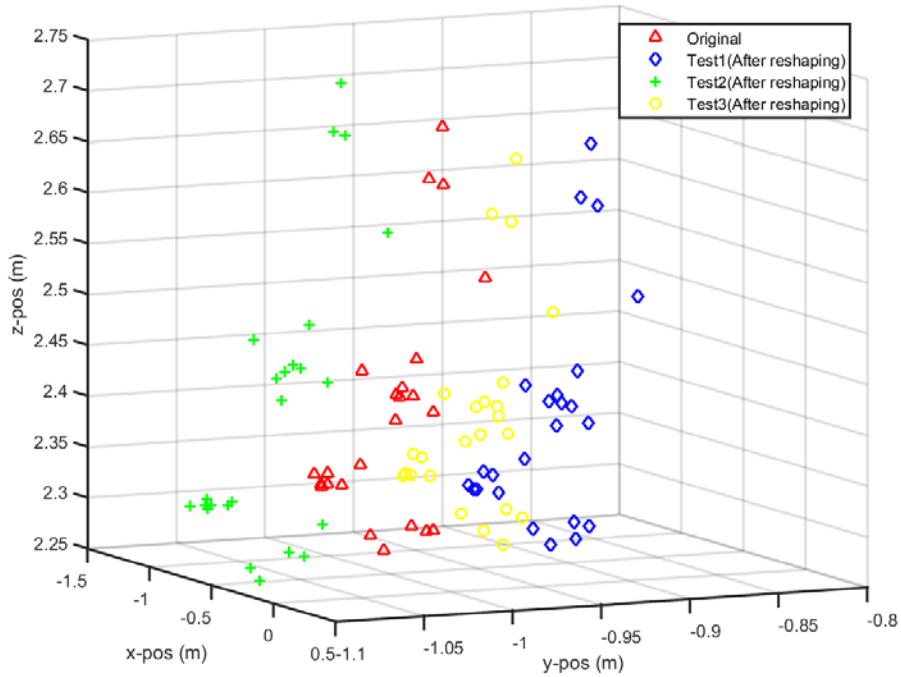

(b)

Figure 6.19 Foot Joint position in one gait cycle. (a) Sequence1. (b) Sequence2.

Chapter 7 Conclusions and Future Work

In this dissertation, I have described several novel systems that can be used to conceal the identity of the person in the captured video frame while preserving the person's pose and facial expression. It has been demonstrated that unlike existing visual privacy protection methods that often lead to loss of significant social cues, my dissertation work provides a way to protect privacy and maintain utility for behavior observation. The key ideas behind the proposed visual privacy protection are reshaping of body shape and facial image manipulation. To the best of knowledge, we are the first to propose the usage of body shape reshaping as an effective solution for visual privacy protection while preserving the underlying affect states.

In addition to the target goal of privacy protection, I have also made fundamental contributions to computer vision. Our proposed pose estimation scheme is robust under heavy occlusion using multiple depth sensors. With a wide-baseline RGB-D camera calibration algorithm, the point set registration procedure with local structure constraints, the rigid bone-based pose transformation and the holes filling scheme, the reconstruction of detailed human model is greatly improved. Even for the case with a single depth sensor, I have presented a new method to accurately estimate the complex movement pose, though the detailed human shape model have been shown to be too difficult to capture. With the help of morphable model, all aforementioned models have been used to reshape a human body through deformation transfer.

I have also presented two approaches for facial image manipulation. The first method combines recoloring and composition of facial component to produce a new face

image while preserving the general configuration of different facial features so as to preserve the expression. The second method transfers both the facial expression and the eye gaze from source input image to target input image by first reconstructing the 3D face from single image in an illumination-invariant manner and then capturing person specific details with a coarse-to-fine scheme. The final manipulated output images have demonstrated the effectiveness of our system.

In the future, I plan to improve the speed of the system for pose estimation to make it run in real-time and improve eye gaze rendering by taking reflection caused by local illumination into consideration. In addition, more challenging tasks such as multiple people interacting, detailed human model from one depth sensor, will be investigated.

Bibliography

[1] M. Afifi and K. F. Hussain, MPB: A modified poisson blending technique. *Springer Comput. Vis. Media*, pages 331–341, 2015.

[2] A. Agarwal and B. Triggs. Recovering 3d human pose from monocular images. *IEEE Trans. Pattern Anal. Mach. Intell.*, pages 44–58, 2006.

[3] P. Agrawal and P. J. Narayanan. Person de-identification in videos. *IEEE Trans. Circuits Syst. Video Technol.*, 2011.

[4] E. de Aguiar, C. Stoll, C. Theobalt, N. Ahmed, H. P. Seidel, and S. Thrun. Performance capture from sparse multi-view video. *ACM Trans. Graph., (Proc. of SIG-GRAPH)*, pages 1-10, 2008.

[5] D. S. Alexiadis, D. Zarpalas, and P. Daras. Real-time, full 3-d reconstruction of moving foreground objects from multiple consumer depth cameras. *IEEE Trans. Multimedia*, vol. 15, no. 2, pp. 339–358, 2013.

[6] B. Allen, B. Curless, and Z. Popovic. The space of human body shapes: Reconstruction and parameterization from range scans. *ACM Trans. Graph., (Proc. of SIG-GRAPH)*, pages 587-594, 2003.

[7] B. Allen, B. Curless, Z. Popović, and A. Hertzmann. 2006. Learning a correlated model of identity and pose-dependent body shape variation for real-time synthesis. In: *Proc. ACM SIGGRAPH/Eurographics Symp. on Comp. Anim.*, pages 147–156, 2006.

[8] M. Andriluka, L. Pishchulin, P. Gehler, and B. Schiele. 2d human pose estimation: New benchmark and state of the art analysis. In *IEEE Conf. on Comput. Vision and Patt. Recog (CVPR)*, 2014.

[9] M. Andriluka, S. Roth, and B. Schiele. Monocular 3d pose estimation and tracking by detection. In *IEEE Conf. on Comput. Vision and Patt. Recog (CVPR)*, 2010.

[10] D. Anguelov, P. Srinivasan, D. Koller, S. Thrun, J. Rodgers, and J. Davis. SCAPE: Shape completion and animation of people. In *ACM Trans. Graph., (Proc. of SIG-GRAPH)*, pages 408–416, New York, NY, USA, 2005.

[11] A. Asthana, S. Zafeiriou, S. Cheng, and M. Pantic. Robust discriminative response map fitting with constrained local models. In *IEEE Conf. on Comput. Vision and Patt. Recog (CVPR)*, 2013.

[12] J. J. Atick, P. A. Griffin, and N. A. Redlich. Statistical approach to shape from shading: Reconstruction of 3d face surfaces from single 2d images. *Neural Computation*, pages 1321–1340, 1996.

[13] A. Baak, M. Muller, G. Bharaj, H.-P. Seidel, and C. Theobalt. A data-driven approach for real-time full body pose reconstruction from a depth camera. In *IEEE International Conference on Computer Vision (ICCV)*, pages 1092–1099, 2011.

[14] M.C. Bakkay, M. Arafa, and E. Zagrouba. Dense 3D SLAM in dynamic scenes using Kinect. In *Proceedings of 7th Iberian Conference on Pattern Recognition and Image Analysis*, Santiago de Compostela, Spain, 17–19 June 2015; pp. 121–129.

[15] A. Balan, L. Sigal, M. Black, J. Davis, and H. Haussecker. Detailed human shape and pose from images. In *IEEE Conf. on Comput. Vision and Patt. Recog (CVPR)*, 2007.

[16] V. Belagiannis, S. Amin, M. Andriluka, B. Schiele, N. Navab, and S. Ilic. 3d pictorial structures for multiple human pose estimation. In *IEEE Conf. on Comput. Vision and Patt. Recog (CVPR)*, 2014.

[17] I. Baran and J. Popovic. Automatic rigging and animation of 3d characters. *ACM Trans. Graph., (Proc. of SIG-GRAPH)*, 2007.

[18] P. J. Besl and N. D. McKay. A method for registration of 3-d shapes. *IEEE Trans. Pattern Anal. Mach. Intell.*, pages 239–256, 1992.

[19] C. M. Bishop. Neural Networks for Pattern Recognition, *Oxford University Press, Inc.*, New York, NY, USA, 1995.

[20] D. Bitouk, N. Kumar, S. Dhillon, P. Belhumeur, and S. K. Nayar. Face swapping: Automatically replacing faces in photographs. In *ACM Trans. Graph., (Proc. of SIG- GRAPH)*, pages 1–8, 2008.

[21] V. Blanz and T. Vetter. Face recognition based on fitting a 3D morphable model. *IEEE Trans. Pattern Anal. Mach. Intell.*, pages 1063–1074, 2003.

[22] A. Bleiweiss, E. Kutliroff, and G. Eilat. Markerless motion capture using a single depth sensor. In *ACM SIGGRAPH ASIA Sketches*, 2009.

[23] F. Bogo, A. Kanazawa, C. Lassner, P. Gehler, J. Romero, and M. J. Black. Keep it smpl: Automatic estimation of 3d human pose and shape from a single image. In *European Conf. on Comput. Vision (ECCV)*, pages 561–578, 2016.

[24] J. Booth, E. Antonakos, S. Ploumpis, G. Trigeorgis, Y. Panagakis, and S. Zafeiriou. 3D face morphable models “in-the-wild”. In *IEEE Conf. on Comput. Vision and Patt. Recog (CVPR)*, 2017.

[25] M. Burenius, J. Sullivan, and S. Carlsson. 3d pictorial structures for multiple view articulated pose estimation. In *IEEE Conf. on Comput. Vision and Patt. Recog (CVPR)*, 2013.

[26] N. Burrus, Nicolas Burrus Homepage: Kinect Calibration. http://nicolas.burrus.name/index.php/Research/KinectCalibration. Accessed February 5, 2017.

[27] Z. Cao, T. Simon, S.-E. Wei, and Y. Sheikh. Realtime multi-person 2d pose estimation using part affinity fields. arXiv:1611.08050v1, 2016

[28] Z. Cao, T. Simon, S. -E. Wei, and Y. Sheikh. Realtime multi-person 2d pose estimation using part affinity fields. In *IEEE Conf. on Comput. Vision and Patt. Recog (CVPR)*, 2017.

[29] C. Cao, Y. Weng, S. Lin, and K. Zhou. 3D shape regression for real-time facial animation. *ACM Trans. Graph., (Proc. of SIG-GRAPH)*, 2013.

[30] C. Cao, Y. Weng, S. Zhou, Y. Tong, and K. Zhou. Facewarehouse: A 3d facial expression database for visual computing. *IEEE Trans. Vis. Comput. Graph.*, pages 413–425, 2014.

[31] Z. Cao, T. Simon, S.-E. Wei, and Y. Sheikh. Realtime multi-person 2d pose estimation using part affinity fields. In *IEEE Conf. on Comput. Vision and Patt. Recog (CVPR)*, 2017.

[32] Y. Chen, Z. Cheng, and R. R. Martin. Parametric editing of clothed 3d avatars. *Visual Comput*, pages 1405-1414, 2016.

[33] Y. Chen, Z. Liu, and Z. Zhang. Tensor-based human body modeling. In *IEEE Conf. on Comput. Vision and Patt. Recog (CVPR)*, pages 105-112, 2013.

[34] X. Chen and A. Yuille. Articulated pose estimation with image-dependent preference on pairwise relations. In *Proc. NIPS*, 2014.

[35] X. Chu, W. Yang, W. Ouyang, C. Ma, A. L. Yuille, and X. Wang. Multi-context attention for human pose estimation. arXiv preprint arXiv:1702.07432, 2017.

[36] https://www.cgal.org

[37] https://en.wikipedia.org/wiki/Delaunay_triangulation

[38] M. Dantone, J. Gall, C. Leistner, and L. van Gool. Body parts dependent joint regressors for human pose estimation in still images. *IEEE Trans. Pattern Anal. Mach. Intell.*, 2014.

[39] A. Dempster, N. Laird, and D. Rubin. Maximum likelihood from incomplete data via the (EM) Algorithm. *Journal of the Royal Statistical Society. Series B (Methodological)*, pages 1-38, 1977.

[40] E. Dibra, H. Jain, C. O¨ztireli, R. Ziegler, and M. Gross, HS-Nets: Estimating human body shape from silhouettes with convolutional neural networks. In *3D Vision (3DV)*, 2016.

[41] D. Doria and R. J. Radke. Filling large holes in lidar data by inpainting depth gradients. In *IEEE Conf. on Comput. Vision and Patt. Recog Workshops (CVPRW)*, pages 65–72, 2012.

[42] M. Dou, S. Khamis, Y. Degtyarev, P. Davidson, S. R. Fanello, A. Kowdle, S. O. Escolano, C. Rhemann, D. Kim, J. Taylor, et al. Fusion4d: real-time performance capture of challenging scenes. *ACM Trans. Graph., (Proc. of SIG-GRAPH)*, 35(4):114, 2016.

[43] P. Dou, S. K. Shah, and I. A. Kakadiaris. End-to-end 3D face reconstruction with deep neural networks. In *IEEE Conf. on Comput. Vision and Patt. Recog (CVPR)*, 2017.

[44] R. Dovgard and R. Basri. Statistical symmetric shape from shading for 3D structure recovery of faces. In *European Conf. on Comput. Vision (ECCV)*, 2004.

[45] J. Fan, H. Luo, M.-S. Hacid, and E. Bertino. A novel approach for privacy-preserving video sharing. In: *Proc. CIKM*, pages 609–616, 2005.

[46] H.-S. Fang, S. Xie, Y.-W. Tai, and C. Lu. RMPE: Regional multi-person pose estimation. In *IEEE International Conference on Computer Vision (ICCV)*,, 2017.

[47] V. Ferrari, M. Marin-Jimenez, and A. Zisserman, Progressive Search Space Reduction for Human Pose Estimation. In *IEEE Conf. on Comput. Vision and Patt. Recog (CVPR)*, 2008.

[48] V. Ferrari, M. Marın-Jimenez, and A. Zisserman. 2d human pose estimation in tv shows. In *Statistical and Geometrical Approaches to Visual Motion Analysis*, pages 128–147, 2009.

[49] D. Fidaleo and G. Medioni. Model-assisted 3D face reconstruction from video. *Lecture Notes in Computer Science*, pages 124–138, 2007.

[50] R.A. Fisher, Statistical methods and scientific inference. Math. Gaz. 1956, 58, 297. Available online: http://psycnet.apa.org/record/1957-00078-000 (accessed on 9 January 2018).

[51] A. Feng, D. Casas, A. Shapiro. Avatar reshaping and automatic rigging using a deformable model. In: *Proceedings of the 8th ACM SIGGRAPH Conference on Motion in Games*, pages 57–64, 2015.

[52] S. Fleishman, I. Drori, and D. Cohen-Or. Bilateral Mesh Denoising. *ACM Trans. Graph., (Proc. of SIG-GRAPH)*, vol. 22, no.3, New York, pages 950-953, July 2003.

[53] A. Flores and S. Belongie. Removing pedestrians from Google street view images. In: *International Workshop on Mobile Vision*, June 2010.

[54] J. J. Fu, D. Miao, W. R. Yu, S. Q. Wang, Y. Lu, and S. P. Li. Kinect-Like Depth Data Compression. *IEEE Trans. Multimed*, pages 1340–1352, 2013.

[55] J. Gall, C. Stoll, E. de Aguiar, C. Theobalt, B. Rosenhahn, and H.-P. Seidel. Motion capture using joint skeleton tracking and surface estimation. In *IEEE Conf. on Comput. Vision and Patt. Recog (CVPR)*, pages1746–1753, 2009.

[56] V. Ganapathi, C. Plagemann, S. Thrun, and D. Koller. Real time motion capture using a single time-of-flight camera. In *IEEE Conf. on Comput. Vision and Patt. Recog (CVPR)*, pages 755-762, 2010.

[57] V. Ganapathi, C. Plagemann, D. Koller, and S. Thrun. Real-time human pose tracking from range data. In *European Conf. on Comput. Vision (ECCV)*, pages 738–751, 2012.

[58] S. Ge and G. Fan. Non-rigid articulated point set registration with Local Structure Preservation. In *Proc. IEEE Conf. Comput. Vis. Pattern Recognit. Work. (CVPRW)*, pages 126-133, 2015.

[59] G. Gkioxari, B. Hariharan, R. Girshick, and J. Malik. Using k-poselets for detecting people and localizing their keypo-ints. In *IEEE Conf. on Comput. Vision and Patt. Recog (CVPR)*, 2014.

[60] R. Gross, E. Airoldi, B. Malin, and L. Sweeney. Integrating utility into face de-identification. In *Workshop on Privacy Enhancing Technologies (PET)*, pages 227– 242, June 2005.

[61] R. Gross, L. Sweeney, F. de la Torre, and S. Baker. Model-based face de-identification. In *IEEE Workshop on Privacy Research in Vision*, 2006.

[62] P. Guan, A. Weiss, A. O. Balan, and M. J. Black. Estimating human shape and pose from a single image. In *IEEE International Conference on Computer Vision (ICCV)*, 2009.

[63] N. Hasler, C. Stoll, M. Sunkel, B. Rosenhahn, H.-P. Seidel. 2009. A statistical model of human pose and body shape. In *Comput. Graph. Forum*, volume 28, pages 337– 346, 2009.

[64] G.R. Hayes and G. D. Abowd. Tensions in designing capture technologies for an evidence-based care community. In: *Proceedings of the SIGCHI Conference on Human Factors in Computing Systems*, pages 937–946, 2006.

[65] G.R. Hayes, L. M. Gardere, G. D. Abowd, and K. N. Truong. Carelog: A selective archiving tool for behavior management in schools. In *Proceedings of the SIGCHI Conference on Human Factors in Computing Systems*, pages 685–694, 2008.

[66] G. R. Hayes and K. N. Truong. Selective archiving: A model for privacy sensitive capture and access technologies. In *Protecting Privacy in Video Surveillance*, pages 165–184, 2009.

[67] L. He and S. Schaefer. Mesh denoising via l0 minimization. *ACM Trans. Graph., (Proc. of SIG-GRAPH)*, 1–8 2013.

[68] T. Helten, A. Baak, G. Bharaj, M. Muller, H.-P. Seidel, and C. Theobalt. Personalization and evaluation of a real-time depth-based full body tracker. In *3D Vision (3DV)*, pages 279–286, 2013.

[69] T. Helten, A. Baak, M. Muller, and C. Theobalt. Full-body human motion capture from monocular depth images. In *Time-of-Flight and Depth Imaging. Sensors, Algorithms, and Applications*, pages 188–206, 2013.

[70] T. Helten, M. Muller, H. Seidel, and C. Theobalt. Real-time body tracking with one depth camera and inertial sensors. In *IEEE International Conference on Computer Vision (ICCV)*, 2013.

[71] D. Hogg. Model-based vision: A program to see a walking person. *Image and Vision Computin*g, pages 5–20, 1983.

[72] B. K. P. Horn. Closed-form solution of absolute orientation using unit quaternions. *Journal of the Optical Society of America*, 1987.

[73] B. Horn. Obtaining shape from shading information. In *P. Winston, editor, The Psychology of Computer Vision*, 1975.

[74] P.-L. Hsieh, C. Ma, J. Yu, and H. Li. Unconstrained realtime facial performance capture. In *IEEE Conf. on Comput. Vision and Patt. Recog (CVPR)*, 2015.

[75] C.H. Huang, E. Boyer, N. Navab, and S. Ilic. Human shape and pose tracking using keyframes. In *IEEE Conf. on Comput. Vision and Patt. Recog (CVPR)*, pages 3446–3453, June 2014.

[76] G. B. Huang, M. Ramesh, T. Berg, and E. Learned-miller. Labeled faces in the wild: A database for studying face recognition in unconstrained environments. In *European Conf. on Comput. Vision Workshop (ECCVW) on Faces in Real-life Images*, 2008.

[77] H. Huang, D. Li, H. Zhang, U. Ascher, and D. Cohen-Or. Consolidation of unorganized point clouds for surface reconstruction. *ACM Trans. Graph., (Proc. of SIG-GRAPH)*, pages 176:1–176:78, 2009.

[78] H. Huang, S. Wu, M. Gong, D. Cohen-Or, U. Ascher, and H. Zhang. Edge-aware point set resampling. *ACM Trans. Graph., (Proc. of SIG-GRAPH)*, pages 1–12, 2013.

[79] http://fei.edu.br/~cet/facedatabase.html.

[80] A. Ichim, S. Bouaziz, and M. Pauly. Dynamic 3D avatar creation from hand-held video input. In *ACM Trans. Graph., (Proc. of SIG- GRAPH)*, pages 1–14, 2015.

[81] E. Insafutdinov, L. Pishchulin, B. Andres, M. Andriluka, and B. Schiele. Deepercut: A deeper, stronger, and faster multi-person pose estimation model. In *European Conf. on Comput. Vision (ECCV)*, 2016.

[82] U. Iqbal, A. Milan, and J. Gall. Posetrack: Joint multi-person pose estimation and tracking. In *IEEE Conf. on Comput. Vision and Patt. Recog (CVPR)*, 2017.

[83] A. Jacobson, I. Baran, J. Popovi´c, and O. Sorkine. Bounded biharmonic weights for real-time deformation. *ACM Trans. Graph., (Proc. of SIG-GRAPH)*, 2011.

[84] A. Jain, T. Thormählen, H.-P. Seidel, C. Theobalt. MovieReshape: Tracking and reshaping of humans in videos. *ACM Trans. Graph., (Proc. of SIG-GRAPH)*, pages 148:1-148:10, 2010.

[85] H. Jiang and D. Martin. Global pose estimation using non-tree models. In *IEEE Conf. on Comput. Vision and Patt. Recog (CVPR)*, 2008.

[86] L. Jiang, J. Zhang, B. Deng, H. Li, and L. Liu. 3d face reconstruction with geometry details from a single image. *arXiv preprint arXiv: 1702.05619*, 2017.

[87] S. Johnson and M. Everingham. Learning effective human pose estimation from inaccurate annotation. In *IEEE Conf. on Comput. Vision and Patt. Recog (CVPR)*, 2011.

[88] H. Joo, T. Simon, X. Li, H. Liu, L. Tan, L. Gui, S. Banerjee, T. Godisart, B. Nabbe, I. Matthews, et al. Panoptic studio: A massively multiview system for social interaction capture. *IEEE Trans. Pattern Anal. Mach. Intell.*, 2017.

[89] H. Joo, T. Simon, and Y. Sheikh. Total Capture: A3D deformation model for tracking faces, hands, and bodies. arXiv preprint arXiv:1801.01615, 2018.

[90] A. Jourabloo, X. Yin, and X. Liu. Attribute preserved face de-identification. In *International Conference on Biometrics (ICB)*, pages 278– 285, 2015.

[91] A. Kanazawa, M. J. Black, D. W. Jacobs, and J. Malik. End-to-end recovery of human shape and pose. In *IEEE Conf. on Comput. Vision and Patt. Recog (CVPR)*, 2018.

[92] S. Katz, A. Tal, and R. Basri. Direct visibility of point sets. *ACM Trans. Graph., (Proc. of SIG-GRAPH)*, 2007.

[93] M. Kazhdan, M. Bolitho, and H. Hoppe. Poisson surface reconstruction. In *Proc. of the Eurographics Symposium on Geometry Processing*, 2006.

[94] I. Kemelmacher-Shlizerman and R. Basri. 3D face reconstruction from a single image using a single reference face shape. *IEEE Trans. Pattern Anal. Mach. Intell.*, pages 394–405, 2011.

[95] I. Kemelmacher-Shlizerman and S. M. Seitz. Face reconstruction in the wild. In *IEEE International Conference on Computer Vision (ICCV)*, 2011.

[96] Kinect For Windows SDK 2.0. http://www. microsoft.com/en-us/kinectforwindows/ develop/.

[97] C. -C. Kuo, and H. -T. Yau. A Delaunay-Based Region-Growing Approach to Surface Reconstruction from Unorganized Points. *Computer-Aided Design*, vol. 37, no. 8, pages 825-835, 2005.

[98] E. Lachat, H. Macher, T. Landes, and P. Grussenmeyer. Assessment and Calibration of a RGB-D Camera (Kinect v2 Sensor) Towards a Potential Use for Close-Range 3D Modeling. *Remote Sensing*, vol. 7, no. 10, pages 13070–13097, 2015.

[99] L. Ladicky, P. H. S. Torr, and A. Zisserman. Human pose estimation using a joint pixel-wise and part-wise formulation. 2013.

[100] S. R. H. Langton, R.J. Watt, and V. Bruce. Do the eyes have it? Cues to the direction of social attention. *Trends in cognitive sciences*, pages 50-59, 2000.

[101] B. H. Le and Z. Deng. Smooth skinning decomposition with rigid bones. *ACM Trans. Graph., (Proc. of SIG-GRAPH)*, pages 199:1– 199:10, 2012.

[102] B. H. Le and Z. Deng. Robust and accurate skeletal rigging from mesh sequences. *ACM Trans. Graph., (Proc. of SIG-GRAPH)*, pages 84:1–84:10, 2014.

[103] S. Lee, K. Park, and J. Kim. A SfM-based 3D face recon- struction method robust to self-occlusion by using a shape conversion matrix. *Pattern Recognition*, pages 1470 – 1486, 2011.

[104] G. Letournel, A. Bugeau, V. T. Ta, and J. P. Domenger. Face de-identification with expressions preservation. In: *IEEE International Conference on Image Processing (ICIP)*, pages 4366-4370, 2015.

[105] H. Li, B. Adams, L.J. Guibas, M. Pauly. Robust Single-View Geometry and Motion Reconstruction. *ACM Trans. Graph., (Proc. of SIG-GRAPH)*, volume 28, pages 1-10, 2009.

[106] H. Li, T. Weise, and M. Pauly. Example-based facial rigging. *ACM Trans. Graph., (Proc. of SIG-GRAPH)*, vol. 29, no. 4, pages 1–6, Jul. 2010.

[107] K. Li, F. Xu, J. Wang, Q. Dai, and Y. Liu. A data-driven approach for facial expression synthesis in video. In *IEEE Conf. on Comput. Vision and Patt. Recog (CVPR)*, pages 57–64, 2012.

[108] S. Li, W. Zhang and A. B. Chan. Maximum-Margin Structured Learning with Deep Networks for 3D Human Pose Estimation. In *IEEE International Conference on Computer Vision (ICCV)*, 2015.

[109] Y. Lin, S. Wang, Q. Lin, and F. Tang. Face swapping under large pose variations: A 3D model based approach. In *IEEE International Conference on Multimedia and Expo (ICME)*, pages 333–338, July 2012.

[110] Y. Liu, J. Gall, C. Stoll, Q. Dai, H.P. Seidel, and C. Theobalt. Markerless motion capture of multiple characters using multiview image segmentation. *IEEE Trans. Pattern Anal. Mach. Intell.*, pages 2720–2735, 2013.

[111] Z. Liu, Z. Lin, X. Wei and S. –C. Chan. A new model-based method for multi-view human body tracking and its application to view transfer in image-based rendering. *IEEE Trans. Multimedia, (Early access)*, 2017.

[112] Y. Liu, C. Stoll, J. Gall, H.-P. Seidel, and C. Theobalt. Markerless motion capture of interacting characters using multi-view image segmentation. In *IEEE Conf. on Comput. Vision and Patt. Recog (CVPR)*, pages 1249–1256, 2011.

[113] X. Lu, X. Liu, Z. Deng, and W. Chen. An efficient approach for feature-preserving mesh denoising. *Opt. Lasers Eng.*, 2017.

[114] S. Lu, X. Ren, and F. Liu. Depth enhancement via low-rank matrix completion. In *IEEE Conf. on Comput. Vision and Patt. Recog (CVPR)*, June 2014.

[115] Y. Luo and S.-C.S. Cheung. Privacy information management for video surveillance. In: *Proceedings of SPIE–The International Society for Optical Engineering*, 2013.

[116] M. A. Magnor, O. Grau, O. Sorkine-Hornung, C. Theobalt. Digital Representations of the Real World: How to Capture Model and Render Visual Reality, *A K Peters*, 2015.

[117] L. Middleton, A. Buss, A. Bazin, and M. Nixon. A floor sensor system for gait recognition. In *Proc. 4th IEEE Workshop Autom. Identification Adv. Technol.*, Buffalo, NY, USA, Oct. 2005, pp. 171–176.

[118] T. Moeslund, A. Hilton, and V. Krger. A survey of advances in vision-based human motion capture and analysis. *Computer Vision and Image Understanding*, pages 90-126, 2006.

[119] S. Mosaddegh, L. Simon, and F. Jurie. Photorealistic face de-identification by aggregating donors' face components. *Asian Conference on Computer Vision (ACCV)*, pages 1–16, 2014.

[120] A. Myronenko and X. Song. Point set registration: Coherent point drift. *IEEE Trans. Pattern Anal. Mach. Intell.*, pages 2262-2275, 2010.

[121] R. A. Newcombe, D. Fox, and S. M. Seitz. DynamicFusion: Reconstruction and tracking of non-rigid scenes in real-time. In *IEEE Conf. on Comput. Vision and Patt. Recog (CVPR)*, pages 343–352, June 2015.

[122] R. Newcombe, A. Davison, S. Izadi, P. Kohli, O. Hilliges, J. Shotton, D. Molyneaux, S. Hodges, D. Kim, and A. Fitzgibbon. KinectFusion: Real-time dense surface mapping and tracking. In *Proc. IEEE Int. Symp. Mixed Augmented Reality*, pages 127–136, 2011.

[123] A. Newell, Z. Huang, and J. Deng. Associative embedding: End-to-end learning for joint detection and grouping. In *Proc. NIPS*, 2017.

[124] A. Newell, K. Yang, and J. Deng. Stacked hourglass networks for human pose estimation. In *European Conf. on Comput. Vision (ECCV)*, 2016.

[125] E. M. Newton, L. Sweeney, and B. Malin. Preserving privacy by de-identifying face images. *IEEE Transactions on Knowledge and Data Engineering*, pages 232–243, 2005.

[126] A. Nodari, M. Vanetti, and I. Gallo. Digital privacy: Replacing pedestrians from Google street view images. In *International Conference on Pattern Recognition (ICPR)*, pages 2889—2893, 2012.

[127] J. R. Padilla-Lopez, A. A. Chaaraoui, and F. Florez-Revuelta. Visual privacy protection methods: A survey. *Expert Syst. Appl.*, pages 4177–4195, 2015.

[128] J. R. Padilla-Lopez, A. A. Chaaraoui, F. Gu, and F. Flórez-Revuelta. Visual privacy by context: Proposal and evaluation of a level-based visualisation scheme. *Sensors*, pages 12959– 12982, 2015.

[129] G. Papandreou, T. Zhu, L. -C. Chen, S. Gidaris, J. Tompson, and K. Murphy. PersonLab: Person Pose Estimation and Instance Segmentation with a Bottom-Up, Part-Based, Geometric Embedding Model. *Technical report*, arxiv: 1803.08225, 2018.

[130] G. Papandreou, T. Zhu, N. Kanazawa, A. Toshev, J. Tompson, C. Bregler, and K. Murphy. Towards accurate multi-person pose estimation in the wild. In *IEEE Conf. on Comput. Vision and Patt. Recog (CVPR)*, 2017.

[131] P. Paysan, R. Knothe, B. Amberg, S. Romdhani, and T. Vetter. A 3d face model for pose and illumination invariant face recognition. In *Advanced Video and Signal Based Surveillance*, pages 296–301, 2009.

[132] P. Perez, M. Gangnet, and A. Blake. Poisson image editing. *ACM Trans. Graph., (Proc. of SIG-GRAPH)*, pages 313–318, 2003.

[133] T. Pfister, J. Charles, and A. Zisserman. Flowing convnets for human pose estimation in videos. In *IEEE International Conference on Computer Vision (ICCV)*, 2015.

[134] L. Pishchulin, M. Andriluka, P. Gehler, and B. Schiele. Strong appearance and expressive spatial models for human pose estimation. In *IEEE International Conference on Computer Vision (ICCV)*, 2013.

[135] L. Pishchulin, S. Wuhrer, T. Helten, C. Theobalt, and B. Schiele. Building statistical shape spaces for 3d human modeling. *Pattern Recognition*, pages 276–286, 2017.

[136] R. Poppe. Vision-based human motion analysis: An overview. *Computer Vision and Image Understanding*, pages 4-18, 2007.

[137] V. Ramakrishna, D. Munoz, M. Hebert, J. A. Bagnell, and Y. Sheikh. Pose machines: Articulated pose estimation via inference machines. In *European Conf. on Comput. Vision (ECCV)*, 2014.

[138] D. Ramanan. Learning to parse images of articulated bodies. In *Neural Information and Processing Systems*, 2006.

[139] E. Reinhard, M. Adhikhmin, B. Gooch, and P. Shirley. Color transfer between images. *IEEE Computer Graphics and Applications*, pages 34–41, 2001.

[140] S. Ren, X. Cao, Y. Wei, and J. Sun. Face alignment at 3000 fps via regressing local binary features. In *IEEE Conf. on Comput. Vision and Patt. Recog (CVPR)*, 2014.

[141] H. Rhodin, N. Robertini, D. Casas, C. Richardt, H. -P. Seidel, and C. Theobalt. General automatic human shape and motion capture using volumetric contour cues. In *European Conf. on Comput. Vision (ECCV)*, 2016.

[142] S. Ribaric, A. Ariyaeeinia, and N. Pavesic. De-identification for privacy protection in multimedia content: A survey. *Signal Processing: Image Communication*, pages 131–151, 2016.

[143] E. Richardson, M. Sela, and R. Kimmel. 3d face reconstruction by learning from synthetic data. In *Int. Conf. on 3D Vision*, 2016.

[144] E. Richardson, M. Sela, R. Or-El, and R. Kimmel. Learning detailed face reconstruction from a single image. In *IEEE Conf. on Comput. Vision and Patt. Recog (CVPR)*, pages 1259– 1268, 2017.

[145] N. Robertini, D. Casas, H. Rhodin, H.-P. Seidel, and C. Theobalt. Model-based outdoor performance capture. In *3D Vision (3DV)*, pages 166–175, 2016.

[146] J. Roth, Y. Tong, and X. Liu. Unconstrained 3D face reconstruction. In *IEEE Conf. on Comput. Vision and Patt. Recog (CVPR)*, 2015.

[147] J. Roth, Y. Tong, and X. Liu. Adaptive 3D face reconstruction from unconstrained photo collections. In *IEEE Conf. on Comput. Vision and Patt. Recog (CVPR)*, 2016.

[148] N. Ruchaud and J. L. Dugelay. De-genderization by body contours reshaping. In *2017 IEEE International Conference on Identity, Security and Behavior Analysis (ISBA)*, pages 1-6, 2017.

[149] M. Saini, P. Atrey, S. Mehrotra, and M. Kankanhalli. W^3-privacy: Understanding what, when, and where inference channels in multi-camera surveillance video. *Multimed. Tools Appl.*, pages 135–158, 2014.

[150] J. M. Saragih, S. Lucey, and J. F. Cohn. Real-time avatar animation from a single image. In *Int. Conf. on Automatic Face and Gesture Recognition*, pages 117–124, 2011.

[151] Y. A. Sekhavat. Privacy preserving cloth try-on using mobile augmented reality. *IEEE Trans. Multimedia*, pages 1041-1049, 2017.

[152] M. Sela, E. Richardson, and R. Kimmel. Unrestricted facial geometry reconstruction using image-to-image translation. In *IEEE International Conference on Computer Vision (ICCV)*, 2017.

[153] A. Senior, S. Pankanti, A. Hampapur, L. Brown, Y.-L. Tian, and A. Ekin. Blinkering surveillance: Enable video privacy through computer vision. *IBM, Research report*, August 2003.

[154] H. Seo, F. Cordier, and N. Magnenat-Thalmann. Synthesizing Animatable Body Models with Parameterized Shape Modifications. In: *Proc. ACM SIGGRAPH/Eurographics Symp. Computer Animation*, pages 120-125, 2003.

[155] J. Shen, W. Xu, Y. Luo, P.-C. Su, and S.-C.S. Cheung. Extrinsic calibration for wide-baseline RGB-D camera network. In *IEEE International Workshop on Multimedia Signal Processing (MMSP)*, 2014.

[156] J. Shotton, A. Fitzgibbon, M. Cook, T. Sharp, M. Finocchio, R. Moore, A. Kipman, and A. Blake. Real-time human pose recognition in parts from a single depth image. In *IEEE Conf. on Comput. Vision and Patt. Recog (CVPR)*, 2011.

[157] L. Sigal, A. Balan, and M. Black. Humaneva: Synchronized video and motion capture data set and baseline algorithm for evaluation of articulated human motion. *Int'l J. Computer Vision*, pages 4-27, 2010.

[158] L. Sigal, A. Balan, M. J. Black. Combined discriminative and generative articulated pose and non-rigid shape estimation. In *Advances in Neural Information Processing Systems (NIPS)*. pages 1337–1344, 2008.

[159] M. Song, Z. Dong, C. Theobalt, H. Wang, Z. Liu, and H.-P. Seidel. A generic framework for efficient 2d and 3d facial expression analogy. *IEEE Trans. Multimedia*, pages 1384–1395, 2007.

[160] R. W. Sumner and J. Popovic. Deformation transfer for triangle meshes. *ACM Trans. Graph., (Proc. of SIG-GRAPH)*, pages 399–405, 2004.

[161] S. Suwajanakorn, I. Kemelmacher-Shlizerman, and S. M. Seitz. Total moving face reconstruction. In *European Conf. on Comput. Vision (ECCV)*, pages 796–812, 2014.

[162] S. Suwajanakorn, S. M. Seitz, and I. Kemelmacher-Shlizerman. Synthesizing obama: Learning lip sync from audio. In *ACM Trans. Graph., (Proc. of SIG-GRAPH)*, pages 1-13, 2017.

[163] V. Tan, I. Budvytis, R. Cipolla. Indirect deep structured learning for 3D human body shape and pose prediction. In: BMVC. (2017)

[164] S. Tansuriyavong and S.-I. Hanaki. Privacy protection by concealing persons in circumstantial video image. In *Proceedings of the 2001 Workshop on Perceptive User Interfaces*, 2001.

[165] J. Taylor, J. Shotton, T. Sharp, and A. Fitzgibbon. The vitruvian manifold: Inferring dense correspondences for one-shot human pose estimation. In *IEEE Conf. on Comput. Vision and Patt. Recog (CVPR)*, 2012.

[166] A. Tewari, M. Zollhofer, H. Kim, P. Garrido, F. Bernard, P. Perez, and C. Theobalt. MoFA: Model-based deep convolutional face autoencoder for unsupervised monocular reconstruction. In *IEEE International Conference on Computer Vision (ICCV)*, 2017.

[167] J. Thies, M. Zollhöfer, M. Stamminger, C. Theobalt, and M. Nießner. FaceVR: Real-Time Facial Reenactment and Eye Gaze Control in Virtual Reality. arXiv preprint arXiv:1610.03151, 2016.

[168] J. Thies, M. Zollhofer, M. Nießner, L. Valgaerts, M. Stamminger, and C. Theobalt. Real-time expression transfer for facial reenactment. *ACM Trans. Graph., (Proc. of SIG- GRAPH)*, 2015.

[169] T.-P. Tian and S. Sclaroff. Fast globally optimal 2d human detection with loopy graph models. In *IEEE Conf. on Comput. Vision and Patt. Recog (CVPR)*, pages 81–88, 2010.

[170] C. Tomasi and R. Manduchi. Bilateral filtering for gray and color images. In *IEEE International Conference on Computer Vision (ICCV)*, pages 839–846, 1998.

[171] A. Toshev and C. Szegedy. Deeppose: Human pose estimation via deep neural networks. In *IEEE Conf. on Comput. Vision and Patt. Recog (CVPR)*, 2014.

[172] A. Tran, T. Hassner, I. Masi, and G. Medioni. Regressing robust and discriminative 3D morphable models with a very deep neural network. In *IEEE Conf. on Comput. Vision and Patt. Recog (CVPR)*, 2017.

[173] A. T. Tran, T. Hassner, I. Masi, E. Paz, Y. Nirkin, and G. Medioni. Extreme 3D face reconstruction: Looking past occlusions. arXiv preprint arXiv:1712.05083v2, 2018.

[174] The Health Insurance Portability and Accountability Act of 1996. United States Federal Law.

[175] The Family Educational Rights and Privacy Act of 1974. United States Federal Law.

[176] The Children's Online Privacy Protection Act of 1998. United States Federal Law.

[177] J. Thies, M. Zollhofer, M. Stamminger, C. Theobalt, and M. Niener. Face2Face: Real-time face capture and reenactment of RGB videos. In *IEEE Conf. on Comput. Vision and Patt. Recog (CVPR)*, 2016.

[178] J. Tong, J. Zhou, L. Liu, Z. Pan, and H. Yan. Scanning 3d full human bodies using kinects. *IEEE Trans. on Visualization and Computer Graphics*, 18(4):643–650, 2012.

[179] G. Varol, D. Ceylan, B. Russell, J. Yang, E. Yumer, I. Laptev, and C. Schmid. BodyNet: Volumetric inference of 3D human body shapes. arXiv preprint arXiv:1804.04875, 2018.

[180] D. Vlasic, M. Brand, H. Pfister, and J. Popovic. Face transfer with multilinear models. In *ACM Trans. Graph., (Proc. of SIG- GRAPH)*, pages 426–433, 2005.

[181] C. Wang, F. Shi, S. Xia, and J. Chai. Realtime 3D eye gaze animation using a single RGB camera. *ACM Trans. Graph., (Proc. of SIG-GRAPH)*, 2016.

[182] F. Wang and Y. Li. Beyond physical connections: Tree mod- els in human pose estimation. In *IEEE Conf. on Comput. Vision and Patt. Recog (CVPR)*, 2013.

[183] R. Wang, L. Wei, E. Vouga, Q. Huang, D. Ceylan, G. Medioni, and H. Li, Capturing Dynamic Textured Surfaces of Moving Targets. 2016.

[184] M. Weber. Caltech face dataset, http://www.vision.caltech.edu/archive.html.

[185] S. -E. Wei, V. Ramakrishna, T. Kanade, and Y. Sheikh. Convolutional pose machines. In *IEEE Conf. on Comput. Vision and Patt. Recog (CVPR)*, 2016.

[186] A. Weiss, D. Hirshberg, M.J. Black. Home 3D body scans from noisy image and range data. In *IEEE International Conference on Computer Vision (ICCV)*, 2011.

[187] Q. Wen, F. Xu, M. Lu, and J.-H. Yong. Real-time 3d eyelids tracking from semantic edges. In *ACM Trans. Graph., (Proc. of SIG-GRAPH)*, pages 1-11, 2017.

[188] N. Werghi. Segmentation and modeling of full human body shape from 3-D scan data: A survey. *IEEE Trans. Syst. Man Cybern. Part C: Appl. Rev*, pages 1122–1136, 2007.

[189] F. Wilcoxon, Individual Comparisons by Ranking Methods, *Biometrics Bull.*, vol. 1, no.6, pp. 80–83, Dec. 1945.

[190] A. Williams, D. Xie, S. Ou, R. Grupen, A. Hanson, and E. Riseman. Distributed smart cameras for aging in place. In *ACM SenSys workshop on distributed smart cameras*, 2006.

[191] T. Winkler and B. Rinner. Security and privacy protection in visual sensor networks: A survey. *ACM Computing Surveys*, pages 1–42, July 2014.

[192] W. Xu, P.-C. Su, S.-C.S. Cheung. Human pose estimation using two RGB-D sensors. In: *IEEE International Conference on Image Processing (ICIP)*, pages 1279-1283, 2016.

[193] W. Xu, S.-C.S. Cheung, and N. Soares. Affect-preserving privacy protection of video. In: *IEEE International Conference on Image Processing (ICIP)*, pages 158-162, 2015.

[194] W. Xu, A. Chatterjee, M. Zollhoefer, H. Rhodin, D. Mehta, H.-P. Seidel, and C. Theobalt. Monoperfcap: Human performance capture from monocular video. *ACM Trans. Graph., (Proc. of SIG-GRAPH)*, 2018.

[195] L. Xu, L. Fang, W. Cheng, K. Guo, G. Zhou, Q. Dai, and Y. Liu. Flycap: Markerless motion capture using multiple autonomous flying cameras. arXiv preprint arXiv:1610.09534, 2016.

[196] J. Yang, J. Franco, F. Hetroy-Wheeler, and S. Wuhrer. Estimation of human body shape in motion with wide clothing. In *European Conf. on Comput. Vision (ECCV)*, pages 439-454, 2016.

[197] W. Yang, S. Li, W. Ouyang, H. Li, and X. Wang. Learning feature pyramids for human pose estimation. In *IEEE International Conference on Computer Vision (ICCV)*, 2017.

[198] Y. Yang and D. Ramanan. Articulated human detection with flexible mixtures of parts. *IEEE Trans. Pattern Anal. Mach. Intell.*, 35(12), 2013.

[199] G. Ye, Y. Liu, N. Hasler, X. Ji, Q. Dai, and C. Theobalt. Performance capture of interacting characters with handheld kinects. In *European Conf. on Comput. Vision (ECCV)*, pages 828–841, 2012.

[200] M. Ye, X. Wang, R. Yang, L. Ren, and M. Pollefeys. Accurate 3d pose estimation from a single depth image. In *IEEE International Conference on Computer Vision (ICCV)*, 2011.

[201] M. Ye and R. Yang. Real-time simultaneous pose and shape estimation for articulated objects using a single depth camera. In *IEEE Conf. on Comput. Vision and Patt. Recog (CVPR)*, pages 2353–2360, 2014.

[202] T. Yu, K. Guo, F. Xu, Y. Dong, Z. Su, J. Zhao, J. Li, Q. Dai, and Y. Liu. Bodyfusion: Real-time capture of human motion and surface geometry using a single depth camera. In *IEEE International Conference on Computer Vision (ICCV)*, 2017.

[203] T. Yu, Z. Zheng, K. Guo, J. Zhao, Q. Dai, H. Li, G. Pons-Moll, and Y. Liu. DoubleFusion: Real-time Capture of Human Performances with Inner Body Shapes from a Single Depth Sensor. In *IEEE Conf. on Comput. Vision and Patt. Recog (CVPR)*, 2018.

[204] Q. Zhang. High quality human 3D body modeling, tracking and application. *Theses and Dissertations--Computer Science*. 39, 2015.

[205] Q. Zhang, B. Fu, M. Ye, and R. Yang. Quality Dynamic Human Body Modeling Using a Single Low-Cost Depth Camera. In *IEEE Conf. on Comput. Vision and Patt. Recog (CVPR)*, pages 676–683, June 2014.

[206] Z. Zhang. A flexible new technique for camera calibration. *IEEE Trans. Pattern Anal. Mach. Intell.*, pages 1330– 1334, 2000.

[207] W. Zhao and R. Chellappa. Illumination-Insensitive Face Recognition using Symmetric Shape-from-Shading. In *IEEE Conf. on Comput. Vision and Patt. Recog (CVPR)*, pages 286–293, 2000.

[208] S. Zhou, H. Fu, L. Liu, D. Cohen-Or, and X. Han. Parametric reshaping of human bodies in images. *ACM Trans. Graph., (Proc. of SIG- GRAPH)*, pages 1-10, 2010.

[209] X. Zhou, M. Zhu, G. Pavlakos, S. Leonardos, K. G. Derpanis, and K. Daniilidis. Monocap: Monocular human motion capture using a cnn coupled with a geometric prior. arXiv preprint arXiv:1701.02354, 2017.

[210] X. Zhu, Z. Lei, J. Yan, D. Yi, and S. Z. Li. High-fidelity pose and expression normalization for face recognition in the wild. In *IEEE Conf. on Comput. Vision and Patt. Recog (CVPR)*, pages 787–796, 2015.

[211] X. Zhu, J. Yan, D. Yi, Z. Lei, and S. Z. Li. Discriminative 3D Morphable Model Fitting. *Automatic Face and Gesture Recognition (FG)*, 2015.

[212] S. Zuffi and M. Black. The stitched puppet: A graphical model of 3D human shape and pose. In *IEEE Conf. on Comput. Vision and Patt. Recog (CVPR)*, 2015.

Vita

EDUCATION

B.S. in Communications Engineering, University of Electronic Science and Technology of China, 2011

M.S. in Electrical Engineering, University of Kentucky, 2013

INTERNSHIP

Mobile Platform Lab, Samsung Research American, 2017
Computer Vision Lab, Rakuten, Inc., 2016

PUBLICATION

(1) P.-C. Su, J. Shen, **W. Xu**, S.-C. Cheung and Y. Luo, "*A Fast and Robust Extrinsics Calibration for RGB-D Camera Network*", Sensors, 18, 235, 2018.

(2) Po-Chang Su, **Wanxin Xu**, Ju Shen, Sen-ching (Samson) Cheung, "*Real-time rendering of physical scene on virtual curved mirror with RGB-D camera networks*". IEEE International Conference on Multimedia & Expo Workshop, 2017. (ICMEW 2017)

(3) **Wanxin Xu**, Po-chang Su, Sen-ching (Samson) Cheung, "*Human Pose Estimation using Two Kinect Sensors*". IEEE International Conference on Image Processing, 2016. (ICIP 2016).

(4) Yuqi Zhang, Nkiruka Uzuegbunam, **Wanxin Xu**, Sen-ching (Samson) Cheung, "*Robomirror: Simulating a Mirror with A Robotic Camera*". IEEE International Conference on Image Processing, 2016. (ICIP 2016).

(5) **Wanxin Xu**, Sen-ching(Samson) Cheung, Neelkamal Soares, "*Affect-Preserving Privacy Protection of Video*". IEEE International Conference on Image Processing, 2015. (ICIP 2015).

(6) Shen, J., **W. Xu**, Y. Luo, P.-C. Su, and S.-C. Cheung, "*Extrinsic Calibration for Wide-baseline RGB-D Camera Networks*". IEEE International Workshop on Multimedia Signal Processing, 2014. (MMSP 2014).

(7) **W.X. Xu**, M.K. Qiu, Z. Chen, H. Su, "*Intelligent Vehicle detection and tracking for highway driving*", IEEE International Conference on Multimedia & Expo Workshop, 2012. (ICMEW 2012)

(8) **Wanxin Xu**, Po-chang Su, Sen-ching Cheung, "*Human Body Reshaping using Multiple RGB-D Sensors*", IEEE Transactions on Multimedia. (Submitted)